CENTRAL NORTH ATLANTIC PALEOCEANOGRAPHY DURING THE MIDDLE PLEISTOCENE (ca. 726–603 ka): INSIGHTS FROM THE DINOFLAGELLATE CYST RECORD

Fernando Mantilla Duran

Department of Earth Sciences

A thesis submitted in partial fulfillment of the degree of

M.Sc. In Earth Sciences

Faculty of Mathematics and Science, Brock University

St. Catharines, Ontario

ABSTRACT

Integrated Ocean Drilling Program (IODP) Site U1313, located at the northern boundary of the subtropical gyre in the central North Atlantic, lies within the southern part of the ice-rafted debris belt. Seventy-three palynological samples were studied from an uninterrupted interval ca. 726–603 ka (upper Marine Isotope Stage [MIS] 18 through lower MIS 15) to resolve conflicting paleoceanographic interpretations. Glacial stages were characterized by high productivity surface waters reflecting a southward shift of the Arctic Front. Sea surface salinities (SSSs) and sea surface temperatures (SSTs) were obtained by transfer functions using the Modern Analogue Technique. The lowest SSTs of 9ºC (±1.3) and 10ºC (±1.3) were recorded in glacial MIS 16 and MIS 18 respectively. However, these reconstructions are influenced by abundant heterotrophic taxa and may reflect elevated nutrient levels rather than lowered temperatures. Reworked palynomorphs uniquely indicate a Cretaceous as well as Paleozoic provenance for the first Heinrich-like events.

ACKNOWLEDGMENTS

I am grateful to my supervisor Prof. Martin J. Head for his guidance throughout this research and for sharing his valuable knowledge. My appreciation also goes to Dr. Stijn De Schepper, who suggested this project, and Dr. Thomas Verleye for their insightful comments and discussions on dinoflagellate cysts and transfer functions, and to Dr. Patrizia Ferretti whose advice and information on foraminifera and stable isotopes were extremely helpful. Dr. David Naafs is also thanked for his insights into biomarkers. Helpful comments on the thesis by Prof. Francine McCarthy sharpened my discussion on paleoproductivity.

This research was supported by a Natural Sciences and Engineering Research Council of Canada (NSERC) Discovery Grant to Prof. Martin J. Head. I acknowledge with gratitude the Dean of Graduate Studies Spring 2012 Research Scholarship (Brock University), and the Canadian Consortium for Ocean Drilling (CCOD) Student Travel Grant 2012 for support during the execution of this research.

Last but not least, I deeply thank and dedicate this work to my parents and siblings for their love and support from afar, and to my best friend and love Ruth for her unconditional support.

TABLE OF CONTENTS

LIST OF FIGURES

LIST OF TABLES

1. INTRODUCTION

During the transition from Early to Middle Pleistocene, the Earth experienced a dramatic change in its climatic cyclicity. It shifted from dominantly 41-kyr cyclicity controlled by obliquity, to a quasi-100-kyr periodicity thought to be associated with precession (e.g. Hays et al., 1976; Imbrie et al., 1992; Head and Gibbard, 2005; Huybers, 2007). This transition, known as the Mid-Pleistocene Revolution (Berger and Jansen, 1994) or Mid-Pleistocene Transition (e.g. Head and Gibbard, 2005; Clark et al., 2006), occurred from ca. 1.2 Ma to 500 ka (Head and Gibbard, 2005). However, quasi-100 kyr cycles became dominant only around 700 ka when the first strong glaciation of the Mid-Pleistocene Transition took place in the Northern Hemisphere (e.g. Maslin and Ridgwell, 2005; Head et al., 2008; Lang and Wolff, 2011). This glaciation corresponds to Marine Isotope Stage (MIS) 16 in the "LR04" stack of the benthic $\delta^{18}O$ isotope record (Lisiecki and Raymo, 2005) (Fig. 1).

The particular importance of MIS 16 relies not only on the fact that it constitutes the first cold stage of the quasi-100 kyr climate system but also because it bears the earliest layers of ice-rafted debris (IRD) derived from the Laurentide Ice Sheet, specifically from carbonate units of the Hudson Strait region of Canada (e.g. Hodell et al., 2008; Naafs et al., 2011). These layers rich in detrital carbonate have been documented extensively for the last glacial cycle (e.g. Bond et al., 1992; Broecker et al., 1992; Hemming et al., 2000; Hemming, 2004; Parnell et al., 2007) and represent the so-called Heinrich events of Broecker et al. (1992). The earliest occurrence of these Heinrich-like events in the sedimentary record, during MIS 16, appears to represent the first time the Laurentide Ice

Sheet attained sufficient thickness to produce significant iceberg discharges (Hodell et al., 2008).

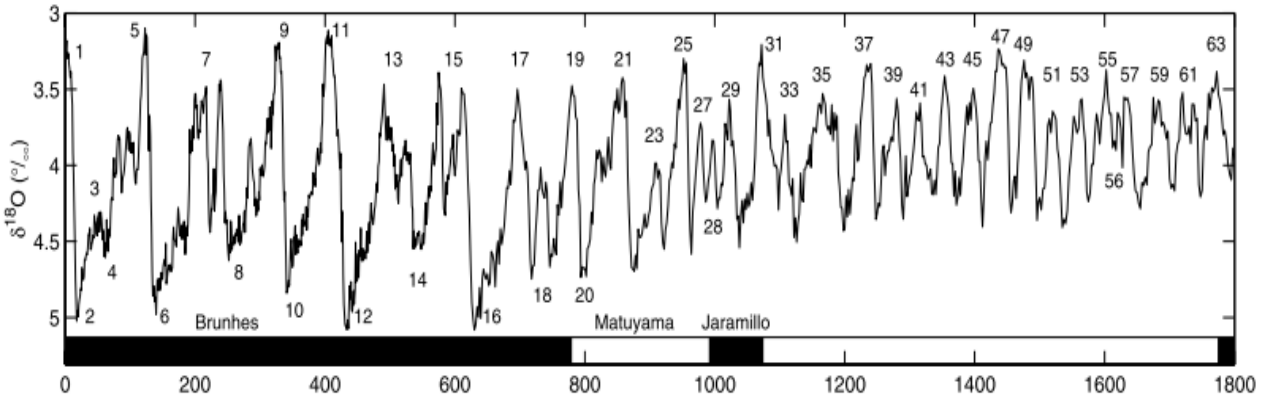

Figure 1: The LR04 benthic $\delta^{18}O$ stack. X axis corresponds to thousands of years (from Lisiecki and Raymo, 2005, fig. 4).

In the North Atlantic, the area with major IRD influence is found between 38º and 55ºN and is known as the IRD-belt or Ruddiman belt (Ruddiman, 1977; Robinson et al., 1995) (Fig. 2). Integrated Ocean Drilling Program (IODP) Site U1313, which is the focus of the present study, lies just within the southern boundary of this belt.

Various studies show that surface water characteristics in the North Atlantic are controlled mainly by the North Atlantic Current (NAC) (e.g. Calvo et al., 2001; Lawrence et al., 2009; Naafs et al., 2010). Its strength and position can control the location of the Arctic Front and therefore produce considerable changes in sea-surface temperature (SST) and primary productivity (Naafs et al., 2010). SSTs during MIS 16 have already been reconstructed at high resolution for IODP Site U1313 using Mg/Ca

ratios from the planktonic foraminifer *Globigerina bulloides* and from alkenones (Naafs et al., 2011). Curiously, alkenone paleotemperatures show a muted peak-cooling in mid-MIS 16 followed by a warming, whereas Mg/Ca results suggest increasing cooling until just before the termination (Naafs et al., 2011). This discrepancy in paleotemperatures was explained as reflecting strong stratification of the water column (Naafs et al., 2011), although the mechanism is still not well understood.

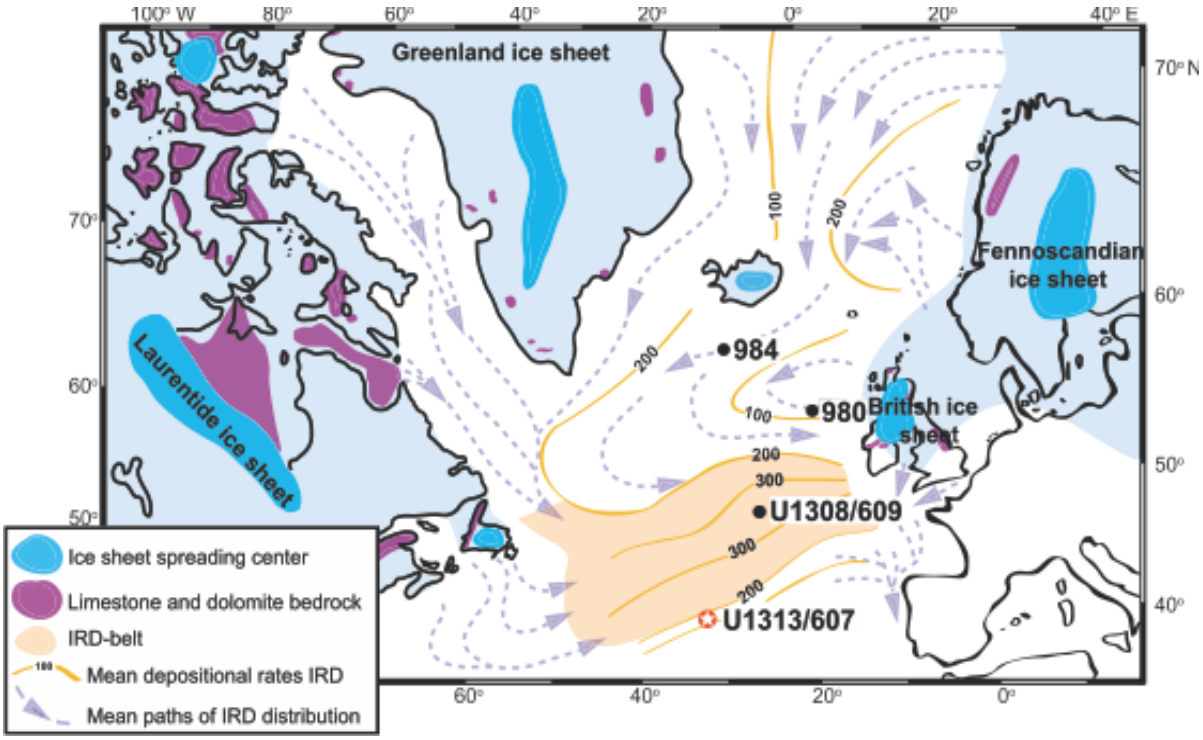

Figure 2: Location of IODP Site U1313 with respect to the IRD belt in the North Atlantic (from Naafs et al., 2011, fig. 1).

Organic-walled dinoflagellate cysts, or dinocysts, have been studied extensively to document how their distribution in modern marine environments is controlled by such parameters as SST, sea-surface salinity (SSS), sea-ice cover and nutrient availability (e.g.

Rochon et al., 1999; de Vernal et al., 2001, 2005; Radi and de Vernal, 2008a, b; Bonnet et al., 2012). This understanding has permitted dinocysts to be used as a tool for paleoceanographic and paleoecological reconstructions in Quaternary sequences, although differential preservation of certain taxa can sometimes affect the accuracy of these reconstructions. For older periods, paleoenvironmental interpretations may be limited by the absence of a modern analog to compare with the fossil assemblages, and this is exacerbated by the presence of extinct species. However, the geographical distributions of extinct species and their relationships to coeval paleoenvironmental proxies, both paleontological and nonpaleontological, have provided qualitative insights into their environmental tolerances (e.g. Head, 1994; Sluijs et al., 2006; De Schepper et al., 2009b; Donders et al., 2009; Sluijs and Brinkhuis, 2009). More recently, extinct Pliocene species have been calibrated directly to foraminiferal Mg/Ca paleotemperatures, allowing their temperature tolerances to be estimated quantitatively (De Schepper et al., 2011).

The present study represents the most detailed dinocyst record yet obtained for MIS 16. It uses dinocysts to investigate shifts in water mass properties during MIS 16 and bounding interglacials at IODP Site U1313, and attempts to resolve the discrepancy between alkenone and foraminiferal Mg/Ca paleotemperatures. The use of transfer functions using the Modern Analogue Technique on a North Atlantic Ocean subset of the n=1419 Northern Hemisphere dataset (Radi and de Vernal, 2008a) is implemented to obtain quantitative values of such parameters as SST and SSS. Additionally, interpretations based on the ecological distributions of selected extant species and on the latitudinal ranges of selected extinct taxa are generated to test the reliability of the output from the

transfer functions. Reworked dinocysts and acritarchs are also tracked to identify the source of Heinrich-like events in the palynological record.

2. STUDY AREA

2.1. IODP Site U1313

IODP Site U1313 (41°00′N, 32°57′W) was drilled at the base of the upper western flank of the Mid-Atlantic Ridge approximately 386 km northwest of the Azores in a water depth of 3426 m (Fig. 2). This site is located in open marine conditions and lies at the northern margin of the North Atlantic subtropical gyre. Site U1313, drilled in 2005, constitutes a reoccupation of Deep Sea Drilling Project (DSDP) Site 607 drilled during Leg 94 in 1983. The rationale for re-drilling this site was that it represents the only site in the high-latitude North Atlantic where North Atlantic Deep Water (NADW) circulation can be monitored throughout the Pleistocene (Expedition 306 Scientists, 2006). Therefore, this site has played an important role in such aspects as the acquisition of benthic $\delta^{18}O$, $\delta^{13}C$, and $CaCO_3$ records for the Pleistocene (Ruddiman et al., 1989). A reoccupation of this site using more advanced coring technology would allow a more complete recovery of the sediment sequence. Indeed, offset drilling techniques to construct composite sections became available in 1992 (Mayer et al., 1992). The acquisition of new cores would allow magnetic susceptibility and geochemical proxies, as well as other measurements, to be acquired for very high resolution stratigraphy and paleoceanographic reconstructions.

Four holes were drilled at Site U1313 during IODP Expedition 306 to produce a composite stratigraphic section. In total, a 308-m sequence was recovered from four holes (U1313A, U1313B, U1313C and U1313D). In general, the sediment is composed of nannofossil ooze with varying quantities of foraminifers and fine to very fine terrigenous material (Expedition 306 Scientists, 2006).

Two major lithologic units were defined at Site U1313 based on visual observations of sediment colour, percentage of carbonate, and physical properties data (Expedition 306 Scientists, 2006). The general characteristics of Unit I are described below following the reported lithology of Expedition 306 Scientists (2006) and summarized in Figure 3. The sediments used for this study only involve Unit I. Therefore, lithological descriptions of Unit II are omitted.

2.1.1. Unit I

This unit comprises silty clay nannofossil ooze, nannofossil ooze with clay, and nannofossil ooze, and displays centimeter- to decimeter-scale variability in detrital clay and biogenic carbonate. Occasional millimeter- to centimeter-scale diffuse green and gray bands are distributed throughout the unit. Boundaries between intervals are often gradational and bioturbated. Bioturbation is rare to moderate throughout the unit. Gamma ray attenuation density as well as magnetic susceptibility and intensity measurements display large variability in this unit. Dropstones are recorded frequently.

This unit spans 0–111.86 meters below sea floor (mbsf) in Hole U1313A, 0–111.28 mbsf in Hole U1313B, 0–112 mbsf in Hole U1313C and 0–113.14 mbsf in Hole U1313D and

represents deposition spanning the Holocene–Early Pleistocene (based on the current time scale; Gibbard and Head, 2010).

2.1.1.1. Subunit IA

Subunit IA is distinguished by high-amplitude fluctuations in detrital clay and biogenic carbonate. This is discernible by colour changes, gamma ray attenuation density and magnetic susceptibility. The uppermost ~65 cm consists of yellowish brown nannofossil silty clay and represents the Holocene. The remainder of the subunit is dominated by nannofossil silty clay, silty clay nannofossil ooze, nannofossil ooze with clay, nannofossil ooze, and minor intervals of silty clay nannofossil ooze with diatoms and nannofossil ooze with diatoms and clay. The colour varies from white to light gray and gray with minor light olive-gray to olive-gray. Colour changes are gradational and reflect variations in carbonate versus clay content. Bioturbation is rare to moderate.

Depths of Subunit IA are 0–41.00 mbsf in Hole U1313A, 0–39.38 mbsf in Hole U1313B, 0–41.08 in Hole U1313C, and 0–39.7 in Hole U1313D, this subunit representing deposition mostly during the Middle Pleistocene–Holocene. The present interval of study occurs within Subunit IA.

2.1.1.2. Subunit IB

This subunit consists of nannofossil ooze, nannofossil ooze with clay, and silty clay nannofossil ooze. In general, the amount of biogenic carbonate is higher than for Subunit

IA and the detrital clay percentage is lower. Colours vary from white to light gray and gray, showing decimeter-scale variation in clay and biogenic carbonate content.

Subunit IB spans 41–111.86 mbsf in Hole U1313A, 39.38–111.28 mbsf in Hole U1313B, 41.08–112.00 mbsf in Hole U1313C, and 39.7–113.14 mbsf in Hole U1313D. The time interval represented by Subunit IB is Early Pleistocene (based on the current time scale; Gibbard and Head, 2010).

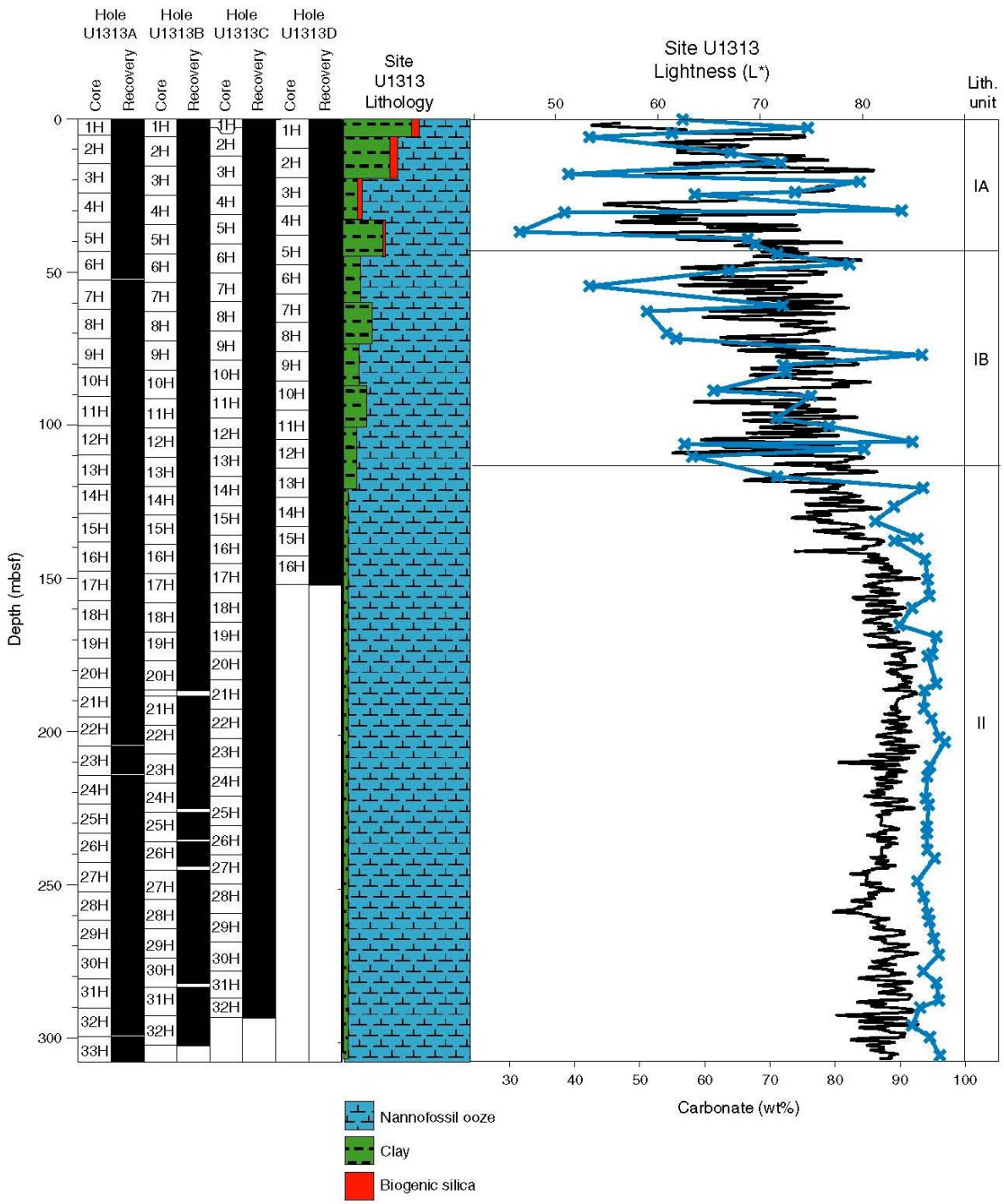

Figure 3: Summarized lithologic units and lithologies at Site U1313. The black line corresponds to sediment lightness determined from colour reflectance data. The blue line shows sediment lightness from carbonate values (from Expedition 306 Scientists, 2006, fig. F7).

2.2. Oceanographic setting

Site U1313 is an open ocean site in the central part of the North Atlantic, located within the northernmost part of the oligotrophic subtropical gyre. The site is currently positioned south of the warm and saline waters of the North Atlantic current (NAC), although surface waters in this area are derived from the NAC (Voelker et al., 2010). Site U1313 is also affected by the cold North Atlantic Deep Water (NADW) current (Ferretti et al., 2010) (Fig. 4). During the Middle Pleistocene, this site was similarly influenced by these oceanic currents (cf. Wright and Flower, 2002; Expedition 306 Scientists, 2006; Naafs et al., 2011). Its relative proximity to the boundary between the subpolar gyre and the subtropical gyre makes this site ideally positioned for studying the response of the central North Atlantic during major climatic events to shifts in the two different regimes: subpolar cold waters with high nutrient content, and warm and oligotrophic waters from the subtropical gyre.

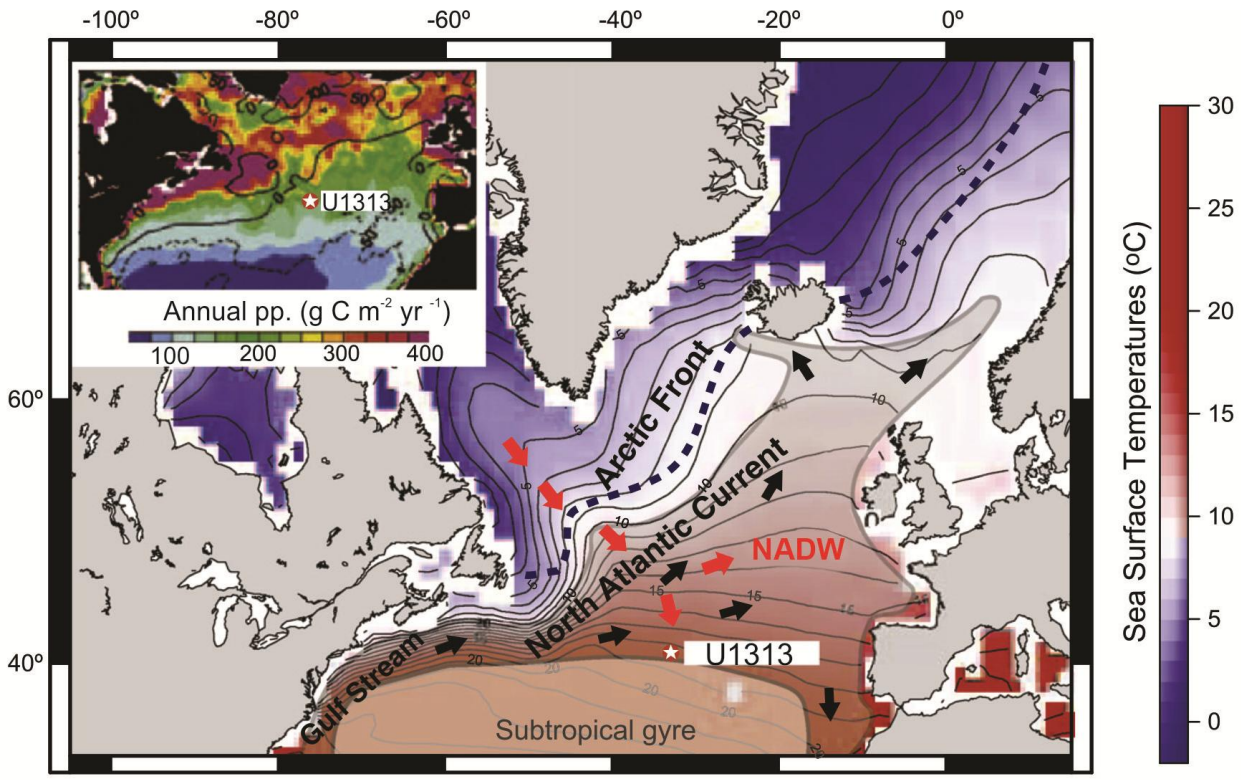

Figure 4: The North Atlantic Ocean showing the modern mean SSTs, North Atlantic Current, Gulf Stream, North Atlantic Deep Water (NADW) and Arctic Front. Black arrows indicate surface currents. Red arrows indicate deep water mass. Insert shows annual primary productivity (modified from Naafs et al., 2010, fig. 1).

3. BACKGROUND INFORMATION

3.1. Overview of dinoflagellate cyst applications

Organic-walled dinoflagellate cysts (dinocysts) in the fossil record are generally regarded as representing hypnozygotes, or resting stages, produced by certain species of marine and fresh water dinoflagellate as part of their life cycle (Fig. 5). The preserved walls of these dinocysts are mainly composed of aromatic biomacropolymer(s) known as dinosporin (Fensome et al., 1993; Kokinos et al., 1998). Their chemical composition makes dinocysts highly resistant to acid dissolution in contrast to carbonate and siliceous fossil groups. The geological record of dinocysts extends from the Triassic to present (Traverse, 2007), with the highest diversity reached during the Cretaceous (Miller et al., 2005). However, geochemical evidence suggests the existence of this group, or a direct ancestor, as far back as the Early Cambrian or Proterozoic (Moldowan et al., 1996; Moldowan and Talyzina, 1998).

Dinocysts are commonly used in studies of biostratigraphy, chronostratigraphy, and paleoecology. Dinocyst extinctions, originations, and even characteristic assemblages, permit correlations at different time frames (e.g. Head et al., 2004; Simaeys et al., 2005; Scott et al., 2009). They are also commonly used in paleoceanographic research as they are controlled by such hydrographic parameters as sea-surface temperature, salinity, sea-ice cover, and nutrient availability (e.g. Wall et al., 1977; Harland, 1983; de Vernal et al., 2001, 2005; Marret and Zonneveld, 2003; Radi and de Vernal, 2008a, b; Pospelova et al., 2008; De Schepper et al., 2009a; Bonnet et al., 2012). Dinocysts are abundant in a wide range of ecological settings from tropical waters to environments where other fossil

groups are scarce or absent, such as the circumpolar waters in both hemispheres (e.g. Wrenn et al., 1998; de Vernal et al., 2001; Kunz-Pirrung, 2001; Harland and Pudsey, 2002) and anoxic basins (e.g. Pospelova et al., 2006; Mertens et al., 2009; Verleye et al., 2009). This results from the capacity of certain dinoflagellates to thrive in unfavorable conditions such as polar waters with seasonal ice cover, presumably though their ability to produce a resting cyst. This versatility as a group, together with the sensitivity of individual species to environmental change, makes dinocysts an effective proxy for paleoclimatic studies in a wide variety of scenarios.

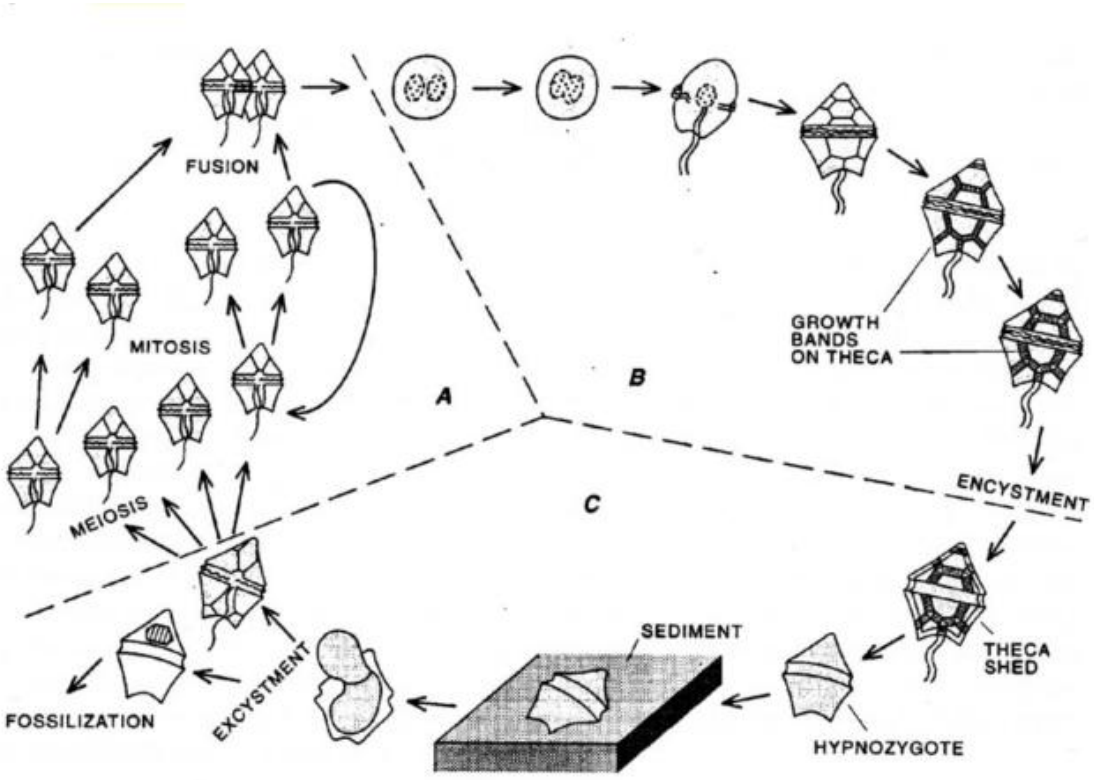

Figure 5: Life cycle of dinoflagellates (from Traverse, 2007, fig. 12.5).

Numerous dinocyst studies have been conducted in the North Atlantic Ocean and adjacent seas to identify changes in hydrographic parameters during the Quaternary, and transfer functions are presently the most widely applied statistical method for quantitative reconstructions. De Vernal et al. (1993) adapted transfer functions based on the best analogue method (MAT; Modern Analogue Technique) for dinocyst assemblages. In essence, the MAT measures the degree of similarity between fossil dinocyst assemblages and modern distributions, assuming that they represent comparable environmental conditions. Since this technique is based on a comparison between the fossil assemblage and the *k*-nearest modern neighbors, the accuracy of MAT-based reconstructions is directly controlled by the quantity of modern data points available. Consequently, in the past two decades the quantity of information on modern dinocyst distribution has increased substantially (e.g. Devillers and de Vernal, 2000; de Vernal et al., 2001; Marret and Zonneveld, 2003; Pospelova et al., 2008; Radi and de Vernal, 2008a, b; Bonnet et al., 2012), providing a wider spectra of geographical datasets for analyses using the MAT.

3.2. The Mid-Pleistocene Transition

The Mid-Pleistocene Transition constitutes one of the most important climatic events in the Quaternary. This transition is characterized by a progressive shift from low-amplitude 41-ka cycles to high-amplitude cycles of around 100 ka. This shift resulted in increasingly strong glaciations and hence an increase in the volume of the northern hemisphere ice sheets as shown by the $\delta^{18}O$ isotope record (e.g. Head and Gibbard, 2005; Head et al., 2008). The quasi-100-ka cycles that characterize the Mid-Pleistocene

Transition (MPT) were initially thought to have been driven by orbital eccentricity (e.g. Imbrie et al., 1993). However, more recent studies have demonstrated that changes in eccentricity cause only small variations in the total annual insolation and do not constitute a significant parameter for controlling the post-MPT glacial–interglacial cycles (e.g. Maslin and Ridgwell, 2005). On the other hand, the influence of precession seems to play a direct forcing role. The low-frequency post-MPT cycles seem to occur synchronously with every fourth or fifth precessional cycle (e.g. Maslin and Ridgwell, 2005; Head et al., 2008). Studies have proposed ice-sheet dynamics (Clark et al., 2006) or a decline in atmospheric CO_2 (Maslin and Ridgwell, 2005) as the factors triggering the MPT, although the originating mechanisms remain speculative.

In a broad sense, the MPT began around 1.2 Ma (MIS 38–36) and had become fully established by ca. 500 ka (MIS 14–12). Yet, in the $\delta^{18}O$ isotope record, the typical asymmetrical post-MPT "saw-tooth" pattern of slow buildup resulted from large ice sheets, and subsequent rapid melting is first noticed around 700 ka (MIS 16) (*see* Figure 1). Hence, MIS 16 represents the first time northern hemisphere ice sheets attained substantial thickness and extent, resulting in the first isotopically strong glaciation experienced in the northern hemisphere during the Quaternary (Lang and Wolff, 2011).

3.3. Ice-rafted debris and Heinrich(-like) events

Ice-rafted debris (IRD) corresponds to erratic rocks and minerals derived mainly from massive discharges of icebergs. When the icebergs melt, the debris is unloaded and deposited onto the sea floor. Analyses of such parameters as mineral composition,

biochemical signature, and palynology of IRD layers are frequently used to investigate the provenance of this material and its relationship to the collapse of particular ice sheets (e.g. Bond et al., 1992; Bischof et al., 1997; Rosell-Melé et al., 1997; Snoeckx et al., 1999; Hemming, 2004; Parnell et al., 2007; Hodell et al., 2008, 2010).

One of the first studies involving IRD in the North Atlantic Ocean was conducted by Ruddiman (1977). He recognized that an area with major IRD influence, called the IRD-belt or later the Ruddiman belt, was located between 38º and 55ºN in the North Atlantic (Fig. 2). Later, in the late 1980s, Hartmut Heinrich reported prominent peaks of lithic grains while studying sediments spanning the last glacial cycle from the Dreizack seamounts in the North Atlantic (Heinrich, 1988). In this study, he noticed six layers with high amounts of detrital limestone and dolostone as well as poor concentrations of foraminifera. These layers became the focus of several studies and were named "Heinrich events" by Broecker et al. (1992). They proposed that the material forming these Heinrich events was derived from massive discharges of ice from the Laurentide ice sheet, specifically from the Hudson Strait region of Canada.

The definition of what constitutes a Heinrich event has been an active topic of discussion. The most widely accepted definition is that proposed by Broecker et al. (1992) which requires the presence of detrital limestone and dolostone derived from Paleozoic basins of northern Canada.

Hence, a Heinrich event *sensu stricto* makes reference only to the IRD layers of detrital limestone and dolostone derived from the Hudson Strait area of Canada and found in sediments of the last glacial cycle. However, more recent studies have identified other

layers with the same characteristics in older glacial cycles (e.g. Hodell et al., 2008). A varied terminology has therefore emerged with reference to these older IRD layers. Examples are *"Hudson Strait" Heinrich events* of Hodell et al. (2008) or *Heinrich(-like) events* of Naafs et al. (2011). This study adopts the term used by Naafs et al. (2011).

Besides abundant lithic grains, Heinrich events and other IRD layers bear such characteristics as high magnetic susceptibility, high lithic/foraminiferal ratios, and elevated relative abundances of the polar planktonic foraminifer *Neogloboquadrina pachyderma* sinistral (Heinrich, 1988). The last of these characteristics reflects the colder surface waters present during iceberg discharge that allowed this foraminifer to live in lower than normal latitudes. The high magnetic susceptibility signal in these layers is explained by the presence of ferromagnetic minerals derived from the continents. Other characteristics involve high peaks in Ca/Sr and Si/Sr ratios due to inorganically precipitated carbonates and continent-derived silicates respectively.

Several studies have investigated the presence, distribution, and characteristics of Heinrich(-like) events in the North Atlantic (e.g. Bond et al., 1992; Rosell-Melé et al., 1997; Hemming, 2004; Parnell et al., 2007; Hodell et al., 2008, 2010; Stein et al., 2009; Naafs et al., 2011). In general, four Heinrich(-like) events in each of MIS 2 and MIS 4, three in MIS 8, one Heinrich-like layer in termination V of MIS 12, and two in MIS 16, have been identified. Other pre-MIS 16 IRD layers have been recorded in North Atlantic sediments but they lack the carbonate composition associated with ice-rafted material from the Hudson Strait. Consequently, MIS 16 corresponds to the first glacial interval registering the influence of detrital carbonates from this region of Canada, and hence

could represent the first time the Laurentide Ice Sheet gained sufficient thickness to release massive iceberg discharges into the North Atlantic (Hodell et al., 2008).

3.4. Differential preservation of dinocysts.

One of the strengths of palynology is the acid-resistant nature of palynomorphs, this providing a significant advantage over other microfossil groups that are usually more prone to dissolution due to their mineral composition. Nevertheless, certain dinocysts are more sensitive to taphonomic processes than others. A documented sensitivity to oxidation in (heterotrophic) protoperidinioid cysts (e.g. *Brigantedinium*) has been widely documented (e.g. Dale, 1976; Hopkins and McCarthy, 2002; Versteegh and Zonneveld, 2002; Zonneveld et al., 2007) and therefore can notably skew assemblages towards more resistant cysts (Hopkins and McCarthy, 2002). This selective degradation can have important implications for interpretations conducted, for instance, in areas with highly oxygenated bottom waters and low sedimentation rates in which susceptible cysts are prone to oxidative destruction (McCarthy et al., 2004; Zonneveld et al., 2007). Cyst concentrations calculated in palynological analyses may therefore underestimate original concentrations and hence estimations of primary productivity.

Reichart and Brinkhuis (2003), however, investigated the degree of influence of oxygenated bottom waters on the preservation of *Protoperidinium* cysts using sediments from the Arabian Sea, which are characterized by well-ventilated waters and high seasonal primary productivity. Their results suggested that *Protoperidinium* cyst preservation can sometimes be comparable to the preservation of pollen grains, and

showed that abundances of *Protoperidinium* cysts can reliably reflect high-productivity zones even when significant cyst degradation has taken place.

3.5. Palynofacies

The term palynofacies was first introduced by Combaz (1964) with reference to the total acid-resistant organic matter component deposited in sediments. Several variations of this term have been introduced, including palynodebris (Boulter, 1994), sedimentary organic matter (Tyson, 1995), and dispersed organic matter (Oboh-Ikuenobe et al., 1998). Powell et al. (1990) defined palynofacies as a specific assemblage of organic debris that reflects a particular depositional environment.

Various classification schemes have been used to categorize the organic debris within sediments (e.g. Combaz, 1964; Tyson, 1995; Oboh-Ikuenobe et al., 2005), and are usually based in the morphological aspect of the particles (i.e. structured and unstructured) and origin (e.g. marine and continental).

Amorphous organic material (AOM) constitutes one of the organic particles present in a palynological sample. This material is generally present in lacustrine samples and also those from marine settings in which it may constitute the principal component, especially in areas without continental influence (Tyson, 1995). AOM results from the anaerobic/dysaerobic degradation of algal matter (Oboh-Ikuenobe et al., 2005). It is itself easily degraded in oxic settings and therefore appears to be especially diagnostic of dysoxic to anoxic facies in marine sediments (Tyson, 1995). This sensitivity allows its

presence or absence in marine palynological samples to be used for ascertaining whether the samples have been subjected to oxidation during their taphonomic history.

4. MATERIALS AND METHODS

In this study, 73 samples from IODP Expedition 306, Site U1313 Hole A were processed for palynological analysis with the intention of assessing the dinocyst signal throughout MIS 16 and its transition to bounding interglacials. The sediment used represents the <63 μm filtrate saved during foraminiferal processing by Patrizia Ferretti at the University of Cambridge (Naafs et al., 2011). The selected samples cover an interval of 29.83 to 35.68 amcd (adjusted meter composite depth. *See below*).

4.1. Age Model at Site U1313

Four holes were drilled in 2005 at Site U1313 during Expedition 306 with the reoccupation of DSDP Site 607. A preliminary age model for Site U1313 was developed using biostratigraphic and paleomagnetic data (Expedition 306 Scientists, 2006). Then followed chronologies by Stein et al. (2009), Ferretti et al. (2010), and Voelker et al. (2010) which were constructed by correlating benthic $\delta^{18}O$ values with the global stacked $\delta^{18}O$ record of Lisiecki and Raymo (2005). Subsequently Naafs et al. (2011) updated the original meter composite depth (mcd)-scale to an adjusted meter composite depth (amcd) scale to enhance the correlation of certain features in the lightness, magnetic susceptibility and paleomagnetic data between the four holes. The age model constructed by Naafs et al. (2011) is based on composite benthic foraminiferal $\delta^{18}O$ data from Stein et al. (2009), Ferretti et al. (2010), Voelker et al. (2010), and Naafs et al. (2011), obtained from *Cibicidoides wellerstorfi.* The obtained composite section was subsequently tuned to the LR04 stack (Lisiecki and Raymo, 2005). Additionally, the lightness from U1313

was tuned to the carbonate content of DSDP Site 607 (Ruddiman et al., 1989) to add more tie points for depth-age consistency. This study adopts the MIS boundaries and age model postulated by Naafs et al. (2011).

4.2. Mg/Ca and alkenone-based SSTs

Naafs et al. (2011) used alkenones along with Mg/Ca ratios on the planktonic foraminifer *Globigerina bulloides* to identify mean sea-surface paleotemperatures at IODP Site U1313. Interestingly, the results show a strong discrepancy; alkenone-based SSTs show a muted trend whereas Mg/Ca results show significantly increased cooling until about 10 kyr before the termination of MIS 16 (Fig. 6). The foraminifer *G. bulloides* is found throughout the upper 60 m of the water column in the North Atlantic (Schiebel et al., 1997) whereas alkenones are thought to represent the upper 10 m (Müller et al., 1998). Naafs et al. (2011) attributed this mismatch to possible strong water stratification.

4.3. Sample selection

The material used in the present study corresponds to the <63 μm sieved material previously used by Naafs et al. (2011) who processed 146 samples for foraminifera. Within this batch, alternate samples were selected for palynological treatment (73 samples) with an average sample resolution of 10 cm. Afterwards, the selected samples were randomized and separated into three different batches for processing.

Randomization was aimed to avoid the occurrence of systematic errors during palynological processing.

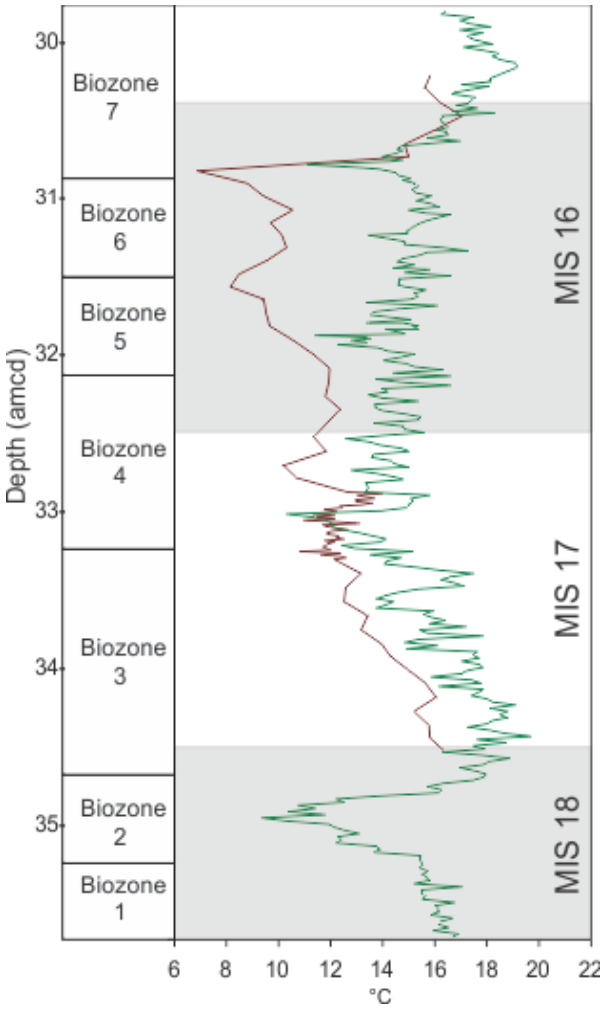

Figure 6: Mg/Ca (red) and alkenone (green) paleotemperatures at IODP Site U1313. Depth in amcd is shown on the left axis. Grey bars indicate glacial stages. (Modified from Naafs et al. 2011, fig. 6). Biozones correspond to the palynological biozonation proposed in this study (see Results section). Resolving the discrepancy between Mg/Ca (red) and alkenone (green) paleotemperatures in MIS 16 is a primary aim of the present study.

4.4. Palynological processing

The protocol for palynological sample processing was adapted from methods already used at Brock University. This protocol was tailored to deep-sea sediments that had been previously disaggregated in distilled water, and wet sieved at <63 µm to remove foraminifera. The filtrate had been retained in a 1L glass beaker, allowed to settle, and decanted. This dried sediment was then scraped from the base of each glass beaker and stored in plastic bags. This part of the procedure was conducted at the University of Cambridge under the direction of Dr Patrizia Ferretti who then supplied the dried sediment for the current palynological analysis. Of the 73 samples chosen for palynology, 28 were subsequently analyzed for Mg/Ca foraminiferal paleotemperature analysis (Naafs et al., 2011, Table 4).

Each sample was weighed, transferred to a plastic 400 ml beaker, and sealed with Parafilm to avoid any airborne contamination prior to and during processing. Cold 20% conc. HCl was added to dissolve all carbonates. Due to the carbonate-rich composition of the samples, the HCl was introduced in small increments to avoid a vigorous reaction that could induce overspill. After several hours, samples were neutralized using distilled water and then treated with cold 38% conc. HF to remove the silicate fraction. After about four or five days in HF, with periodic swirling, the HF was decanted and the residue neutralized once more. Residues were briefly treated again with cold 20% conc. HCl to remove any fluorosilicates. At this point, tablets of *Lycopodium clavatum* (Batch # 1031; x=20848, s= ± 3457) were added to each sample. The residue was then sieved through a 10-µm nylon mesh. Up to 2 minutes of ultrasound was applied to certain samples to deflocculate agglomerates and remove excessive amorphous organic material.

Table 1 summarizes the applied ultrasound for each sample. Sieved residues were stained in safranin-o and mounted on standard microscope slides using glycerine jelly. Surplus residue was stored in vials containing glycerine to which one drop of liquefied phenol had been added to prevent microbial growth.

Samples were labeled giving the core, drilling type, section number, half (working or archival), and sample interval in cm. For example, sample 4H2W 50–51 corresponds to Core 4, type H (advanced hydraulic piston corer), Section 2, working half (W), and interval 50–51 cm. Since all samples correspond to Hole A (U1313A) this information was excluded. Each sample was also labeled with a consecutive identification number corresponding to the randomized order in which each sample was processed. The sample numbers therefore follow no particular relationship to depth.

Table 1 shows detailed information regarding weight, ultrasound times and number of tablets of *L. clavatum* added to each sample. A detailed explanation of the protocol used for sample preparation is given in Appendix 3. For practical purposes, samples are here referred to their corresponding depth (amcd).

4.5. Dinocyst analysis

Palynological analyses were conducted at Brock University using a Leica DM2500 transmitted light microscope. During counting, each palynological slide was scanned using a 40X objective lens. A 100X oil immersion objective was used for detailed morphological analyses of key and problematic dinocysts and small acritarch species. Palynomorphs were counted until a minimum of 300 dinocysts had been enumerated for

each sample, wherever possible. However, low concentrations in some intervals yielded reduced counts (see Results section).

ID #	Sample	Depth (amcd)	Total dry weight (<63 + >63 µm) (gr)	Tablets of *L. clavatum*	Ultrasound treatment (mins and secs)
12	4H2W 50-51	29.83	13.64	1	0:00
39	4H2W 58-59	29.92	16.1	1	1:15
63	4H2W 66-67	30.01	15.47	1	1:15
40	4H2W 74-75	30.09	15.6	1	1:30
11-S	4H2W 82-83	30.18	16.27	1	1:30
34	4H2W 90-91	30.27	15.72	1	1:45
60	4H2W 98-99	30.36	16.06	1	0:30
32	4H2W 106-107	30.45	15.75	1	1:30
67	4H2W 114-115	30.53	16.27	1	0:00
64	4H2W 122-123	30.62	11.64	1	1:30
28	4H2W 129-130	30.70	13.18	1	1:15
66	4H2W 134-135	30.75	16.45	1	1:10
20	4H2W 142-143	30.84	12.84	1	0:00
33	4H2W 146-147	30.88	7.92	1	1:15
73	4H3W 4-5	30.96	11.81	1	0:00
26	4H3W 12-13	31.04	12.28	1	1:30
52	4H3W 18-19	31.11	13.82	1	0:40
36	4H3W 24-25	31.17	13.74	1	1:10
57	4H3W 32-33	31.25	13.46	1	0:40
13	4H3W 40-41	31.33	14.52	1	0:00
35	4H3W 48-49	31.41	12.72	1	1:15
62	4H3W 56-57	31.50	12.69	1	0:00
1	4H3W 64-65	31.58	11.94	1	2:00
65	4H3W 72-73	31.66	8.46	1	0:25
14	4H3W 76-77	31.70	14.98	1	0:45
44	4H3W 84-85	31.79	12.55	1	1:10
59	4H3W 92-93	31.88	13.84	1	0:00
46	4H3W 100-101	31.97	14.1	1	0:45
50	4H3W 108-109	32.05	15.35	1	0:45
6	4H3W 116-117	32.14	15.76	1	1:15
49	4H3W 120-121	32.19	9.78	1	1:00
42	4H3W 128-129	32.28	14.98	1	1:45
61	4H3W 136-137	32.36	16.1	1	0:45
5	4H3W 144-145	32.45	11.97	1	0:00

Table 1: Total sample weight, number of *Lycopodium* tablets added, and duration of ultrasound treatment (minutes and seconds) for each sample. The total dry weight was measured before wet sieving at 63 µm for foraminifera (supplied by P. Ferretti).

68	4H4W 2-3	32.54	13.21	1	0:40
4	4H4W 10-11	32.63	12.56	1	0:15
8	4H4W 18-19	32.72	10.98	1	1:00
45	4H4W 26-27	32.80	10.72	1	1:30
69	4H4W 34-35	32.89	13	1	0:00
9	4H4W 42-43	32.98	12.75	1	1:00
3	4H4W 50-51	33.07	12.81	1	1:00
54	4H4W 58-59	33.16	14.77	1	0:00
7	4H4W 66-67	33.25	15.61	1	0:00
58	4H4W 71-72	33.30	11.21	1	1:10
38	4H4W 78-79	33.38	14.43	1	1:30
53	4H4W 85-86	33.46	16.27	1	1:15
37	4H4W 93-94	33.55	13.95	1	1:30
10	4H4W 101-102	33.63	13.93	1	1:30
16	4H4W 109-110	33.72	16.62	1	1:15
55	4H4W 117-118	33.81	16.72	1	1:00
27	4H4W 125-126	33.90	21.88	1	1:45
43	4H4W 133-134	33.99	16.32	1	1:30
72	4H4W 141-142	34.08	14.25	1	0:40
29	4H5W 2-3	34.20	16.34	1	1:45
17	4H5W 10-11	34.29	15.47	1	1:15
71	4H5W 18-19	34.38	16.9	1	1:00
19	4H5W 26-27	34.46	14.63	1	1:45
47	4H5W 34-35	34.54	17.62	1	1:30
15	4H5W 42-43	34.61	16.55	1	1:00
18	4H5W 50-51	34.69	16.11	1	1:30
48	4H5W 58-59	34.77	7.09	1	1:45
21	4H5W 62-63	34.82	13.17	1	0:00
41	4H5W 69-70	34.89	10.98	1	1:00
56	4H5W 74-75	34.95	11.53	1	1:00
25	4H5W 82-83	35.03	13.17	1	1:00
2	4H5W 90-91	35.12	14.31	1	1:00
70	4H5W 95-96	35.18	13.34	1	1:00
23	4H5W 102-103	35.25	9.54	1	1:30
51	4H5W 110-111	35.34	15.08	1	0:45
30	4H5W 118-119	35.42	14	1	1:30
22	4H5W 126-127	35.51	13.1	1	2:00
31	4H5W 134-135	35.60	14.55	1	2:00
24	4H5W 142-143	35.68	15.04	1	1:45

Table 1 (continued).

4.6. AOM analysis

Sixteen samples from depths of particular interest such as troughs and peaks of cyst concentrations were chosen to establish the percentage of AOM (Table 2). The percentage was calculated based on the number of AOM particles counted within the total particles (excluding spores of *L. clavatum*) present in five separate visual fields using 400X magnification. The analysis was aimed to identify possible oxic decay. Therefore, the remaining organic particles were not classified.

ID #	Sample (core, section, interval)	Depth (amcd)	cysts/gram of sediment
11-S	4H2W 82-83	30.18	20
64	4H2W 122-123	30.62	133
26	4H3W 12-13	31.04	5368
13	4H3W 40-41	31.33	444
62	4H3W 56-57	31.50	6673
1	4H3W 64-65	31.58	1114
44	4H3W 84-85	31.79	2449
42	4H3W 128-129	32.28	700
5	4H3W 144-145	32.45	298
3	4H4W 50-51	33.07	2724
37	4H4W 93-94	33.55	426
29	4H5W 2-3	34.20	100
48	4H5W 58-59	34.77	237
41	4H5W 69-70	34.89	1033
51	4H5W 110-111	35.34	1652
24	4H5W 142-143	35.68	1037

Table 2: Samples selected for AOM analysis.

4.7. Taxonomy

The dinocyst nomenclature follows Rochon et al. (1999), Fensome and Williams (2004), and De Schepper and Head (2008). Some dinocysts were assigned as unidentified due to poor preservation. Poorly preserved reworked dinocysts were similarly identified as reworked unidentified. In addition, some specimens were identified only to genus level due either to their poor preservation or unfavourable orientation.

4.8. Dinocyst concentrations

The concentration of in situ dinocysts per gram of dried sediment was calculated using the equation proposed by Benninghoff (1962) and is described as follows:

$C = (d_c \times L_t \times t) / (L_c \times w)$

Where:

C Concentration of dinocysts / gram of dried sediment

d_c Number of counted dinocysts

L_t Number of *Lycopodium* spores / tablet

t Number of tablets added to the sample

L_c Number of counted *Lycopodium* spores

w Weight of dried sediment (g)

The weight of dried sediment corresponds to the total dry weight of the sample as specified in Table 1. This refers to the true weight of the original sample (supplied by Patrizia Ferretti) prior to the removal of the >63 µm fraction. Unidentified cysts were included for the calculation since they constitute part of the productivity signal.

4.9. Modern dinocyst dataset

A North Atlantic subset of the modern northern hemisphere dinocyst database from Radi and de Vernal (2008a) was used to produce a quantitative reconstruction of the surface water parameters at Site U1313 during MIS 16 and bounding interglacials. In total, the North Atlantic subset contains dinocyst counts from 524 surface sediment samples. Each of these samples includes information on sea-surface temperature and salinity, sea-ice cover, and primary productivity interpolated and compiled from different sources (for details see Radi and de Vernal, 2008a). Figure 7 shows the location of the surface sediment samples used in the database.

4.10. Modern Analogue Technique

Transfer functions using the Modern Analogue Technique were employed to produce a quantitative reconstruction of past water mass parameters based on dinocyst assemblages. This method assumes that both the modern dinocyst assemblages and the fossil assemblages were deposited under the same environmental conditions. In addition, there are instrumental errors relating to the measured environmental records, and the

measurements have been taken over a duration of a year or less, whereas the modern and fossil dinocyst assemblages will typically represent more than 100 years of sedimentation. Moreover, the assumption is made that there has been no transport of cysts from the surface waters to the ocean floor, whereas long-distance transport is a documented fact (Dale, 1976). This would not affect the accuracy of the reconstructions if this long-distance transport equally affected the modern and fossil assemblages. But this cannot be assumed, especially when during glacial intervals surface and bottom water currents will have been quite different from those of today. This produces an uncertainly which unfortunately cannot be measured, and affects not only dinocyst transfer functions but those based on all micropaleontological and geochemical proxies in oceanic settings. A unique potential problem with dinocysts, however, is the species-specific response to the damaging effects of oxidizing bottom waters which can cause bias in the preserved assemblages (usually against protoperidiniacean taxa). As with long-distance transport, this potentially affects the calibration set as well as the fossil assemblages used in transfer functions.

As mentioned, a North Atlantic subset of modern dinocyst distributions was chosen as the calibration set to conduct quantitative reconstructions using transfer functions. The total relative dinocyst abundances of both the North Atlantic subset and Site U1313 (this study) were converted to per thousand to avoid negative values during a subsequent logarithmic transformation when running the MAT. The underlying principle of the logarithmic transformation is that dominant taxa are usually opportunistic and ubiquitous whereas accompanying taxa have a narrower range of environmental conditions (e.g. de

Vernal et al., 2001, 2005; Verleye and Louwye, 2010). Thus, logarithmically-transformed relative abundances enhance the signal of species with lower occurrences.

The MAT was run using the software R (R Core Team, 2012) with scripts adapted from GEOTOP (http://www.geotop.uqam.ca). Reconstructions were made using the leave-one-out method for validation and calculations of the Root Mean Square Error (RMSE). The leave-one-out procedure uses 1/6th of the calibration data for verification purposes of the reconstruction.

The dinocysts *Impagidinium cantabrigiense* and *Corrudinium*? *labradori* were excluded from the MAT analysis because they are extinct. "*Pyxidinopsis striatoconulus*" was also removed due to its uncertain presence in the modern database. Samples from depths 30.18 and 30.27 amcd were also removed from the MAT to avoid statistical noise caused by their low cyst concentrations (see Results).

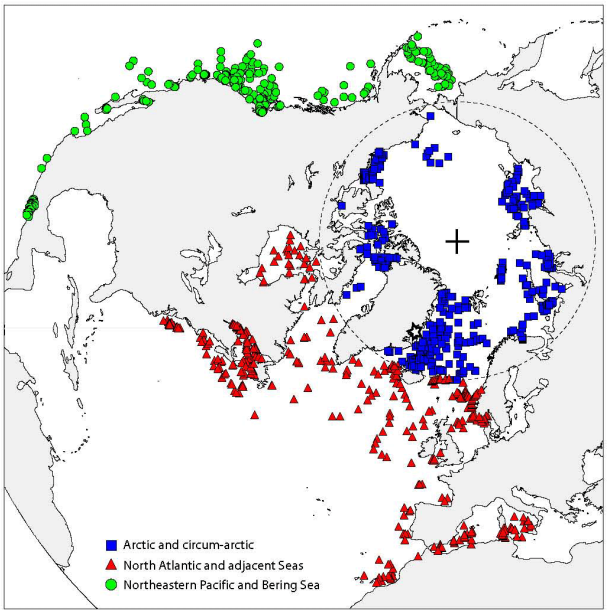

Figure 7: Northern Hemisphere database of modern dinocyst assemblages. Surface sediment samples in red represent the North Atlantic subset used for the present MAT reconstructions of Site U1313 (from Radi and de Vernal, 2008a, fig. 4a).

4.11. Multivariate analyses

Detrended correspondence analysis (DCA) was conducted using the PAST statistical package (Hammer et al., 2001). DCA constitutes in some respects a normalized form of correspondence analysis that 'spreads out' the variables to produce a cleaner plot, hence allowing easier interpretation of the parameters controlling assemblages. Relative abundances of dinocysts and the acritarch *Lavradosphaera* cf. *crista* were used in the dataset. Even though many studies do not include acritarchs in their statistical analyses (e.g. De Schepper et al., 2009a), the presence of *L.* cf. *crista* remains fairly constant in Hole U1313A. Hence, this acritarch was included in the analysis to try to investigate its ecology. The dinocysts *Achomosphaera andalousiensis* and *Spiniferites ramosus* were removed from the analysis due to their scarcity. All specimens of the genus *Brigantedinium* were placed under *Brigantedinium* spp. owing to preservational difficulties. Reworked palynomorphs were excluded from the analysis since they mainly represent iceberg discharge. Categories that could represent more than one genus (i.e. reworked unidentified and unidentified dinocysts) were also excluded. Samples from 30.18 and 30.27 amcd were also removed due to their low cyst concentrations (*see* section 5.1.). The abbreviations of species used in the DCA plot are given in Table 3.

In addition, a constrained R-mode cluster analysis was performed using the PAST statistical package. This analysis was carried out with the Unweighted pair-group average logarithm (UPGMA) and used the Morisita Index. This index was selected because it measures similarities from 0 (no similarity) to 1 (identical) and is independent of any possible effects produced by sample size (Hammer and Harper, 2006). It also produced

the clearest diagram compared to other indexes including Chord, Euclidean, Hamming, Manhattan, and Simpson that were experimented with in the present study.

The constrained cluster analysis was here used to generate a biostratigraphic zonation for Hole U1313A since it maintains the stratigraphic position of samples. Reworked palynomorphs and foraminiferal linings were included to generate a more detailed biozonation.

ABBREVIATION	SPECIES
BRIG	*Brigantedinium* spp.
BTEP	*Bitectatodinium tepikiense*
CLAB	*Corrudinium ? labradori*
DCHA	*Dalella chathamensis*
IACU	*Impagidinium aculeatum*
ICANTA	*Impagidinium cantabrigiense*
IMSPP	*Impagidinium* spp.
IPAL	*Impagidinium pallidum*
IPAR	*Impagidinium paradoxum*
IPAT	*Impagidinium patulum*
IPLIC	*Impagidinium plicatum*
ISPH	*Impagidinium sphaericum*
ISTRI	*Impagidinium strialatum*
LCRI	*Lavradrosphaera* ? cf. *crista*
NLAB	*Nematosphaeropsis labyrinthus*
OCEN	*Operculodinium centrocarpum*
OCEN SRT	*Operculodinium centrocarpum* short processes
PDAL	Cysts of *Pentapharsodinium dalei*
PRET	*Pyxidinopsis reticulata*
PSTRI	*"Pyxidinopsis striatoconulus"*
SELO	*Spiniferites elongatus*
SHYP	*Spiniferites hyperacanthus*
SMIR	*Spiniferites mirabilis*
SNEP	*Selenopemphix nephroides*
SPI/ACH	*Spiniferites/Achomosphaera* indet.
SQUA	*Selenopemphix quanta*

Table 3: Abbreviations of taxa used in the DCA plot.

5. RESULTS

5.1. Dinocyst concentrations

Dinocyst concentrations vary between 20 and 6673 cysts/g with the lowest concentrations obtained in 30.18 and 30.27 amcd, and the highest in 31.50 amcd. As depicted in Figure 8, the lowest sustained concentrations occur during interglacials. For instance, the interval between 34.77 and 33.72 amcd corresponding to the lower part of MIS 17 shows a steady low concentration. The same is obtained during the part of MIS 15 analyzed. On the other hand, the highest concentrations are obtained during MIS 16 except just before the termination where cyst concentrations drop dramatically to values lower that 1000 cysts/g. As a result, counts of fewer than 100 specimens were obtained in a few samples (Table 3). Because low counts can produce unreliable interpretations (e.g. Heiri and Lotter, 2001; Telford, 2006; De Schepper et al., 2011), samples with the lowest concentrations (30.18 and 30.27 amcd) were removed from statistical procedures except for the cluster analysis in which all samples were taken into account. Total counts for each sample are shown in Table 4.

						DINOFLAGELLATE CYSTS																				
ID #	Sample (core, section, interval)	Depth (amcd)	Calibrated age	Marine Isotope Stage	Biozones	*A. orndorffii* var. *andalousiensis*	*Brigantedinium* spp. indet.	*B. cariacoense*	*B. simplex*	*B. tepikiense*	*C.? labradori*	*Dalella chathamensis*	*I. aculeatum*	*I. cantabrigiense*	*I. pallidum*	*I. paradoxum*	*I. patulum*	*I. plicatum*	*I. sphaericum*	*I. striatum*	*Impagidinium* spp. indet.	*N. labyrinthus*	*O. centrocarpum sensu W. & D.*	*O. centrocarpum* short processes	*P. dalei*	
12	4H2W 50-51	29.83	603.30	MIS 15	Biozone 7					17	6		60	24	1	8	6		1	3		56	127	2		
39	4H2W 58-59	29.92	605.00							20	8		64	15	6	8	7		1			81	85			1
63	4H2W 66-67	30.01	606.32							12	3		51	17	4	10			1	1	7	55	90			
40	4H2W 74-75	30.09	608.42							1			2	1		1					2	1	13			
11-S	4H2W 82-83	30.18	610.33										1							1	1	1				
34	4H2W 90-91	30.27	612.33				1						2	2								3	2			
60	4H2W 98-99	30.36	614.34										8	3		2	5			1	1	26				
32	4H2W 106-107	30.45	616.19				3						7	1		1	1			5	2	31	2			
67	4H2W 114-115	30.53	618.95				5			2			8	2		1	1			2	3	55	3			
64	4H2W 122-123	30.62	622.09				3						6	4			4				6	38	4			
28	4H2W 129-130	30.70	624.88				1						47	5	2	7	38				6	109	26	1		
66	4H2W 134-135	30.75	626.62				1			18			72	1	2	4	27			3	7	90	82	2		
20	4H2W 142-143	30.84	629.75			1				5			124	2		32	19	2		1		53	54			3
33	4H2W 146-147	30.88	631.14				1			18			96	10		28	11	4	1		3	36	102	1		1
73	4H3W 4-5	30.96	633.44	MIS 16	Biozone 6		127		1	3	2		24	4	1	10	3			1	12	41	116			
26	4H3W 12-13	31.04	635.67				223		3	3			10	1		4			1		3	17	41			
52	4H3W 18-19	31.11	637.41				93			7	1		24	3		7	5		1		7	98	92	2		1
36	4H3W 24-25	31.17	638.74				70	2	2	7	2		34	7		21	3				2	119	70	1		1
57	4H3W 32-33	31.25	640.53				238	1	3	2			21	1		3				1	7	11	34			
13	4H3W 40-41	31.33	642.32				17		3	21	1		50	6	2	24	4	2		2	1	27	75	1		
35	4H3W 48-49	31.41	644.10				7			110	3		62	3	2	20	1					44	71	1		
62	4H3W 56-57	31.50	646.10				302	4	4	9	2		19		2	11	4		2		1	6	17			1
1	4H3W 64-65	31.58	647.89		Biozone 5		62	2	1	30	15		79		3	40	2	2	2	1	2	29	62			7
65	4H3W 72-73	31.66	649.68				53		1	2	3	1	43	1	2	29	5				11	28	115			2
14	4H3W 76-77	31.70	650.57				43		3		4		31	6	5	29	5		1		1	55	117	1		2
44	4H3W 84-85	31.79	652.52				2				6		55	5	2	12	8					66	182	1		
59	4H3W 92-93	31.88	654.41				33				5	1	52	4	2	20	6		1		6	71	91			
46	4H3W 100-101	31.97	656.21				43		2		2		45	5		10	7		1	1		68	154	5		
50	4H3W 108-109	32.05	657.69				20			1	2	1	75	11	3	25	2	1	1		15	64	106			1
6	4H3W 116-117	32.14	659.36				2			1	5		48	19	10	24	5	3	2		4	84	144	4		
49	4H3W 120-121	32.19	660.30		Biozone 4		4				6		50	19	8	25	3		1	2	10	78	74	2		1
42	4H3W 128-129	32.28	661.96				4			1	8		48	25	5	16	12			1	21	93	53	1		5
61	4H3W 136-137	32.36	663.45				4			3	14	2	59	21	3	27	4	1	1	6	8	63	32	1		2
5	4H3W 144-145	32.45	665.13				7				24		28	32		25	8	1		4	11	75	37	1		1
68	4H4W 2-3	32.54	666.80	MIS 17			8			1	28		45	39	9	14	18		2	1	17	74	34			7
4	4H4W 10-11	32.63	668.47				6			1	6		34	19	2	12	12					131	39	3		1
8	4H4W 18-19	32.72	670.14				9			3	18		47	29	1	14	10				3	86	62			2
45	4H4W 26-27	32.80	671.63				3			1	10		42	14	9	5	1		1		6	148	46			1
69	4H4W 34-35	32.89	673.31				1			2	12		51	25	2	6	7			1	9	142	52			
9	4H4W 42-43	32.98	674.97			1				1	4		29	7	6	9	3		1		1	112	89			1
3	4H4W 50-51	33.07	676.65								2		24	7	5		9					104	159			
54	4H4W 58-59	33.16	678.32				2			3	1		28	19	5	9	11			1	7	95	112	5		
7	4H4W 66-67	33.25	680.00				1		1		1		42	32		12	8				1	135	72	1		1
58	4H4W 71-72	33.30	680.92		Biozone 3		1			2	4		73	34	4	22	8		3		9	75	51	2		5
38	4H4W 78-79	33.38	682.41				7			1			93	45	6	9			2		3	33	78			1
53	4H4W 85-86	33.46	683.90				4			1	3		119	35		18	6		1	1	14	53	53			1
37	4H4W 93-94	33.55	685.57				11				1		62	18	1	14	7	1			11	33	105	2		2
10	4H4W 101-102	33.63	687.06				22		1	1		1	96	12	2	13	13	2	1	1	1	73	70	2		6
16	4H4W 109-110	33.72	688.73				9	1	1	3	1		49	27	4	11	7	2	2	1	2	86	85			4
55	4H4W 117-118	33.81	690.41				13				1		129	8	2	23	3		2	2	15	80	40			
27	4H4W 125-126	33.90	692.07				8		1	2			184	3	2	8	5		1	1	1	65	26			
43	4H4W 133-134	33.99	693.75				6			1			32			1			2		2	23	20			
72	4H4W 141-142	34.08	695.42				9			1			81	9		11	2	1	2	1	7	41	38	1		
29	4H5W 2-3	34.20	697.65				6						28	2		3	2			1	1	10	6			
17	4H5W 10-11	34.29	699.33				50			1	1		99	3	1	12	2			3	6	55	52			1
71	4H5W 18-19	34.38	701.00				7			3			23	2						1	1	18	10			
19	4H5W 26-27	34.46	702.48				32	1	1				109	9		16	1			3	8	48	60	1		1
47	4H5W 34-35	34.54	703.97	MIS 18			21			1			77	8		5	3		2	2	3	49	9			
15	4H5W 42-43	34.61	705.28				36			4			97	4		8	6			4	5	110	22			
18	4H5W 50-51	34.69	706.76				36			4			95	2	3	7	3	1		1	5	68	22			1
48	4H5W 58-59	34.77	708.25		Biozone 2		12			1			12	3		2			1	1	2	10	18	1		
21	4H5W 62-63	34.82	709.17				13			6			46	21	1	13	4	1			3	78	81			
41	4H5W 69-70	34.89	710.48										81	21	16	7	5	1				63	106			
56	4H5W 74-75	34.95	711.60				4			2			61	17	13	2	2		2		8	73	128	3		
25	4H5W 82-83	35.03	713.08				3			3			51	12	3	6	4		1		3	50	171			3
2	4H5W 90-91	35.12	714.75				17			1			44	10		6	2					40	159	5		1
70	4H5W 95-96	35.18	715.87				89						46	7		2	3				4	57	114	2		1
23	4H5W 102-103	35.25	717.26				57	1					56	17	4	5					1	69	86	2		
51	4H5W 110-111	35.34	719.15		Biozone 1		41						106	62	3	10	14	1	3		24	47	17	1		
30	4H5W 118-119	35.42	720.82				72	1	1	1			110	34		10	11				3	108	19			
22	4H5W 126-127	35.51	722.70				117			1			84	10		9	8	1			6	72	6	1		
31	4H5W 134-135	35.60	724.58				19						115	9		19	35			1	2	105	1			
24	4H5W 142-143	35.68	726.26				5	1	1				191	9		23	12		1	1	1	65	12			

Table 4: Raw counts of all palynomorphs in Hole U1313A enumerated in the present study. Mg/Ca-based SSTs in last column are from Naafs et al. (2011).

						DINOFLAGELLATE CYSTS										ACRITARCHS			REWORKED PALYNOMORPHS							
ID #	Sample (core, section, interval)	Depth (amcd)	Calibrated age	Marine Isotope Stage	Biozones	*P. reticulata*	*P. striatoconulus**	*S. elongatus*	*S. hyperacanthus*	*S. mirabilis*	*S. quanta*	*S. nephroides*	*S. ramosus*	Spiniferites/Achomosphaera indet.	Unidentified dinocysts	*Lavradosphaera*? sp.	*L. cf. crista*	*L. cf. crista*?	Unidentified acritarchs (RW)	*Areoligera /Glaphyrocysta* spp. (RW)	*Cerodinium*? sp. (RW)	*Circulodinium* sp. (RW)	*Cyclonephelium*? sp. (RW)	*Geonettia*? sp. (RW)	*H. pulchrum* (RW)	*Hystrichodinium*? sp. (RW)
12	4H2W 50-51	29.83	603.30			3	3	1	22	5				2	10		4		1								
39	4H2W 58-59	29.92	605.00			1	1		5	2		2		10	8	1	7	1								
63	4H2W 66-67	30.01	606.32				2	1	20	6				5	4		8									
40	4H2W 74-75	30.09	608.42							2																
11-S	4H2W 82-83	30.18	610.33																							
34	4H2W 90-91	30.27	612.33																							
60	4H2W 98-99	30.36	614.34	MIS 15	Biozone 7	1	4		2					2												
32	4H2W 106-107	30.45	616.19				2		1						2											
67	4H2W 114-115	30.53	618.95				1							2	1											
64	4H2W 122-123	30.62	622.09												2											
28	4H2W 129-130	30.70	624.88											1	1		1		3							
66	4H2W 134-135	30.75	626.62			1		1							3				7	1						
20	4H2W 142-143	30.84	629.75				3			1					6				5							
33	4H2W 146-147	30.88	631.14			2	3	1						1	3			1	4			1				1
73	4H3W 4-5	30.96	633.44								1			1	6		4		4						1	
26	4H3W 12-13	31.04	635.67								1	1			5		2		2							
52	4H3W 18-19	31.11	637.41						1						7		5									
36	4H3W 24-25	31.17	638.74		Biozone 6	2						8		1	4		6		3							
57	4H3W 32-33	31.25	640.53			1						2		2	8		3		1							
13	4H3W 40-41	31.33	642.32				1		1	1		1		4	4		9		4							
35	4H3W 48-49	31.41	644.10			2	1		2	1					6		4		1		1					
62	4H3W 56-57	31.50	646.10				1				1			3	5		1									
1	4H3W 64-65	31.58	647.89						8	1	4	1		18	3		23		3					1		
65	4H3W 72-73	31.66	649.68				1		2	1	1	1		4	7		15									
14	4H3W 76-77	31.70	650.57			1								7	5		1	1	2							
44	4H3W 84-85	31.79	652.52						2	1					3		3									
59	4H3W 92-93	31.88	654.41		Biozone 5	1			1	2	4			1	11		3		3						1	
46	4H3W 100-101	31.97	656.21			1								1	11		3		2							
50	4H3W 108-109	32.05	657.69							1				2	12		9								1	
6	4H3W 116-117	32.14	659.36				1		4	2				2	7		5		5			1				
49	4H3W 120-121	32.19	660.30			3	1	3	3						11	1	1									
42	4H3W 128-129	32.28	661.96						8	3				1	18		11		1							
61	4H3W 136-137	32.36	663.45			2		1	27	4				13	18		24		1							
5	4H3W 144-145	32.45	665.13				1	2	24	4				10	10		10								2	
68	4H4W 2-3	32.54	666.80			1	2		9	3				1	7	1	10								1	
4	4H4W 10-11	32.63	668.47			1	1		14	2				9	11		7		7	1		1	1			2
8	4H4W 18-19	32.72	670.14			2	1	2	11	4				11	7		12	1	9						4	
45	4H4W 26-27	32.80	671.63				1		9	2				3	9	1	2								1	1
69	4H4W 34-35	32.89	673.31			2	2		9	2				2	7		4	1								
9	4H4W 42-43	32.98	674.97			1	1	1	15	1		2		29	6		7		4				1			
3	4H4W 50-51	33.07	676.65					2	3					2	6		2		2							
54	4H4W 58-59	33.16	678.32			1		1	8	4				4	2		2		1							
7	4H4W 66-67	33.25	680.00					2	12	8		1		10	6				5							
58	4H4W 71-72	33.30	680.92			1			5	2				6	10											
38	4H4W 78-79	33.38	682.41			1		2				1		12	15		1									
53	4H4W 85-86	33.46	683.90						4	1				5	5		6									
37	4H4W 93-94	33.55	685.57					1	3				2	7	22		5									
10	4H4W 101-102	33.63	687.06			2								6	12		4									
16	4H4W 109-110	33.72	688.73			1	3		2	3			1	6	14		3									
55	4H4W 117-118	33.81	690.41				2		1	1				8	5		4									
27	4H4W 125-126	33.90	692.07			1	2		5	1				4	11		1									
43	4H4W 133-134	33.99	693.75			2	1		5	1				1	1											
72	4H4W 141-142	34.08	695.42			2			4	1				7	4											
29	4H5W 2-3	34.20	697.65						2	1					3		1									
17	4H5W 10-11	34.29	699.33			1	1		1	1				3	1		1									
71	4H5W 18-19	34.38	701.00				1							1	1											
19	4H5W 26-27	34.46	702.48				4		1	1	1			11	10		7									
47	4H5W 34-35	34.54	703.97					1	5					1	5											
15	4H5W 42-43	34.61	705.28				1		1	1		1		5	4		1									
18	4H5W 50-51	34.69	706.76				1		7	2				4	3											
48	4H5W 58-59	34.77	708.25					1	5						1											
21	4H5W 62-63	34.82	709.17				1		18	7				15	13		1									
41	4H5W 69-70	34.89	710.48					1	1	1			1	10	12		2		1							
56	4H5W 74-75	34.95	711.60					1	10	3		1		9	4		1			1						
25	4H5W 82-83	35.03	713.08			2	1	1	3	2				2	15		1		1							
2	4H5W 90-91	35.12	714.75					3	1	2		2		6	3		3		4							
70	4H5W 95-96	35.18	715.87						4	1		1		1	8		1									
23	4H5W 102-103	35.25	717.26					2	1			1		2	13		6		3							
51	4H5W 110-111	35.34	719.15				1	3	2	3	1			1	15		2									
30	4H5W 118-119	35.42	720.82			1			2			1		8	37		1		4							
22	4H5W 126-127	35.51	722.70			1				2				5	15		2		1							
31	4H5W 134-135	35.60	724.58			1	1		3					3	23		4									
24	4H5W 142-143	35.68	726.26			2		1	15	4				10	3		3									

Table 4 (continued)

						REWORKED PALYNOMORPHS															
ID #	Sample (core, section, interval)	Depth (amcd)	Calibrated age	Marine Isotope Stage	Biozones	*O. centrocarpum sensu lato* (RW)	*O. complex* (RW)	*O. costata* (RW)	*O. operculata* (RW)	*P. infusoricides* (RW)	*Spiniditinium* sp. (RW)	*Spiniferites* spp. (RW)	*Subtilisphaera?* sp. (RW)	Unidentified dinocysts (RW)	*Verrhyachium* sp. (RW)	Foraminiferal lining	Total dinocysts counted	*L. claviatum* spores	Cyst concentration/gram of sediment	Mg/Ca-based SSTs (°C)
12	4H2W 50-51	29.83	603.30											4			357	875	624	
39	4H2W 58-59	29.92	605.00	MIS 15	Biozone 7	2								9			325	1101	382	
63	4H2W 66-67	30.01	606.32											3		1	289	1639	238	
40	4H2W 74-75	30.09	608.42														23	502	61	
11-S	4H2W 82-83	30.18	610.33														4	259	20	
34	4H2W 90-91	30.27	612.33														10	359	37	
60	4H2W 98-99	30.36	614.34														55	1625	44	
32	4H2W 106-107	30.45	616.19				1					1		2			58	1285	60	
67	4H2W 114-115	30.53	618.95										1	2	1		86	1512	73	
64	4H2W 122-123	30.62	622.09											3	1		67	900	133	
28	4H2W 129-130	30.70	624.88	MIS 16							1			5	2		244	957	403	
66	4H2W 134-135	30.75	626.62			3					2		1	9	2		314	676	589	14.99
20	4H2W 142-143	30.84	629.75				1				10	1	4	17	2		306	1156	430	6.88
33	4H2W 146-147	30.88	631.14			1	5	1			9			5	4		322	952	890	
73	4H3W 4-5	30.96	633.44		Biozone 6		1				1			7		12	353	204	3055	
26	4H3W 12-13	31.04	635.67			1					1			6		20	313	99	5368	
52	4H3W 18-19	31.11	637.41								1			1		8	349	300	1755	
36	4H3W 24-25	31.17	638.74			1	2				2			14		27	356	322	1678	9.69
57	4H3W 32-33	31.25	640.53											7	1	9	335	189	2745	10.13
13	4H3W 40-41	31.33	642.32			5	4	2			2	1	3	12	6	9	248	802	444	10.3
35	4H3W 48-49	31.41	644.10			5	1				1			5		2	336	235	2343	9.57
62	4H3W 56-57	31.50	646.10											1		9	394	97	6673	8.48
1	4H3W 64-65	31.58	647.89		Biozone 5	1			1	1	1			7	1	19	374	586	1114	8.15
65	4H3W 72-73	31.66	649.68								1		1	2		12	313	551	1400	9.43
14	4H3W 76-77	31.70	650.57								1	3		5			316	260	1691	
44	4H3W 84-85	31.79	652.52			1						1		4	1		345	234	2449	
59	4H3W 92-93	31.88	654.41											4		12	312	180	2611	
46	4H3W 100-101	31.97	656.21			1					1	1	1	7	1	11	356	204	2580	
50	4H3W 108-109	32.05	657.69								1			2		4	343	434	1073	
6	4H3W 116-117	32.14	659.36				4				3			2	1		371	845	581	
49	4H3W 120-121	32.19	660.30		Biozone 4							5		5			304	662	979	11.93
42	4H3W 128-129	32.28	661.96							1	3		1	5			323	642	700	11.8
61	4H3W 136-137	32.36	663.45			1					1			8			316	785	521	12.36
5	4H3W 144-145	32.45	665.13				2	1		1	6	3	3	23	1	1	305	1784	298	11.86
68	4H4W 2-3	32.54	666.80				2			1	1	2		2	1		320	1042	485	11.35
4	4H4W 10-11	32.63	668.47			4	1				3	1		16	2		304	815	619	11.84
8	4H4W 18-19	32.72	670.14			2	6				6	3	3	26	1		322	1410	434	10.2
45	4H4W 26-27	32.80	671.63				1					2	3	6			311	464	1304	10.69
69	4H4W 34-35	32.89	673.31									2		1			334	279	1920	12.65
9	4H4W 42-43	32.98	674.97								1	1		4			320	248	2110	12.34
3	4H4W 50-51	33.07	676.65														323	193	2724	10.94
54	4H4W 58-59	33.16	678.32														318	279	1609	11.89
7	4H4W 66-67	33.25	680.00				1							7		1	346	429	1077	11.88
58	4H4W 71-72	33.30	680.92		Biozone 3							2					317	720	819	12.38
38	4H4W 78-79	33.38	682.41	MIS 17										2			309	585	763	
53	4H4W 85-86	33.46	683.90											2			324	592	701	
37	4H4W 93-94	33.55	685.57											2			303	1063	426	
10	4H4W 101-102	33.63	687.06											2			337	724	697	
16	4H4W 109-110	33.72	688.73											6			325	1167	349	
55	4H4W 117-118	33.81	690.41											2			335	979	427	
27	4H4W 125-126	33.90	692.07											2			331	985	320	
43	4H4W 133-134	33.99	693.75														98	801	156	
72	4H4W 141-142	34.08	695.42											3			222	1779	183	
29	4H5W 2-3	34.20	697.65											1			65	828	100	16.05
17	4H5W 10-11	34.29	699.33											3	1		294	3944	100	15.2
71	4H5W 18-19	34.38	701.00														68	778	108	15.78
19	4H5W 26-27	34.46	702.48											2			318	2464	184	15.81
47	4H5W 34-35	34.54	703.97	MIS 18		2											192	1465	155	16.35
15	4H5W 42-43	34.61	705.28											1		1	309	1874	208	
18	4H5W 50-51	34.69	706.76			2						2		2			265	2002	171	
48	4H5W 58-59	34.77	708.25		Biozone 2									1	1		70	867	237	
21	4H5W 62-63	34.82	709.17			1						1		3	1		321	1350	376	
41	4H5W 69-70	34.89	710.48											9		1	326	599	1033	
56	4H5W 74-75	34.95	711.60									2		1			343	569	1090	
25	4H5W 82-83	35.03	713.08								1			8			336	224	2374	
2	4H5W 90-91	35.12	714.75											2		8	302	173	2543	
70	4H5W 95-96	35.18	715.87													6	340	146	3639	
23	4H5W 102-103	35.25	717.26											6	1	32	317	186	3724	
51	4H5W 110-111	35.34	719.15		Biozone 1									1		31	355	297	1652	
30	4H5W 118-119	35.42	720.82											3		56	419	280	2228	
22	4H5W 126-127	35.51	722.70											2		14	338	181	2972	
31	4H5W 134-135	35.60	724.58											1		53	337	236	2046	
24	4H5W 142-143	35.68	726.26											4		14	357	477	1037	

Table 4 (continued)

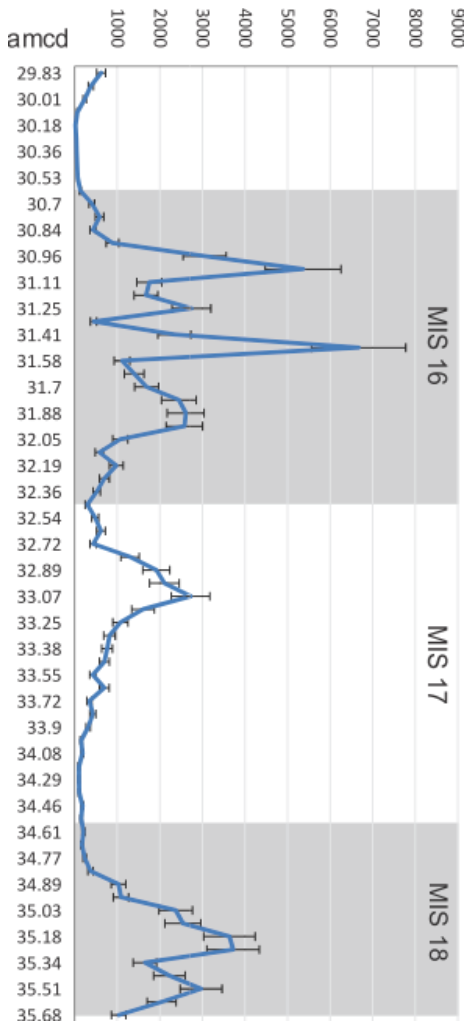

Figure 8: In-situ dinocyst concentrations per gram of total dried sediment. Horizontal lines correspond to error bars calculated from standard deviation of tablets of *Lycopodium clavatum*. Grey bars indicate glacial stages.

5.2. The dinocyst assemblages at IODP Site U1313

Excluding reworked dinocysts and acritarchs, 13 genera and 29 species were recorded in 73 samples (Table 4). In general, the assemblages are dominated by the cosmopolitan

species *Operculodinium centrocarpum* sensu Wall and Dale (1966) (hereafter *O. centrocarpum*) together with the open marine species *Impagidinium aculeatum* and *Nematosphaeropsis labyrinthus.* Other accompanying species include *Impagidinium paradoxum, Impagidinium patulum, Brigantedinium* spp., and dinocysts linked to polar to sub-polar waters including *Bitectadodinium tepikiense, Impagidinium pallidum, Spiniferites elongatus* and cysts of *Pentapharsodinium dalei* (e.g. Rochon et al., 1999; de Vernal et al., 2001, 2005; Marret and Zonneveld, 2003; Bonnet et al., 2012; Zonneveld et al., 2013). The stratigraphic distributions of the main taxa are shown in Figure 9.

5.3. Colder species

Four colder-related species were registered in Hole U1313A. The most abundant is *B. tepikiense,* which occurs continuously but generally in low numbers throughout the entire studied interval, with a peak abundance (33%) during mid-MIS 16 at 31.41 amcd (Fig. 9). This species has been reported frequently in subarctic regions and in the northern North Atlantic. Its modern distribution is associated with the subpolar to temperate boundary (e.g. Dale, 1996; Rochon et al., 1999; de Vernal et al., 2005; Zonneveld et al., 2013). *B. tepikiense* has also been considered characteristic of waters with reduced surfaces salinities due to ice melting (e.g. Dale, 1985; Bakken and Dale, 1986) and stratified waters in regions with large seasonal temperature amplitudes (e.g. Rochon et al., 1999; Van Nieuwenhove and Bauch, 2008a).

Impagidinium pallidum is generally continuous although its relative abundances are low (0–5%). The highest percentage (5%) is recorded in the upper part of MIS 18 at 34.89

amcd (Fig. 9). A slightly increasing trend is observed from mid-MIS 17 towards the boundary between MIS 17 and MIS 16. Afterwards, its concentration gradually decreases during MIS 16. *I. pallidum* is common in polar and subpolar basins (Rochon et al., 1999) with its maximum abundance (39%) registered in the central Greenland Sea (Matthiessen, 1995). The use of this species as a strictly cold-water indicator has, however, been questioned by De Schepper et al. (2011) who recorded abundances in the Plio–Pleistocene of the North Atlantic exceeding 10% where reconstructed SSTs were around 12–14°C. Moreover, its bipolar distribution must have required this species to cross the equator at some time. They also pointed out that its rare occurrence during the last glacial maximum (LGM) in North Atlantic sites in de Vernal et al. (2005) reveals inconsistencies about its value as a truly low-temperature indicator.

Spiniferites elongatus is also typically used as a cold-water indicator. Its maximum occurrence today (up to 49%) is observed in the Barents Sea and Baffin Bay where it has been grouped with the similar morphotypes *Spiniferites frigidus* and *Rottnestia amphicavata* (Rochon et al., 1999). In Hole U1313A, this species is found consistently during MIS 18 (35.68–34.54 amcd) and from mid-MIS 17 to lowest MIS 16 (33.55–32.19 amcd), with two other minor events registered in the upper MIS 16 and lower MIS 15 (Fig. 9). The relative abundances of *S. elongatus* are low, varying from 0 to 1.4% of the total counts, with the highest peak in the upper MIS 18 (34.77 amcd).

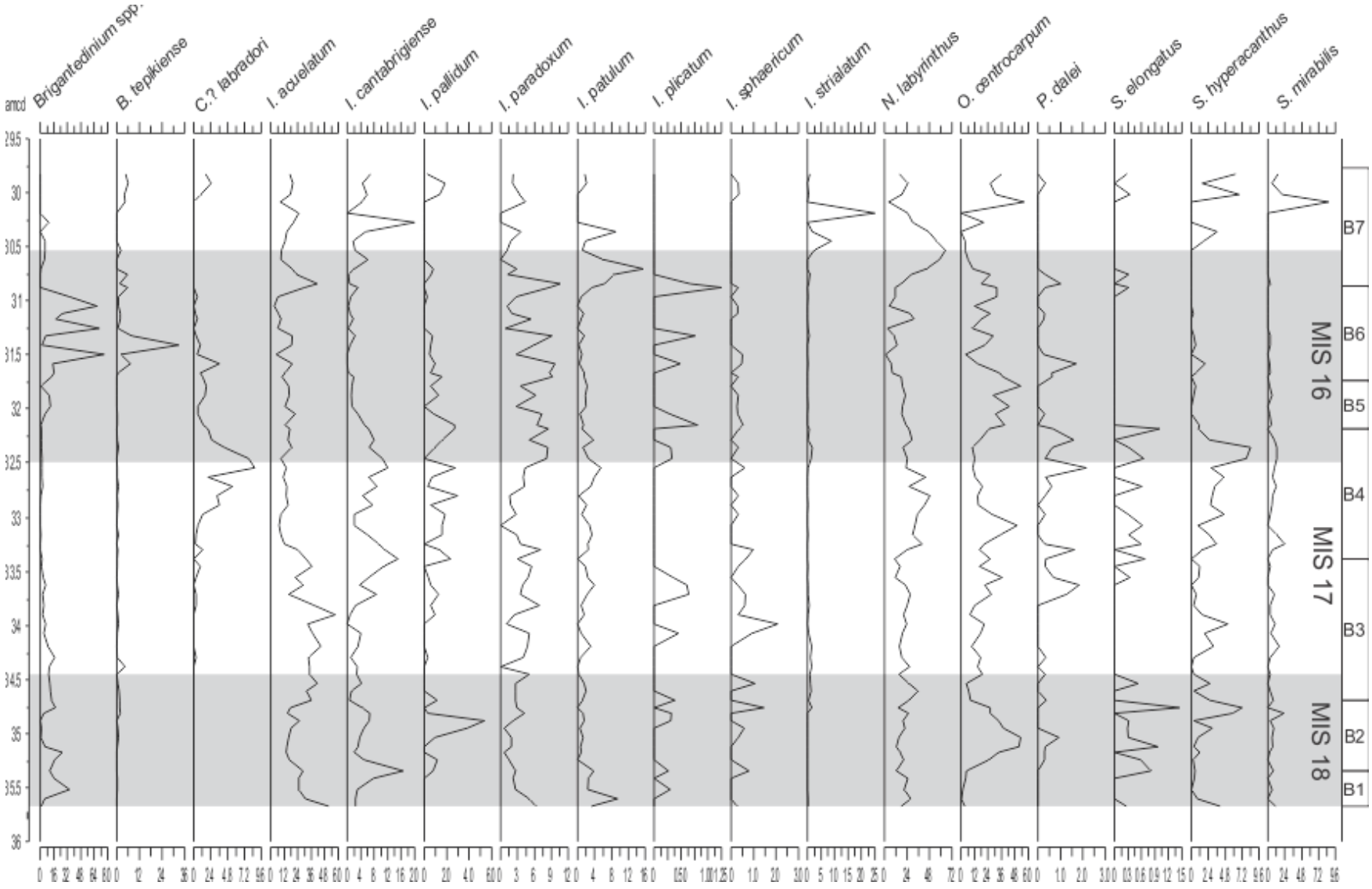

Figure 9: Stratigraphic distribution of the main taxa in Hole U1313A. Grey bars indicate glacial stages.

The fourth species corresponds to cysts of *Pentapharsodinium dalei*. Although *P. dalei* has a relatively wide temperature distribution, it is dominant today in such areas as the north of Iceland, southern Hudson Bay, eastern Barents Sea, and Norwegian fjords (Dale, 1976; Rochon et al., 1999). According to Rochon et al. (1999), this species requires a minimum summer temperature of 4ºC and has preference for locations with large seasonal temperature gradients. In Hole U1313A, *P. dalei* has low abundances (0–2.16%) and poor preservation, occurring more or less consistently through the analyzed interval, with highest peaks in mid-MIS 17, the transition between MIS 17 and MIS 16, and in mid-MIS 16 (Fig. 9). The small central body diameter (16 to 18 µm) and processes with a fibroreticulate base were consistent features of all studied specimens. However, the distinctive process bifurcation in some cysts was not discernible probably as a result of poor preservation. These specimens were classified as *P. dalei* based entirely on the two first characteristics. The poor preservation could indicate significant transportation or reworking, although these specimens have almost the same colouring as their well-preserved counterparts. However, this uncertainty does not significantly affect interpretations because of the low percentages reported.

The relative abundances of the four species mentioned above were combined to identify any trends within the colder-related dinocysts. As seen in Figure 10, the curve of colder species is mainly controlled by the percentage of *B. tepikiense*: its highest relative abundance during mid-MIS 16 coincides with the peak percentage of cold species. The other species exert no significant influence due to their low relative abundances**.**

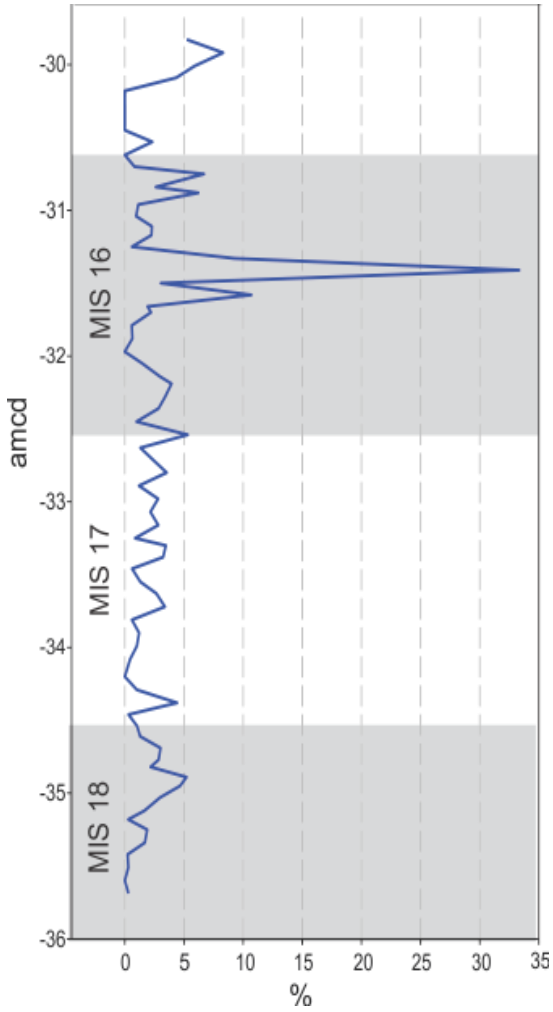

Figure 10: Relative abundance of total cold-related dinocyst species in Hole U1313A. Grey bars indicate glacial stages.

5.4. Heterotrophic dinocysts

Brigantedinium cariacoense, *Brigantedinium simplex*, unidentified *Brigantedinium* species, *Selenopemphix nephroides*, and *Selenopemphix quanta* comprise the

heterotrophic dinocysts. Most *Brigantedinium* specimens could not be identified to species level owing to crumpling or poor orientation and were therefore grouped as *Brigantedinium* spp., although both *Brigantedinium cariacoense* and *B. simplex* were observed.

Brigantedinium is the dominant heterotrophic genus, with relative abundances reaching 80% at 31.50 amcd. The total heterotrophic vs. total autotrophic index shows a substantial increase during the cold stages MIS 16 and MIS 18, with this index dropping significantly during the interglacials (Fig. 11). The distribution of this genus is generally associated with high nutrient/food availability (e.g. Rochon et al., 1999; de Vernal et al., 2005; Susek et al., 2005; Radi et al., 2007; Pospelova et al., 2008; Radi and de Vernal, 2008a, b; Bonnet et al., 2012). Hence, this genus is usually found in upwelling zones as well as areas adjacent to polar fronts where diatoms (i.e. a principal food source) proliferate (e.g. Pospelova et al 2010; Zonneveld et al., 2010; Price and Pospelova, 2011).

5.5. Extinct dinocysts

Only two extinct dinocyst species were recorded in the studied section: *Impagidinium cantabrigiense* and *Corrudinium*? *labradori*.

The relative abundance of *I. cantabrigiense* fluctuates from 0 to 20% with highest peaks registered at the base of MIS 15 (30.27 amcd), middle and upper MIS 17 (33.38 and 32.54 amcd respectively), and MIS 18 (35.34 amcd). The lowest abundances are found during the mid- to upper MIS 16 (31.97–30.45 amcd).

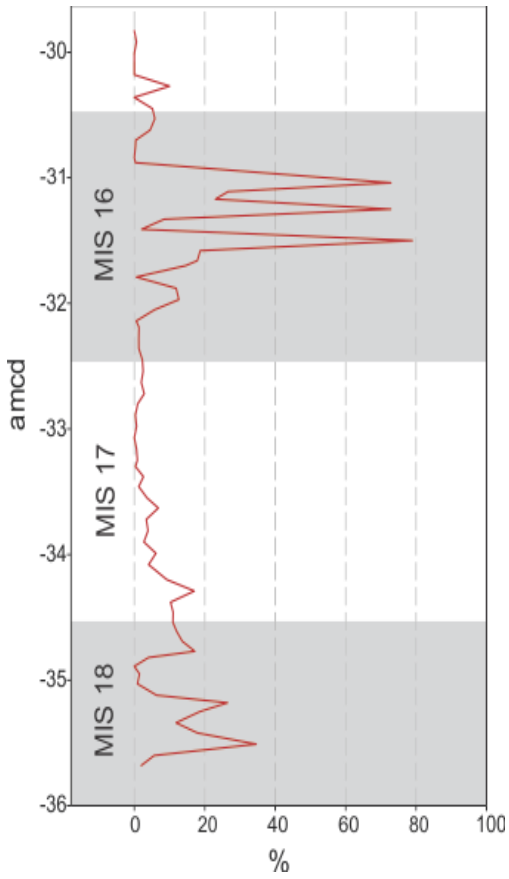

Figure 11: Percentage of heterotrophic dinocyst species in Hole U1313A. Grey bars indicate glacial stages.

The lowest occurrence of *C.*? *labradori* in Hole U1313A is recorded in lower MIS 17 (34.29 acmd) and it ranges to the top of the investigated interval at ca. 603 ka in MIS 15. Its highest relative abundance (8.9%) at a depth of 32.54 amcd corresponds to the transition between MIS 17 and MIS 16.

5.6. Pleistocene acritarchs

Late Cenozoic marine acritarchs are increasingly attracting the attention of palynologists owing to their biostratigraphic value in the northern North Atlantic and adjacent seas (e.g. de Vernal and Mudie, 1989; Head et al., 1989a, b; Head, 2003; Head and Norris, 2003; De Schepper and Head, 2008, in press). *Lavradosphaera* constitutes the only in-situ acritarch genus identified at IODP Site U1313, with only a single species recorded. This species has been provisionally categorized as *L.* cf. *crista* pending a more thorough taxonomic analysis. The occurrence of this acritarch remains fairly constant throughout the analyzed interval. Its highest abundance is registered in the lower part of MIS 16. A few specimens were categorized as *Lavradosphaera*? sp. and *L.* cf. *crista*? due to poor preservation (*see* Table 4).

5.7. Reworked palynomorphs

IODP Site U1313 lies within the southern boundary of the IRD belt. Consequently, material derived from massive iceberg discharges can be found interlayered within the sediments of this site. These IRD layers often contain reworked palynomorphs that can yield the age and provenance of this debris, thereby allowing the source of the icebergs to be determined (e.g. Bischof et al., 1997).

Numerous reworked palynomorphs were identified in Hole U1313A. The reworked assemblages are dominated by the dinocysts *Spinidinium* sp., *Oligosphaeridium complex*, *Hystrichodinium pulchrum*, *Palaeohystrichophora infusorioides*, *Subtilisphaera* sp. and

species of the acritarch genus *Veryhachium*. Also, considerable numbers of reworked palynomorphs were recorded as unidentified reworked cysts due to their poor preservation. The stratigraphic distribution of reworked palynomorphs is shown in Figure 12.

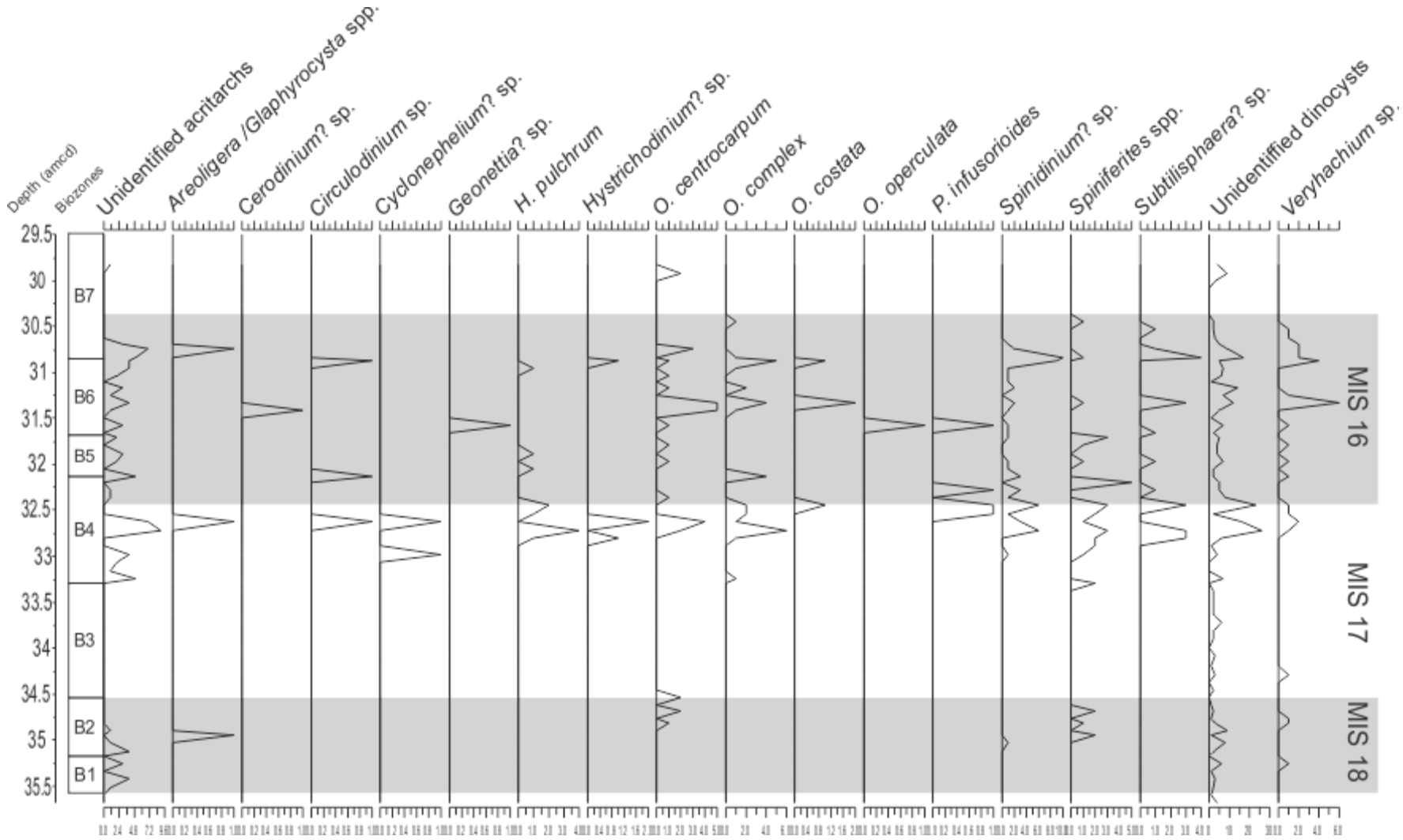

Figure 12: Distributions of the main reworked palynomorph taxa in Hole U1313A. Grey bars indicate glacial stages.

5.8. AOM analysis

The quantification of the AOM present in 16 selected samples showed contents varying from 30 to 100% (Table 5). Ultrasound treatment during sample processing had been performed on some samples to reduce amorphous agglomerate that could hinder the dinocyst analysis, and the percentages of AOM in these samples hence may be under-represented. The influence of ice-rafted material can also produce a misrepresentation of the original palynofacies signal during glacial stages. The duration of ultrasound treatment for each sample is shown in Table 1 and Table 5.

ID #	Sample (core, section, interval)	Depth (amcd)	cysts/gram of sediment	% of AOM	Ultrasound treatment (mins, sec)	Relative abundance of *Brigantedinium* spp.
11-S	4H2W 82-83	30.18	20	99	1:30	0
64	4H2W 122-123	30.62	133	80	1:30	4.5
26	4H3W 12-13	31.04	5368	90	1:15	72
13	4H3W 40-41	31.33	444	45	1:30	8.1
62	4H3W 56-57	31.50	6673	30	0:00	79
1	4H3W 64-65	31.58	1114	40	2:00	17.8
44	4H3W 84-85	31.79	2449	95	1:10	0.6
42	4H3W 128-129	32.28	700	99	1:45	1.2
5	4H3W 144-145	32.45	298	62	0:00	2.3
3	4H4W 50-51	33.07	2724	80	1:00	0
37	4H4W 93-94	33.55	426	99	1:30	3.6
29	4H5W 2-3	34.20	100	99	1:45	9.2
48	4H5W 58-59	34.77	237	100	1:45	17
41	4H5W 69-70	34.89	1033	96	1:00	0
51	4H5W 110-111	35.34	1652	30	0:45	12
24	4H5W 142-143	35.68	1037	35	1:45	2

Table 5: Percentage of AOM in selected samples.

In general, the results show that samples with low cyst concentrations are dominated by high percentages of AOM. For example, the lowest concentrations are found at 30.18 amcd. The palynofacies at this depth is almost entirely composed of AOM. The same abundance of amorphous material occurs at 34.20 amcd in which only 100 cysts per gram of sediment are registered. Samples with high cyst concentrations also show high amounts of AOM. Such is the case with samples at 31.04 amcd (5368 cysts/gram), 31.79 amcd (2449 cysts/gram), and 33.07 amcd (2724 cysts/gram). On the other hand, the lowest percentages of AOM are registered at depths with fairly high cyst concentrations, for instance at 31.50 amcd in which the highest cyst concentrations are recorded but only 30% of the palynofacial material corresponds to AOM. Additionally, some small opaque particles present within the AOM show a cubic symmetry consistent with the mineral pyrite (Fig 13.g). This iron sulfide, sensitive to oxidation, is usually common in sediments deposited in anoxic conditions (Wilkin et al., 1997). Figure 13 shows photographs of AOM in various samples.

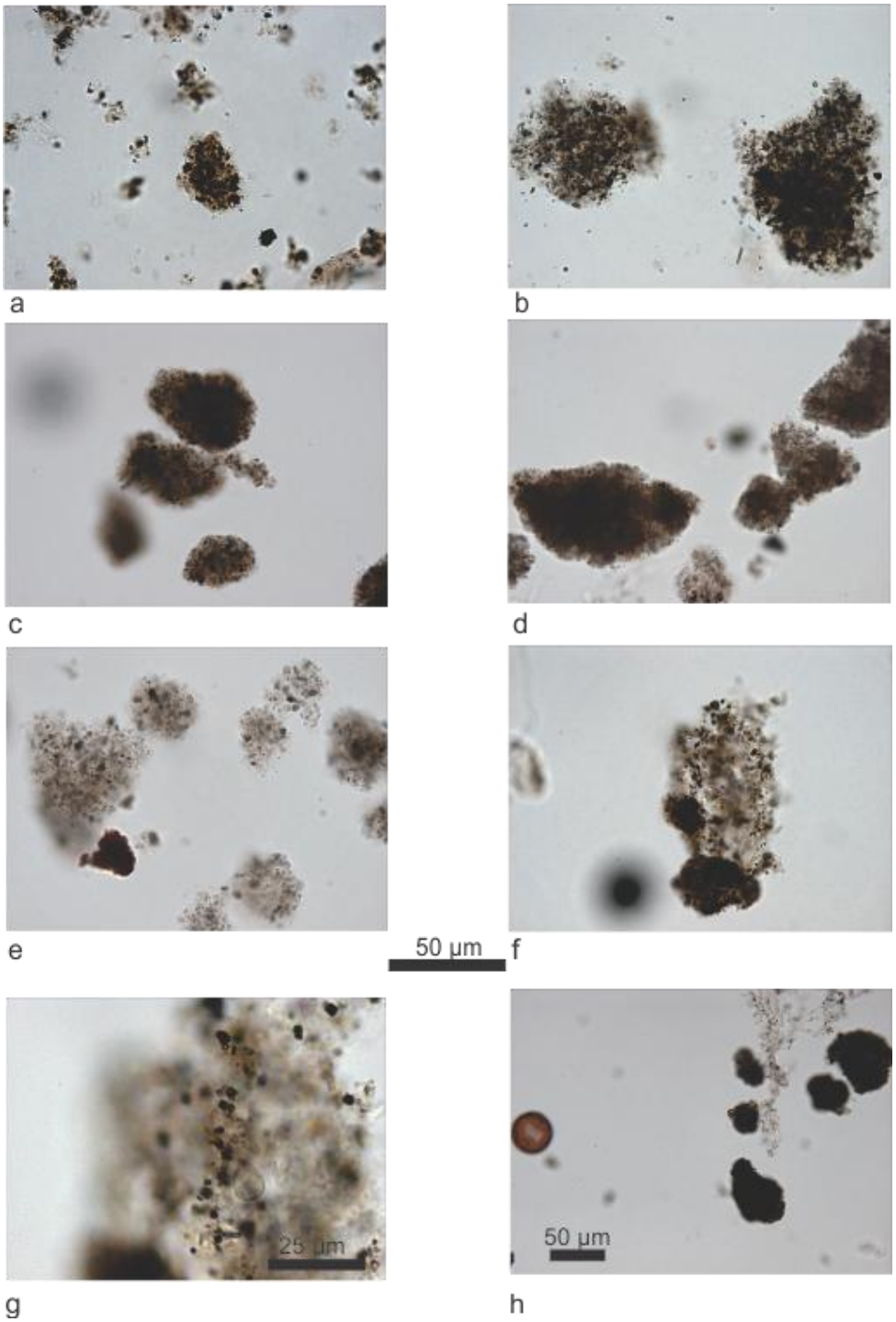

Figure 13: Visual fields with AOM from 30.18 amcd (a), 30.62 amcd (b), 32.28 amcd (c), 33.55 amcd (d), 34.20 amcd (e), 33.07 amcd (f, g) and 34.77 amcd (h). See well-preserved cyst of *Brigantedinium* on the left side of field (h). Horizontal bar shows the scale for the photographs except bottom ones in which a different scale was used.

5.9. Modern Analogue Technique

Before running transfer functions using the MAT, samples 30.18 and 30.27 amcd were removed from the input data to avoid misleading returns (see Methods section). In addition, counts of the extinct *I. cantabrigiense* and *C.*? *labradori* were excluded because they are not in the modern calibration set. "*Pyxidinopsis striatoconulus*" was also removed (see Methods section). Recalculations of the total dinocysts were made after their removal.

The SSTs and SSSs reconstructions yielded values between 9 and 15ºC (±1.3ºC) and 33 and 35 psu (±1.2) respectively. As shown in Figure 14, the obtained coefficients of correlation (r^2) for each parameter show significant accuracy between the predicted and reconstructed data. The best reconstruction corresponds to the winter SSTs (Fig. 14.c) with r^2 higher than 0.95 and a root mean square error (RMSE) of 1.09ºC. These results, however, must be interpreted carefully (see Discussion). The obtained values were subsequently converted to mean annual SSTs and mean annual SSSs (Fig. 14) to display reconstructions more conveniently.

The MAT-based SSTs reconstructions illustrated in Figure 14a show three major cooling peaks: two in the middle of MIS 16 (31.04 and 31.25 amcd) of 9ºC and one within MIS 18 (35.25 amcd) of 10ºC. Apart from these peaks, MAT-based SSTs do not show obvious trends such as warming during MIS 17. This is might be explained by low cyst concentrations in MIS 17 (Figure 7).

MAT-based SSSs show mostly random fluctuations between 32.5 and 35.5 during MIS 18 and MIS 17 (Fig. 15b). The only weak trend is found during MIS 16 where SSSs

reach higher values (34–35 psu) until mid-MIS 16 followed by a slight drop towards the termination (33 psu).

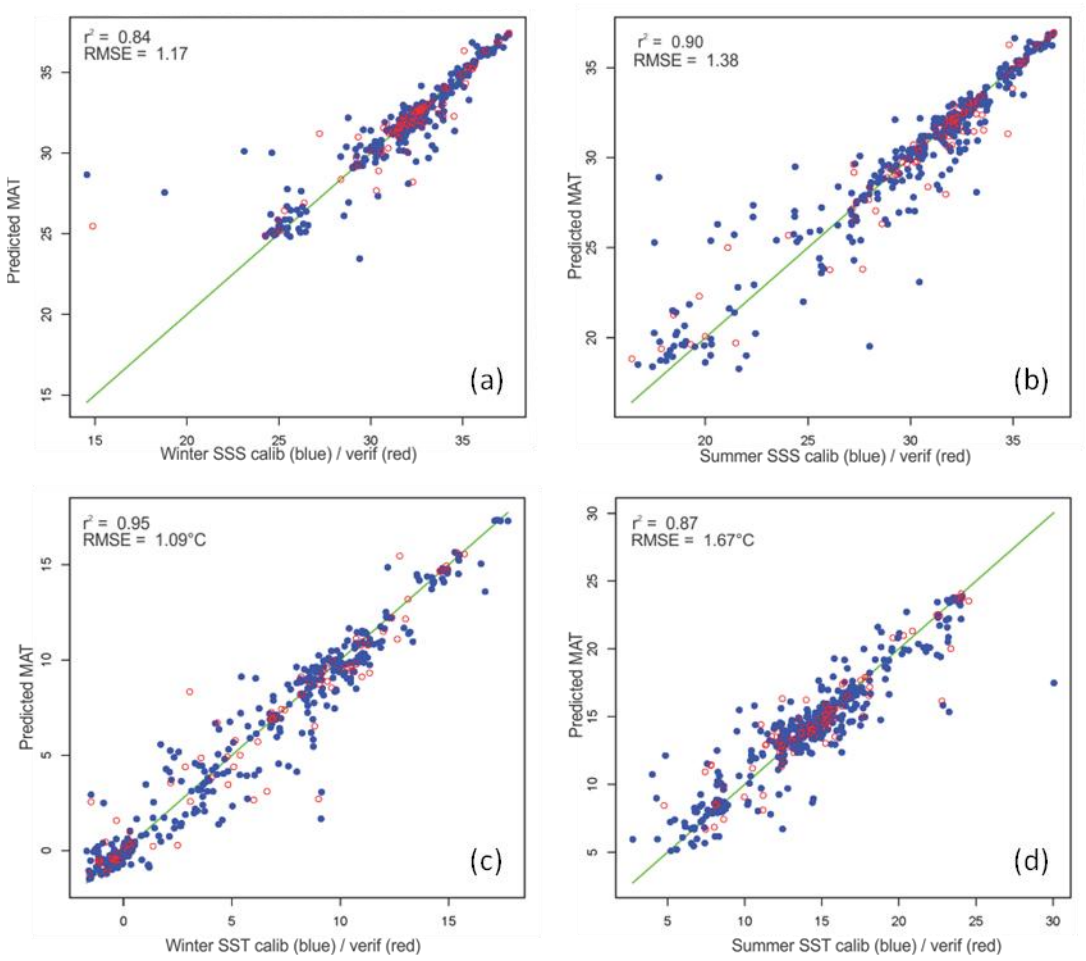

Figure 14: Results of validation tests for winter and summer SSSs (a, b) and SSTs (c, d) carried out with MAT in Hole U1313A. Calibration datasets are plotted as blue dots. Validation datasets plotted as red circles.

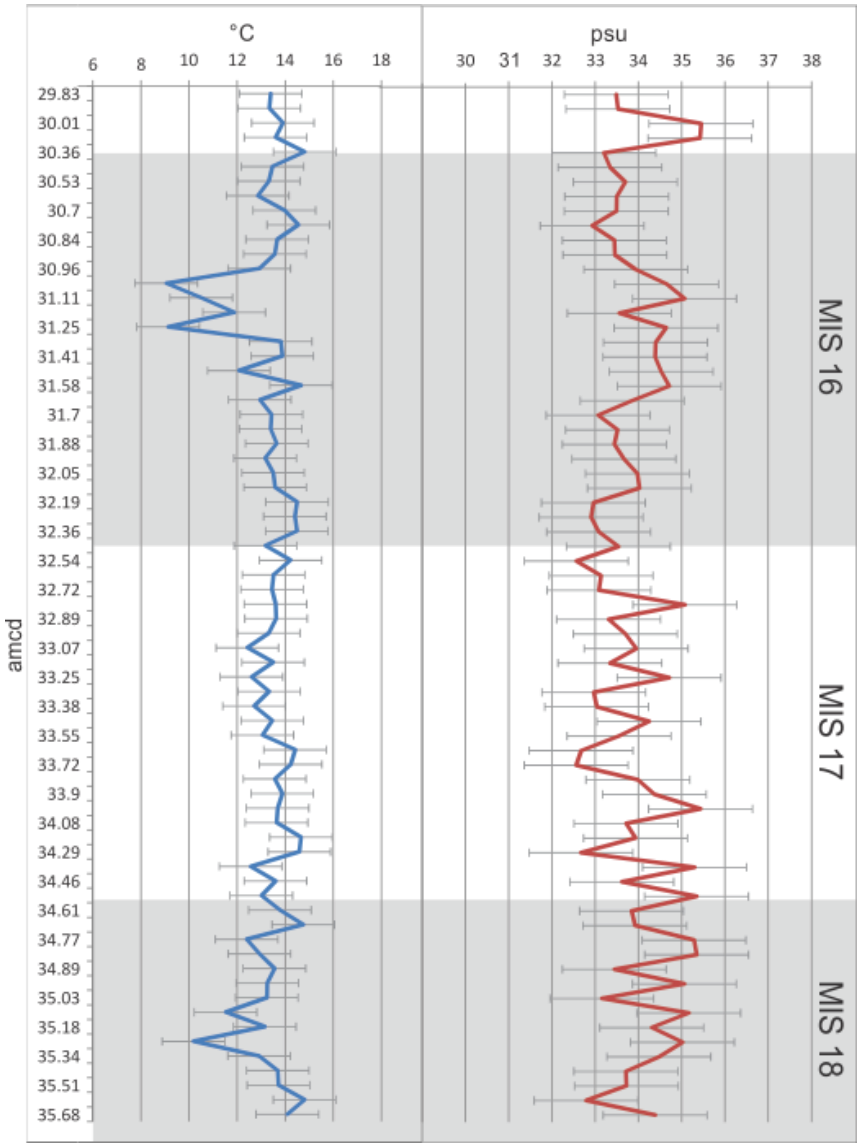

Figure 15: MAT-based sea-surface temperatures in °C (blue) and sea-surface salinities in psu (red) based on dinocysts in Hole U1313A. Horizontal lines correspond to error bars based on average Root Mean Square Errors.

5.10. Statistical analysis

5.10.1. Detrended correspondence analysis

The DCA plot in Figure 16 shows that the dispersion of taxa along the Axis 1 appears to be influenced in part by temperature, with higher values indicating cooler temperatures. Highest values on Axis 1 are represented by *B. tepikiense.* This species is usually associated with sub-polar to temperate regions, and has highest abundances in the North Sea and off eastern Canada near the subtropical front (Zonneveld et al., 2013). The cool water species *S. elongatus, I. pallidum* and cysts of *P. dalei*, also show positive values, although not as prominent as *B. tepikiense.* Negative values of Axis 1 are represented by *I. strialatum*. According to Zonneveld et al. (2013), this oceanic species is characteristic of temperate to equatorial regions.

Axis 2 appears to be influenced by nutrient availability. The protoperidinioids *Brigantedinium* spp., *Selenopemphix nephroides* and *Selenopemphix quanta*, generally restricted to settings with elevated nutrients, are located towards the far right of the diagram at the highest values of Axis 2. The left side, on the other hand, shows "*P. striatoconulus"* as the species with the lowest values. This species therefore seems to reflect oligotrophic conditions, although its modern distribution and (paleo-)ecological preferences are uncertain. *Spiniferites mirabilis* and *S. hyperacanthus* also have low values on the Axis 2. These species are usually plotted together due to their similar morphology (e.g. Marret and Zonneveld, 2003; Bonnet et al., 2012; Zonneveld et al., 2013) and are considered to represent warm water, with particular distributions in areas where subtropical fronts are formed (Zonneveld et al., 2013). Hence, although *S.*

mirabilis and *S. hyperacanthus* can be found in oligotrophic to eutrophic conditions, their response in the DCA is here interpreted as an indicator of water from the subtropical gyre (i.e. warm and oligotrophic).

Impagidinium aculeatum, *I. paradoxum*, and *I. patulum* have rather similar distributions today, namely oceanic and temperate to equatorial (Zonneveld et al., 2013), yet they are quite widely separated in the DCA plot. In Hole U1313A, *I. aculeatum* is the dominant species of these three, reaching its highest relative abundances of 56% during MIS 17 whereas the highest abundances of *I. paradoxum* and *I. patulum* are 11 and 16% respectively (*see* Table 4 and Fig. 8). Even though DCA "stretches out" the data to reduce the arch effect in unimodal distributions, the wide difference in relative abundances could have left some "vestiges" of this effect and produced a scattering of the species in the plot.

In general, the driving parameters controlling the dispersion in the DCA seem to be reflecting shifts in water properties at Site U1313 from warm and oligotrophic waters of the subtropical gyre to more cold and eutrophic waters of the subpolar gyre. This concurs with the close proximity of this site to the boundary between these gyres.

5.10.2. Cluster analysis

A constrained cluster analysis was produced to subdivide the palynological record into assemblage biozones, based on distinctive palynological associations, both for descriptive and biostratigraphic purposes. As a result, seven assemblage biozones, numbered in

ascending order, are proposed based on the obtained dendrogram (Figure 17). Because the dinocyst concentration shows some correlation to the proposed biozones (*see* Figure 17), it was used as an additional criterion. This concentration only involves 'in-situ' dinocysts. Foraminiferal linings, acritarchs, and reworked palynomorphs are described as raw counts per 300 dinocysts counted instead of percentages since they were not used in the calculated concentrations. A concentration scale of low (<1000 cysts/gram), moderate (1000–1500 cysts/gram), and high (>1500 cysts/gram) is implemented here for descriptive purposes. The biozones are described using the taxa with more significance in each biozone. Table 4 provides additional details of accompanying species. The proposed assemblage biozones, in ascending order, are as follows:

- ***Assemblage Biozone 1 (35.68–35.34 amcd; 726.2–719.1 ka)***

This biozone is characterized by a constant presence of foraminiferal linings that can reach up to 40 specimens per 300 dinocysts. Relative abundances of *N. labyrinthus* (13–31%), *Brigantedinium* spp. (2–35%), *I. aculeatum* (25–54%), and *I. cantabrigiense* (3–17%) are also important in this biozone. *Operculodinium centrocarpum* shows a rather low relative abundance (0–4.8%). Total dinocyst concentrations vary between moderate and high.

Figure 16: Detrended correspondence analysis plot with dispersion of species in Hole U1313A. Taxon abbreviations are described in Table 3.

- ***Assemblage Biozone 2 (35.25–34.77 amcd; 717.2–708.2 ka)***

This biozone features a substantial drop in foraminiferal linings to almost none. *Operculodinium centrocarpum* increases significantly, rising to 51% in the middle of the zone. *I. aculeatum* is moderately abundant (14–25%) and *N. labyrinthus* (14–24%) remains constant. *Impagidinium cantabrigiense* drops to 2.0–6.5%. *Impagidinium pallidum* has its lowest occurrence just below the Biozone 1–2 boundary and persists through Biozone 2 although with low relative abundances (0–4.9%). The reworked acritarch *Veryhachium* sp. has its lowest occurrence in Biozone 2. Other reworked palynomorphs such as *Spinidinium* sp., *Areoligera/Glaphyrocysta* sp., and *Spiniferites* spp. occur in this biozone in low numbers (see Table 4). Dinocyst concentrations vary from high at the bottom to moderate to low at the top of the biozone.

- ***Assemblage Biozone 3 (34.69–33.30 amcd; 706.7–680.9 ka)***

Characterized by the lowest occurrence of *C.*? *labradori* in the middle of the biozone. *Impagidinium aculeatum* increases with relative abundances of 15 to 56% and becomes the dominant species along with *N. labyrinthus* (11–36%) and *O. centrocarpum* (5–25%). *Impagidinium strialatum* becomes frequent although with low relative abundances (0–1.5%). *Brigantedinium* spp. decline in abundance towards the top of this biozone to values as low as 0.3% whereas *I. cantabrigiense* increases from 0–4% to 8–15%. The presence of reworked palynomorphs drops significantly, approaching zero. Dinocyst concentrations remain low through this biozone.

- ***Assemblage Biozone 4 (33.25–32.19 amcd; 680–660.3 ka)***

Relative abundances of *C.*? *labradori* become highest in this biozone, with values varying between 0.3 and 8.8%. A similar increase is seen with *S. hyperacanthus* which ranges between 1 and 8.5%. *Spiniferites elongatus* becomes persistent in this biozone although with low relative abundances (0.3–1%). *Brigantedinium* spp. remain scarce with relative abundances not exceeding 2.8%. Although the acritarch *L.* cf. *crista* is persistent throughout the studied interval, its highest abundances are in Biozone 4 reaching up to 23 specimens per 300 dinocysts counted. Reworked palynomorphs become frequent with up to 55 reworked specimens per 300 dinocysts in some samples (see Table 4). The most common identifiable reworked cysts are assignable to *Oligosphaeridium complex, Subtilisphaera* sp., and *Spinidinium* sp. Dinocyst concentrations vary from high to moderate at the bottom to low at the top of this biozone.

- ***Assemblage Biozone 5 (32.14–31.58 amcd; 659.3–647.8 ka)***

Relative abundances of *S. hyperacanthus* and *I. cantabrigiense* decrease to ranges of 0–2% and 0–5% respectively. *Operculodinium centrocarpum* is dominant with abundances of 17–53%. Other common species are *N. labyrinthus* (8–23%), *I. aculeatum* (9.8–22%), and *I. paradoxum* (3–11%). Three specimens of *D. chathamensis* are also recorded. *Brigantedinium* ssp. become frequent again although with low relative abundances (1–17%). Foraminiferal linings also appear again with counts up to 7 specimens counted per 300 dinocysts in some samples. Reworked palynomorphs remain constant with counts

varying from 3 to 12 specimens per 300 dinocysts. *Spinidinium* sp. is the most common identifiable reworked species. Cyst concentrations vary from moderate to high.

- ***Assemblage Biozone 6 (31.50–30.96 amcd; 646.1–633.4 ka)***

This biozone is characterized mainly by highest abundances of *Brigantedinium* spp., reaching more than 70% in some samples. Also, an acme of *B. tepikiense* is registered at the base of this zone (31.41 amcd) with relative abundances of up to 33%. *Spiniferites hyperacanthus* and *I. cantabrigiense* persist with very low abundances (0–0.6% and 0–2% respectively). Foraminiferal linings continue to have a significant presence, with counts varying from 1 to 10 specimens per 300 dinocysts. Reworked palynomorphs continue though this biozone with raw counts varying from 1 to 47 specimens per 300 dinocysts. The most common identifiable reworked palynomorphs are assignable to the dinocysts *Spinidinium* sp. and *O. complex*, and the acritarch *Veryhachium* sp. Dinocyst concentrations are high with the exception of sample 31.33 which has a low concentration.

- ***Assemblage Biozone 7 (30.88–29.83 amcd; 631.1–603.3 ka)***

This biozone is characterized by the high relative abundances of *N. labyrinthus* (5–64%), *I. aculeatum* (9–41%), *I. cantabrigiense*, and *O. centrocarpum* (4–57%). *Brigantedinium* spp. decrease to relative abundances between 0 and 10% in the lower part of this biozone and disappear at the top. *Impagidinium patulum* reaches its highest abundances (up to

9.1%). Reworked palynomorphs are common at the base of the biozone (up to 39 specimens per 300 counted dinocysts) but their presence decreases drastically towards the top. The most common identifiable reworked palynomorphs are *Spinidinium* sp., *Subtilisphaera* sp., and *Veryhachium* sp. Cyst concentrations are the lowest of the studied interval, with values as low as only 20 cysts per gram of sediment (see Table 4).

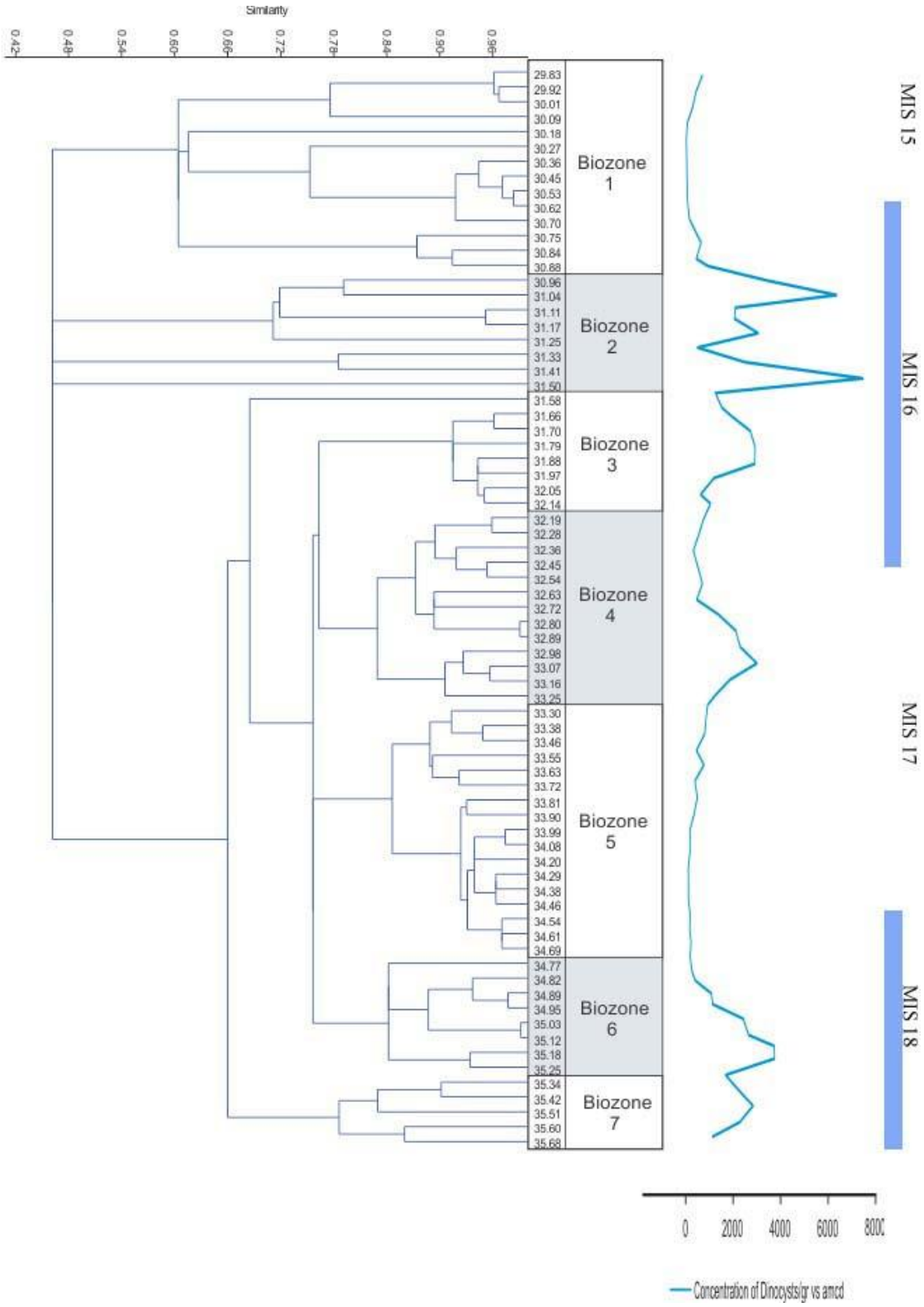

Figure 17: Constrained cluster analysis with assemblage biozones and dinocyst concentrations for Hole U1313A.

6. DISCUSSION

6.1. Cyst preservation and implications for paleoproductivity

Several studies have documented the sensitivity of protoperidinioid cysts to aerobic decay (e.g. Zonneveld et al., 2001; Hopkins and McCarthy, 2002; Versteegh and Zonneveld 2002). This selective degradation can therefore affect the cyst concentrations and reconstructions of primary productivity based on protoperidinioid cysts. The low cyst concentrations in Hole U1313A, however, are not the result of selective degradation produced by taphonomic processes. This interpretation is based on the analysis of amorphous organic matter (AOM) on selected samples with relevant cyst concentrations (high and low) (Table 5).

AOM is rapidly degraded in oxic settings, and therefore appears to be especially diagnostic of dysoxic to anoxic facies in marine sediments (Tyson, 1995). The present study shows high AOM percentages at depths with very low cyst concentrations. This argues against significant oxic decay of susceptible cysts during these intervals. In other words, low concentrations are not being controlled by oxidation. Additionally, some *Brigantedinium* secimens recorded in samples with low concentrations are well preserved (Fig. 18). Moreover, an opaque, cubic mineral, here interpreted to be pyrite, is generally present within all particles of AOM. This sulfide is commonly present in anoxic conditions (e.g. Wilkin et al., 1997) and therefore indicates absence of oxic decay.

In contrast, some samples with low percentages of AOM have elevated cyst concentrations. Hence, if some oxidation took place, the concentrations in these samples are underrepresented. However, it may be that the AOM signal is being suppressed by

reworked non-palynomorph particulate organic matter associated with ice-rafted debris, as it is almost impossible to distinguish between reworked and in-situ debris under transmitted light microscopy, as used in this study.

In general, the protoperidinioids present in intervals with high cyst concentrations are well preserved. However, specimens display variable degradation. Therefore, this group might be somewhat underrepresented due to selective degradation in such samples. Even if so, this does not seem to strongly affect the interpretations here proposed; indeed any allowance for underrepresentation would only make the preserved protoperidinioid signal stronger. A similar conclusion was reached by Reichart and Brinkhuis (2003) who found during their studies of the Arabian Basin that in spite of selective degradation under oxic conditions the marine primary productivity signal based on protoperidinioid cysts remains reliable.

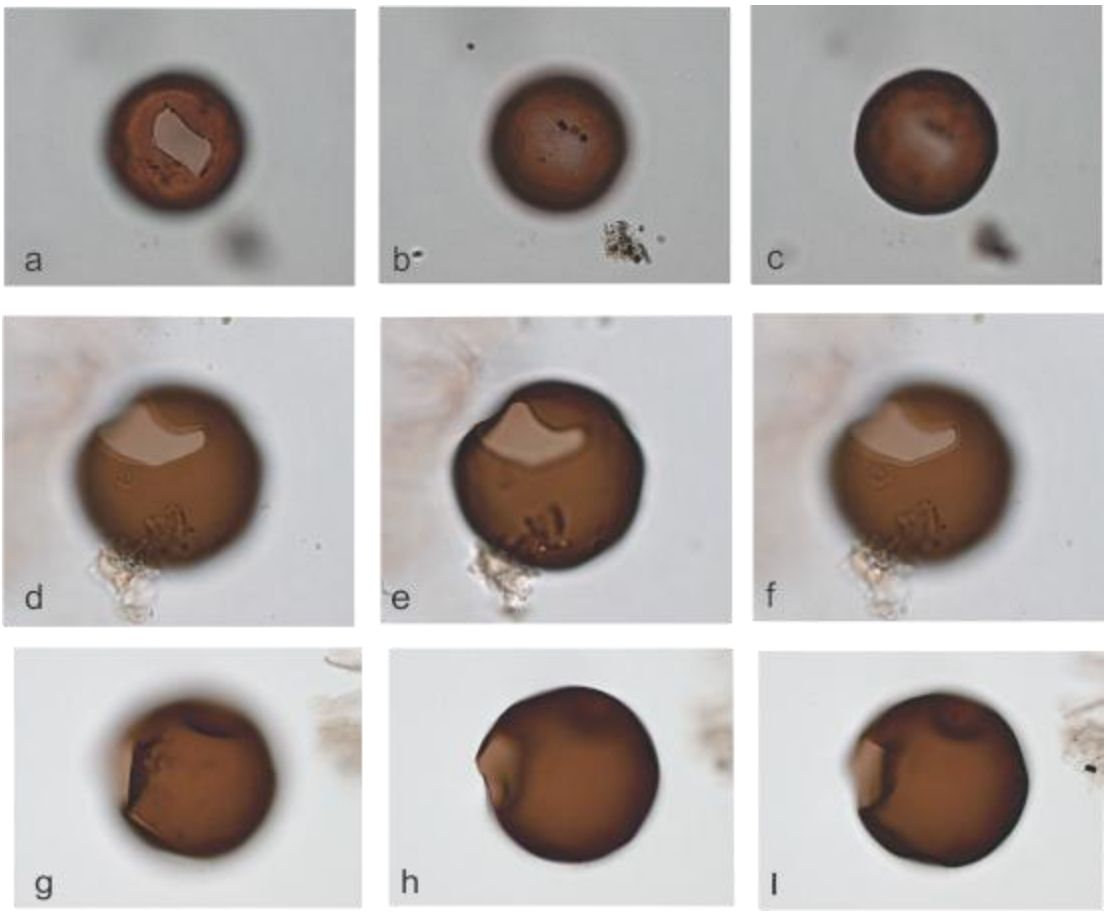

Figure 18: Photomicrographs of *Brigantedinium* spp. from 34.77 amcd (a-c), and 35.18 amcd (d-f), and 35.34 amcd (g-i). Size of specimens: 33 µm (a-c), 36 µm (d-f), and 35 µm (g-i).

6.2. Extinct dinocysts

Impagidinium cantabrigiense has been reported from the latest Gelasian through Middle Pleistocene of eastern North Atlantic DSDP Hole 610A where it extends to the top of the investigated section at 530 ka (De Schepper and Head, 2008, 2009). A single torn specimen reported from modern sediments off Chile may indicate that it is extant, although reworking is clearly also possible (Verleye and Louwye, 2010). It has been reported also from the Early and Middle Pleistocene of Zakynthos, Greece, and ODP Site 963 off Sicily (De Schepper and Head, 2008 and references therein; De Schepper et al., 2011). De Schepper and Head (2008) suggested that this species might be related to transitional phases from warm to cold surface waters with a preference for cooler conditions. Relative abundances of *I. cantabrigiense* recorded in this present study might be following this trend, given that Site U1313 is located near the boundaries of the cold subpolar gyre and the warm subtropical gyre. Hence, high abundances of this species during MIS 18 and MIS 17 could reflect the transition between these two contrasting oceanic gyres. The abundances during MIS 16 are, however, the lowest of the entire analyzed interval. Rather than reflecting a drop in absolute abundance, these low counts are conceivably a consequence of an intense increase in other species associated with subpolar waters, due to the severity of MIS 16 compared to MIS 18. However, the ecological affinities of *I. cantabrigiense* are still not entirely understood.

Corrudinium? *labradori* was first described from the Upper Miocene and Lower Pliocene of the Labrador Sea (Head et al., 1989 a, b), and has since been reported across the eastern North Atlantic and adjacent seas from the Pliocene through Middle Pleistocene

(e.g. Versteegh and Zonneveld, 1994; Head et al., 2004; Louwye et al., 2004; De Schepper et al., 2008, 2009, 2011; De Schepper and Head, 2008, 2009), with the highest occurrence at 530 ka in eastern North Atlantic DSDP Hole 610A (De Schepper and Head, 2008, 2009). The paleoecology of this species is presently unknown although sea-surface temperature appears not to have been the only factor controlling its distribution (De Schepper et al., 2011).

6.3. The acritarch *Lavradosphaera* cf. *crista*

Lavradosphaera De Schepper and Head, 2008 is a distinctive genus containing three species, all of which have restricted stratigraphic ranges (De Schepper and Head, in press). *Lavradosphaera crista* De Schepper and Head, 2008 has a highest common occurrence in the North Atlantic at ca. 2.9 Ma, with sporadic higher records that extend into the lower Pleistocene (ca. 1.8 Ma) presumed to represent reworking (De Schepper and Head, in press). Indeed, the highest presently accepted occurrence of the genus is the highest occurrence of *Lavradosphaera canalis* De Schepper and Head, in press, at 2.6 Ma near the Pliocene–Pleistocene boundary in the North Atlantic (De Schepper and Head, in press).

Samples from IODP Hole U1313A contain a single species of *Lavradosphaera*, which is provisionally identified as *L.* cf. *crista*. This species ranges through the entire analysed interval in Hole U1313A, with its highest observed occurrence therefore at ca. 603 ka in lower MIS 15. Its highest relative abundance (7.6 %) is registered in lowermost MIS 16 at a depth of 32.36 acmd. Consequently the results here presented extend the stratigraphic

record of the genus *Lavradosphaera* into the Middle Pleistocene. Detailed morphological studies using the SEM are needed to clarify the taxonomy of our specimens and determine whether they constitute the highest stratigraphic record of *L. crista*.

6.4. Palynology of Heinrich-like events in Hole U1313A

To reveal the distribution of ice-rafted material at Site U1313, Naafs et al. (2011) used X-ray diffraction (XRD) measurements to identify the abundance of quartz and dolomite in the holes. Quartz and feldspar have been used to identify continent-derived material (e.g. Stein et al., 2009), and within the IRD belt dolomite additionally serves as an indicator of detrital Paleozoic carbonates derived from the Hudson Bay area of Canada (Bond et al., 1992), i.e. Heinrich(-like) Events. Several studies report the lowest occurrence of Heinrich-like events in the North Atlantic during MIS 16 (e.g. Hodell et al., 2008; Stein et al., 2009; Naafs et al., 2011). Hole U1313A contains two of these events: the first one located in mid-MIS 16 and the second, and more intense, in upper MIS 16 (Fig 19c). MIS 18 also contains an increase in IRD material but is not considered a Heinrich-like event due to its low dolomite concentration.

The relative abundances and concentrations of reworked palynomorphs were calculated, and, as expected, a strong correlation was observed between the percentage of reworked palynomorphs and the ratios of quartz/calcite and dolomite/calcite (Fig. 19). This shows the reliability of palynology in identifying Heinrich(-like) events, as well as other IRD layers, with sedimentary sources.

In addition, the stratigraphic ranges of selected reworked palynomorphs provide information on the age of the ice-rafted material. For instance, the record of the ceratioid dinocysts *Odontochitina costata* and *Odontochitina operculata* spans Upper Albian–lowermost Maastrichtian and uppermost Hauterivian–lowermost Maastrichtian, respectively (Williams et al., 2004). These two Cretaceous species were recorded in MIS 16 at 32.45, 31.58, 31.33 and 30.88 amcd (Fig. 12). *Oligosphaeridium complex* was also recorded throughout MIS 16 and upper MIS 17 (33.25–30.45 amcd). The genus *Oligosphaeridium* has a highest occurrence in the Thanetian (Upper Paleocene), and representatives are very common in the Cretaceous, including *O. complex* which has its lowest occurrence in lowermost Valanginian (Lower Cretaceous). Another typical Cretaceous species is the peridinioid *Palaeohystrichophora infusorioides* which spans the Late Albian–Maastrichtian. In Hole U1313A, this species is recorded at 32.54, 32.28 and 31.58 amcd. Other reworked dinocysts including *Cyclonephelium*? sp., *Cerodinium*? sp. and *Areoligera*? sp. may also be derived from Cretaceous sequences, but their poor preservation hinders identification to species level and hence assignment of a precise stratigraphic range. The palynological evidence for a Paleozoic influence could rely on the presence of the acritarch *Veryhachium* sp. Interestingly, this acritarch has its lowest documented occurrence in Hole U1313A at 34.77 amcd, corresponding to upper MIS 18 (Fig. 12). Its occurrence through MIS 16 remains fairly constant. Additional reworked acritarchs were encountered but their poor preservation obstructed further identification.

The multiple ages of the reworked palynomorphs within the IRD layers therefore implies that the provenance of the IRD is derived from more than one source rock. Additionally, the palynological data show an incipient iceberg discharge during MIS 18 also supported

by the quartz/calcite and dolomite/calcite ratios (Figure 19). The presence of *Veryhachium* sp. may be related to Paleozoic material from the Hudson Strait. However, a more detailed study is needed to gain more accurate insights.

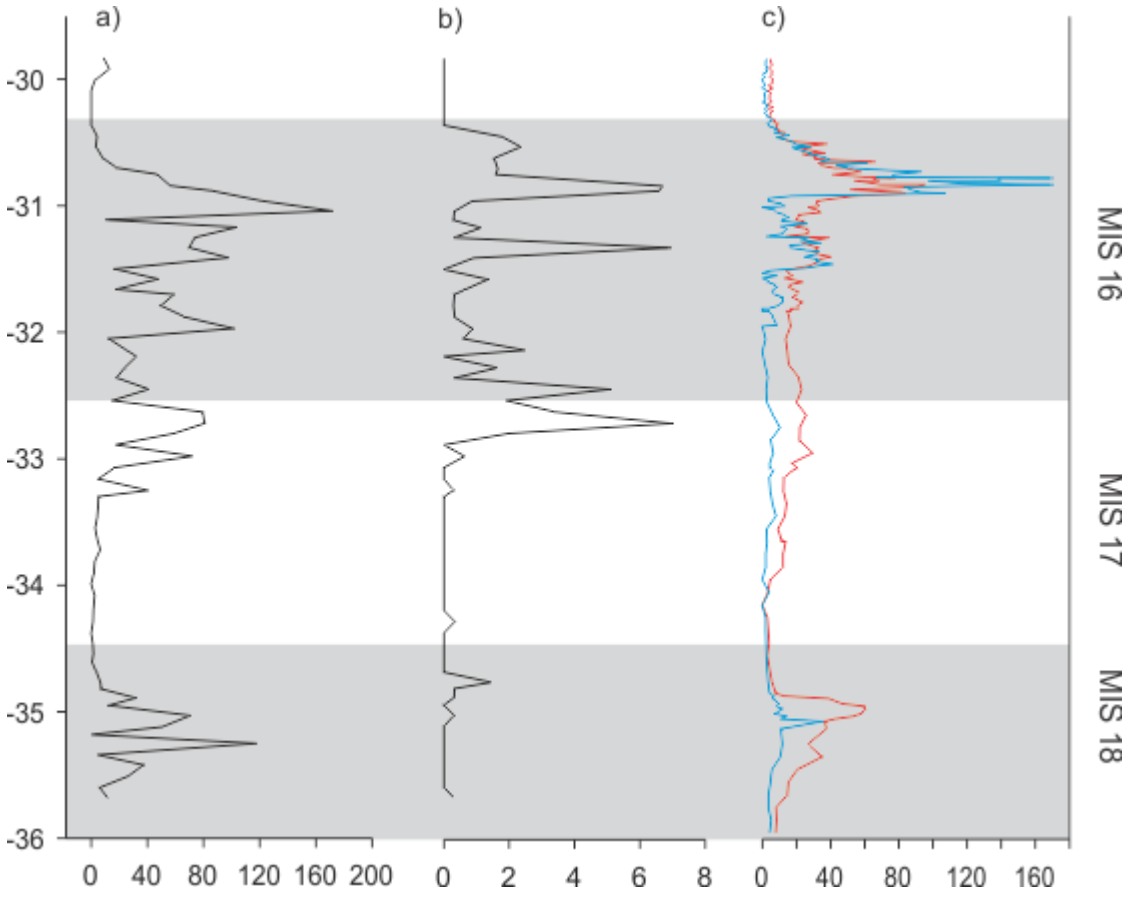

Figure 19: (a) Reworked palynomorph concentrations/gram of sediment. (b) Percentage of reworked palynomorphs. (c) Quartz/calcite (red) and dolomite/calcite (blue) ratios in Hole U1313A based on data from Naafs et al. (2011). Grey bars indicate glacial stages.

6.5. Paleoceanography and shifts of the Arctic Front

Although *O. centrocarpum* is a cosmopolitan species, those sites influenced by the NAC usually display high abundances of this dinocyst (e.g. Rochon et al., 1999; De Schepper

et al., 2009a and references therein). For instance, its abundance in the Norwegian–Greenland Sea has been associated with the inflow of warmer North Atlantic waters today (Matthiessen, 1995) and during the last interglacial (Van Nieuwenhove et al., 2008b).

Site U1313 shows varying peaks and troughs of abundance of this species along the analyzed interval (Fig. 9). These fluctuations attest to changes in the influence of the NAC. Currently, this site is located in the subtropical gyre and therefore not directly affected by the NAC. However, with moderate cooling (e.g. southward shift in the Arctic Front), the NAC can be shifted southwards to influence Site U1313. High abundances of *O. centrocarpum* along with *I. pallidum*, *P. dalei*, and *S. elongatus* during MIS 18 (Biozone 2) indicate a southward shift of the NAC that directly influenced Site U1313 and introduced cold-related species. Reduced values of *O. centrocarpum* in the latest MIS 18 and early part of MIS 17 (Biozone 3) suggest a northward shift of the NAC away from U1313. High levels of *I. aculeatum* also seem to support the oligotrophic conditions for U1313 at this time. The middle to late MIS 17 (upper Biozone 3 to lowermost Biozone 4) shows increasing values of *O. centrocarpum* accompanied by low abundances of the cold-related species *S. elongatus*, *P. dalei*, and *I. pallidum* along with high levels of *N. labyrinthus.* This tendency of increasing *O. centrocarpum* abundance through Biozone 3 and lower Biozone 4 suggests a progressive southward shifting of the NAC prior to the transition to MIS 16 (middle–upper Biozone 4) whereupon values of *O. centrocarpum* drop significantly. These subsequently low values of *O. centrocarpum* during the transition to MIS 16 (middle–upper Biozone 4) suggest a weakened influence of the NAC at this site, perhaps caused by a northward shift of the NAC, although the simultaneous

peak in *C.*? *labradori* suggests unusual oceanographic conditions that are perhaps related to this transition. This setting permitted minor amounts of IRD to reach Site U1313 before full entry into a cold stage (*see* Fig 19). The NAC was then reestablished over Site U1313 during early MIS 16 Biozone 5) with a subsequent southerly shift during mid-MIS 16 (Biozone 6) that reflects significantly cooler conditions than previously.

At this point, massive discharges of IRD (i.e. first Heinrich-like events) occurred in the central North Atlantic (Figs 19 and 20). In the North Atlantic, the cold, high-nutrient, surface waters of the subpolar gyre are separated from the warm and oligotrophic waters of the subtropical gyre by the NAC (e.g. Naafs et al., 2010; Alonso-Garcia et al., 2011). The Arctic Front located just north of the NAC can also be associated with high primary productivity (Naafs et al., 2010). The elevated numbers of heterotrophic species during mid-MIS 16 (Biozone 6) reflect the influence of nutrient-rich, subpolar waters resulting from the close proximity of the Arctic Front at Site U1313. A prominent peak of *B. tepikiense* occurring during mid-MIS 16 (Fig. 9) represents the only significant peak of a cold-to-cool-indicating species through the entire analyzed interval (e.g. see Fig. 10, these cold species being represented mainly by *B. tepikiense*). The modern distribution of *B. tepikiense* is closely related to the transition of subpolar to temperate waters (Dale, 1996) and is also linked to polar front regions with low surface salinities due to ice melting (Bakken and Dale, 1986) and possible water stratification (Rochon et al., 1999). Consequently, its high abundance in the central North Atlantic during mid-MIS 16 supports the interpretation of colder waters caused by the close proximity of the Arctic Front. A link between peaks of *B. tepikiense* and water stratification produced by iceberg melting is therefore suggested at Site U1313. The peak of *B. tepikiense* correlates to the

base of the IRD layer 16.2 (Fig. 20). The second IRD layer (16.1) also coincides with an increase in the relative abundance of *B. tepikiense*. However, this increase is not as significant as the previous one, even though IRD layer 16.1 is more prominent. This increase may have been suppressed by a drop in cyst concentrations immediately following the deposition of IRD layer 16.1. Interestingly, De Schepper et al. (2009a) identified peaks of *B. tepikiense* before rather than during the deposition of IRD layers in a Pliocene glacial event in the eastern North Atlantic. Hence, there are still gaps in our understanding of the precise association of this species with water stratification.

During MIS 16, the Arctic Front was located in the eastern North Atlantic near the Feni Drift, based on abundances of the foraminifers *Turborotalia quinqueloba*, an indicator of sea-ice margins, and *Neogloboquadrina pachyderma* (s), an Arctic water species at ODP Site 980 (Wright and Flower, 2002) (Fig. 21). Additionally, its position was reported south of IODP Site U1314 based on foraminifer data (Alonso-Garcia et al., 2011). This together with the palynological data at Site U1313 suggests that the Arctic Front could have had a pronounced northeast–southwest direction during MIS 16 (Fig. 22), probably as a result of an intense cooling of the subpolar gyre that produced a steep SST gradient between the eastern and western North Atlantic.

A decline in *O. centrocarpum* towards the end of MIS 16 and transition to MIS 15 (middle Biozone 7) suggests a new type of paleoceanographic condition in which *N. labyrinthus* dominates. Today, *N. labyrinthus* is found usually where cold Arctic waters mix with relatively warm North Atlantic waters (e.g. Rochon et al., 1999; Zonneveld et al., 2013). Soon after the beginning of MIS 15, the NAC is re-established with *O. centrocarpum* rising in abundance. Species linked to tropical to temperate waters such as

I. strialatum, *S. hyperacanthus*, and *S. mirabilis* (Zonneveld et al., 2013) reappear in the record.

In summary, the heterotrophic species reflect high primary productivity associated with the influence of subpolar waters during the middle of MIS 16. MIS 18 also shows evidence of such a setting, although to a lesser extent. This can also be seen by the decrease in relative abundances of *S. mirabilis* and *S. hyperacanthus* during MIS 16 (Fig. 9). In mid-Pliocene sediments of the North Atlantic these species were considered to represent waters with summer SSTs above 12ºC (De Schepper et al., 2009a). The high relative abundances of these species during MIS 18 indicate that sea-surface waters were warm enough in the central North Atlantic to allow these species to be present.

The fact that the NADW current becomes weaker during glacial stages and stronger during interglacials as suggested by various authors (e.g. Broecker et al., 1990; Fagel and Hillaire-Marcel, 2006), argues that the high abundances of *Brigantedinium* spp. and *B. tepikiense* during MIS 16 and part of MIS 18 are more likely the result of local conditions than deep-water transport from the north. The NAC constitutes an additional possible source of transport. Nevertheless, this current transports oligotrophic and warm waters from the Gulf Stream to the northeastern Atlantic and would therefore not be expected to supply cold-related and/or high-nutrient-related species. The dinocysts here recorded are therefore thought to represent the water masses present over Site U1313 during the Middle Pleistocene.

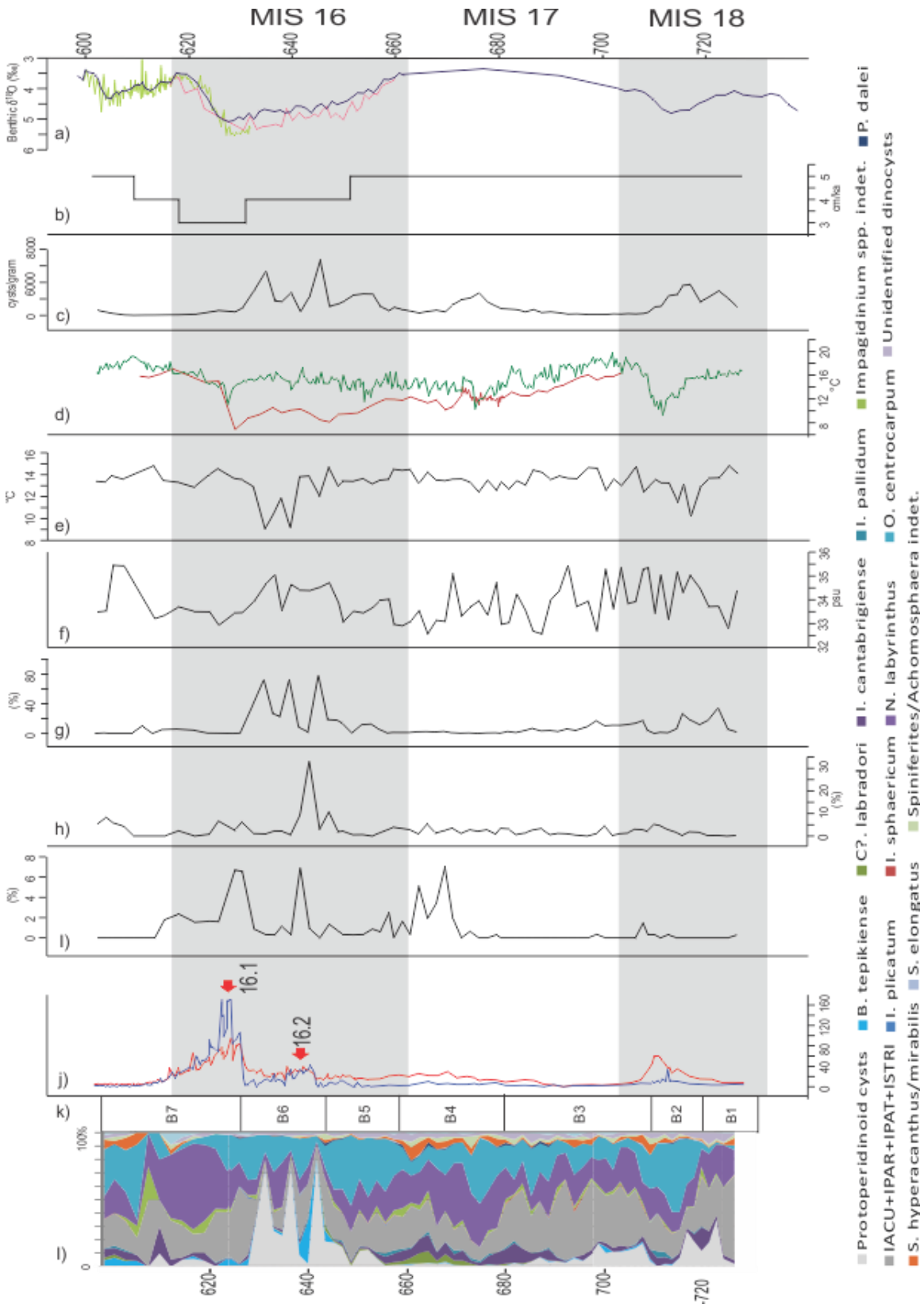
MIS 16
MIS 17
MIS 18
600
620
640
660
680
700
720
Benthic δ18O (‰)
a)
b)
cm/ka
cysts/gram
c)
d)
°C
e)
f)
psu
(%)
g)
h)
i)
16.1
16.2
j)
k)
B7
B6
B5
B4
B3
B2
B1
100%
l)
Protoperidinoid cysts
B. tepikiense
C?. labradori
I. cantabrigiense
I. pallidum
Impagidinium spp. indet.
P. dalei
IACU+IPAR+IPAT+ISTRI
I. plicatum
I. sphaericum
N. labyrinthus
O. centrocarpum
Unidentified dinocysts
S. hyperacanthus/mirabilis
S. elongatus
Spiniferites/Achomosphaera indet.

Figure 20: Summary diagram. (a) Benthic $\delta^{18}O$ of Site U1313 from Naafs et al. (2011) (red), Stein et al. (2009) and Voelker et al. (2010) (green) together with the LR04 Stack of Lisiecki and Raymo (2005) (purple). Modified from Naafs et al. (2011). (b) Sedimentation rate [cm/ka] in Hole U1313A (Naafs et al., 2011). (c) In situ dinocyst concentrations (cyst/gram of dry sediment). (d) Alkenone-based (green) and Mg/Ca-based (red) SSTs (Naafs et al., 2011). (e) MAT-based SSTs using dinocyst data. (f) MAT-based SSSs using dinocyst data. (g) Percentage of heterotrophic dinocysts in Hole U1313A. (h) Percentage of cold-related species. (i) Percentage of reworked palynomorphs. (j) Quartz/calcite (red) and dolomite/calcite (blue) ratios at Site U1313 (Naafs et al., 2011). Red arrows indicate Heinrich[-like] events 16.1 and 16.2 (Naafs et al., 2011). (k) palynological assemblage biozones. (l) Relative abundances of main taxa in Hole U1313A. Abundances of *I. aculeatum, I. paradoxum, I. patulum,* and *I. strialatum* are plotted together because of their oligotrophic affinity.

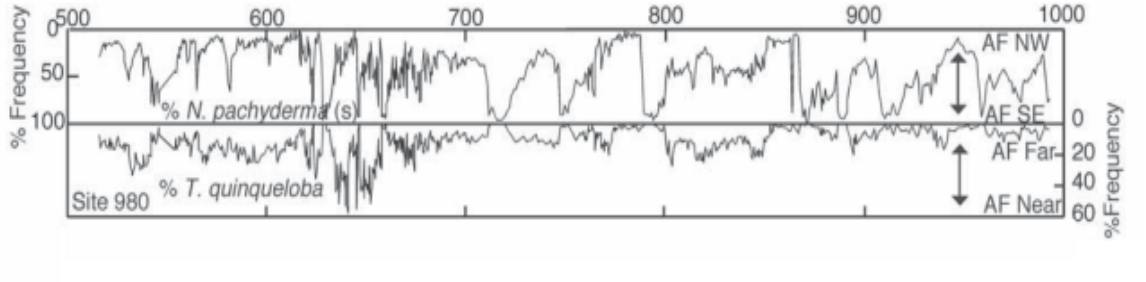

Figure 21: Arctic Front indicator based on percentages of *N. pachyderma* (s) and *T. quinqueloba*. Modified from Wright and Flower (2002).

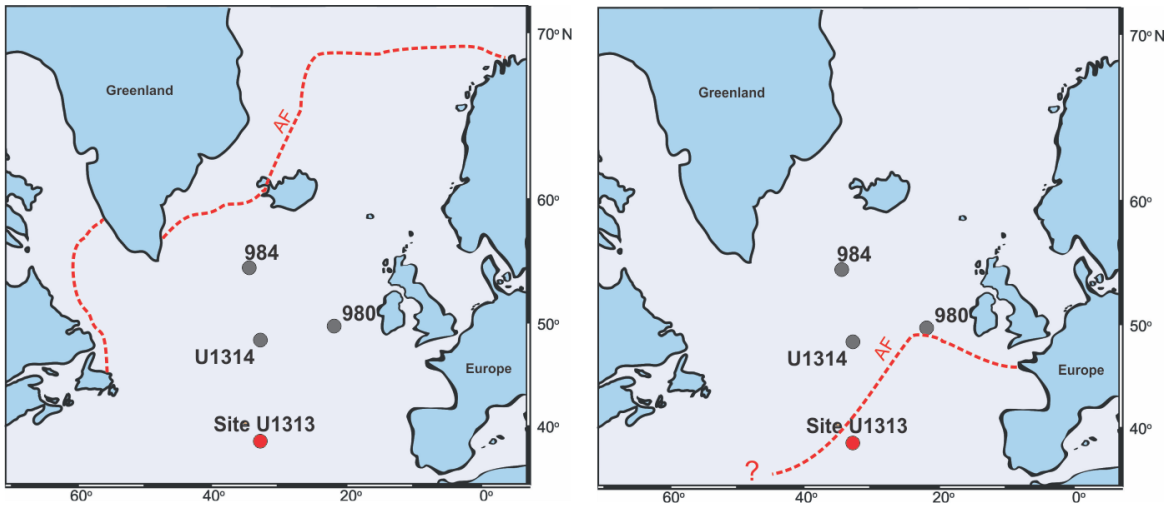

Figure 22: Inferred position of the Arctic Front during the mid-Pleistocene interglacials (left) and mid-MIS 16 (right) based on data from IODP Site U1314 (Alonso-Garcia et al., 2011), ODP Sites 984 and 980 (Wright and Flower, 2002); and IODP Site U1313 (this study).

6.6. Reliability of the MAT in the central North Atlantic

The question of reliability arises when analyzing in detail the outcomes of MAT shown in Figure 14. SSTs show no trends besides the three cooling peaks in MIS 16 and MIS 18 (two and one respectively). These peaks are controlled by the limited presence of cold-related species combined by high abundances of *Brigantedinium* spp., a genus that is controlled primarily not by SSTs but by other factors including food sources which happen to be in the more northerly, colder areas of the modern sample set used for the MAT calibration. These peaks probably do indicate cooling, but as an indirect consequence of high nutrient content at Site U1313 most likely related to the advance of

subpolar waters. A similar issue with MAT and the group *Brigantedinium* was also reported by Pospelova et al. (2006). Additionally, the data obtained at Hole U1313A are being compared with data from the North Atlantic subset, the sample positions of which are not located in the central North Atlantic and are disproportionately positioned in neritic settings, considerably biasing the results. Conversely MAT does not respond to the peak of *B. tepikiense* at the base of Biozone 6 and yielded SSTs of 14ºC. Esper and Zonneveld (2007) noted that the MAT can be biased by preservation when including protoperidinioid species such as *Brigantedinium* spp. due to their easy degradation, and suggest the use of a selective degradation index (kt-index). However, the protoperidinioids recorded in Hole U1313A showed, in general, the appropriate wall thickness and brown colour characteristic of this group indicating good preservation.

SSSs show a slight trend towards higher salinities during mid-MIS 16 and a following drop that could be the response of increasing salinity values during the glaciation followed by a decrease resulting by the discharge of fresh water into the ocean from ice-sheets melting. Yet, during MIS 17 and MIS 18 salinity values show no evident trends but rather seem to fluctuate abruptly between 32.5 and 35.5 psu (Fig. 14). Low counts could strongly affect the accuracy of reconstructions as demonstrated by Heiri and Lotter (2001). Cyst concentrations (i.e. low counts) during Biozone 3 (MIS 17) show low values (Fig 8 and Fig 16) and therefore could be a factor affecting the outcome during this interval. Nevertheless, Biozones 1 and 2 (MIS 18) registered relatively high concentrations that allowed counts of up to 300 specimens per sample, and yet the abrupt fluctuations persist.

A notable constraint of the MAT as applied to dinocysts is that the interaction of such parameters as SSTs, SSSs, primary productivity and light regimes plays an important role in controlling the distribution of dinocysts, but the MAT treats these variables as though they were independent (Verleye and Louwye, 2010). An additional shortcoming is that the accuracy of MAT using dinocysts is strongly reliant on the region analyzed. In this particular study, none of the modern analogue samples used was situated in the open waters of the central North Atlantic, and comparisons of the MAT were therefore conducted using a dataset that does not strictly share the same environmental variables.

Although valuable effort has been expended to refine the MAT using dinocysts, it is imperative to increase the study of modern dinoflagellate cysts in bottom sediments of the open central North Atlantic in order to improve understanding of the modern cyst distributions in this oligotrophic oceanic setting and thereby widen the spectrum for MAT analyses. In addition, MAT-based outcomes must be treated with caution when high abundances of protoperidinioids are involved.

6.7. Comparison of palynological data with Mg/Ca and alkenone paleotemperatures

A primary aim of the present study has been to address the discrepancy between alkenone and foraminiferal Mg/Ca paleotemperature reconstructions for MIS 16. Palynological interpretations and alkenone paleotemperatures coincide to reflect an increased cooling during MIS 18 that produced a deflection of the NAC towards Site U1313. The

subsequent northern shift of the Arctic Front during early MIS 17 allowed an increase in abundances of oligotrophic and tropical to temperate species. Both alkenone and Mg/Ca paleotemperatures also show a warming that supports this explanation. Interestingly, a deflection between Mg/Ca and alkenone paleotemperatures begins during Biozone 4, corresponding to the late MIS 17 and transition to MIS 16; and remains that way until the lowermost Biozone 7, just before the termination of MIS 16. The alkenone SSTs show a muted warming whereas Mg/Ca SSTs reflect an increased cooling. The mismatch between SSTs was explained by Naafs et al. (2011) as a result of strong water stratification. Alkenones are thought to reflect SSTs of the upper 10 meters of the water column (Müller et al., 1998) whereas *G. bulloides* dwells in mixed layers corresponding to the upper 60 meters in the North Atlantic (Schiebel et al., 1997). The only palynological evidence for water stratification relies on *B. tepikiense* as discussed previously. Peaks of this species however, only occur during Biozone 6 at MIS 16 and seem to be linked to massive iceberg discharges. On the other hand, high abundances of heterotrophic dinocysts during the glacial cycles are here attributed to the influence of subpolar waters. This more closely agrees with the cooling trend displayed by Mg/Ca SSTs. Substantial decrease in *S. hyperacanthus* and *S. mirabilis* during MIS 16 also supports this interpretation. Palynological interpretations therefore suggest that dinocysts are more in accord with SSTs of the upper 60 meters. Perhaps more pronounced water stratification during Biozone 6 in MIS 16, resulting from massive iceberg discharges, favoured the growth of *B. tepikiense* at this time.

7. SUMMARY AND CONCLUSIONS

The palynological analysis of 73 samples from IODP Hole U1313A has resulted in the identification of 29 dinocyst taxa, three acritarch taxa, and 16 reworked palynomorph taxa. This constitutes the first study of mid-Pleistocene dinocysts in the central North Atlantic at high resolution.

Seven assemblage biozones are established using constrained cluster analysis on the association of dinoflagellate cysts, acritarchs, foram linings, and reworked palynomorphs. Dinocyst concentrations given for each assemblage biozone provide additional characterization.

The continuous presence of the acritarch *Lavradosphaera* cf. *crista* in Hole U1313A significantly extends the stratigraphic range top of the genus *Lavradosphaera* which is currently recorded near the Pliocene–Pleistocene boundary (De Schepper and Head, in press). Additional morphological studies are needed to clarify the taxonomy of this species.

Reworked palynomorphs from the Paleozoic and Cretaceous have been identified, showing the potential of palynology in recognizing Heinrich-like events and other IRD layers sourced by sedimentary rocks. The presence of Cretaceous material within the Heinrich-like events of MIS 16 constitutes an enhancement in the understanding of the rock sources for these layers, previously thought to be restricted to Paleozoic units from the Hudson Strait.

The data here obtained suggest a southward shift of the NAC during late MIS 18 resulting in the direct influence of this current at Site U1313. This southward shifting also

allowed subpolar, nutrient-rich waters to penetrate this area. A subsequent northward shift of the Arctic Front and hence the NAC during the latest MIS 18 and early MIS 17 allowed oligotrophic waters to return to this area. Increasing values of *O. centrocarpum* along with *I. pallidum, P. dalei,* and *S. elongatus* during the middle to late MIS 17 are interpreted as a progressive southward shifting of the NAC prior to the transition to MIS 16 where values of *O. centrocarpum* decline, possibly as the result of a weakening or more southerly deflection of the NAC associated with the beginning of a glacial stage. Reworked palynomorphs, as well as quartz/calcite and dolomite/calcite ratios, evidence some IRD discharge at this point. The NAC was then reestablished over Site U1313 during the early MIS 16 and shifted southwards during middle part of this stage allowing substantial influence of eutrophic waters from the subpolar gyre as reflected by high values of the heterotrophic genus *Brigantedinium*. An increasing presence of the subpolar species *B. tepikiense* with a peak abundance at the base of Biozone 6 also suggest the presence of cold waters during mid-MIS 16 and probable water stratification as a result of iceberg discharge linked to the first two Heinrich-like events. A subsequent onset of oligotrophic conditions during the uppermost analyzed portion of MIS 15 is registered.

The elevated percentages of AOM in intervals with low cyst concentrations rule out a significant aerobic decay of the sediments that could have seriously compromised the dinocyst assemblages at Site U1313.

Dinocyst data seem more in accord with the cooling trend showed by Mg/Ca records during MIS 16 than with the muted paleotemperature signal based on alkenones (both proxies from Naafs et al., 2011). However the abundance of *B. tepikiense* is consistent with stratified waters during MIS 16 that would have resulted from iceberg discharge.

The lack of modern analogues among modern samples in the central North Atlantic forced the MAT to compare data obtained at Hole U1313A with those from modern neritic settings, considerably biasing the reconstruction. This numerical technique also reveals important weaknesses such as the exclusion of interaction between environmental variables, e.g. the assumption that the genus *Brigantedinium* is a SST-controlled dinocyst when in reality it follows areas with high nutrient/food availability. Additionally, this genus tends to be more susceptible to oxidation. Consequently, MAT-based interpretations must be addressed with caution when high relative abundances of heterotrophic dinocysts are present; even where the modern analogue dataset contains a substantial number of samples representing the same environmental settings as the studied area.

8. REFERENCES

Alonso-Garcia, M., Sierro, F.J., and Flores, J.A., 2011, Arctic front shifts in the subpolar North Atlantic during the Mid-Pleistocene (800–400ka) and their implications for ocean circulation: Palaeogeography, Palaeoclimatology, Palaeoecology, v. 311, no. 3-4, p. 268–280, doi: 10.1016/j.palaeo.2011.09.004.

Bakken, K., and Dale, B., 1986, Dinoflagellate cysts in Upper Quaternary sediments from southwestern Norway and potential correlations with the oceanic record: Boreas, v. 15, p. 185-190.

Benninghoff, W.S., 1962, Calculation of pollen and spores density in sediments by addition of exotic pollen in known quantities: Pollen et Spores, v. 6, p. 332–333.

Berger, W.H., and Jansen, E., 1994, Mid-Pleistocene climate shift – the Nansen connection. In: Johannessen, O.M., Overland, J.E. (Eds.), The Polar Oceans and Their Role in Shaping the Global Environment.: Geophysical Monograph Series, p. 295–311.

Bischof, J., Lund, J.J., and Ecke, H.-H., 1997, Palynomorphs of ice rafted clastic sedimentary rocks in Late Quaternary glacial marine sediments of the Norwegian Sea as provenance indicators: Palaeogeography, Palaeoclimatology, Palaeoecology, v. 129, p. 329–360, doi: 10.1016/S0031-0182(97)88176-X.

Bond, G., Heinrich, H., Broecker, W., and Labeyrie, L., 1992, Evidence for massive discharges of icebergs into the North Atlantic ocean during the last glacial period: Nature, v. 360, p. 345–249.

Bonnet, S., de Vernal, A., Gersonde, R., and Lembke-Jene, L., 2012, Modern distribution of dinocysts from the North Pacific Ocean (37–64°N, 144°E–148°W) in relation to hydrographic conditions, sea-ice and productivity: Marine Micropaleontology, v. 84–85, p. 87–113, doi: 10.1016/j.marmicro.2011.11.006.

Boulter, M.C., 1994, An approach to a standard terminology for palynodebris, in Traverse, A., Sedimentation of organic particles. Cambridge University Press, New York. p. 199–216.

Broecker, W.S., Bond, G., Bonani, G., and Wolfli, W., 1990, A salt oscilator in the glacial Atlantic?: Paleoceanography, v. 5, p. 469–477.

Broecker, W., Bond, G., Klas, M., and Clark, E., 1992, Origin of the northern Atlantic's Heinrich events: Climate Dynamics, v. 6, p. 265–273.

Calvo, E., Villanueva, J., Grimalt, J.O., Boelaert, A., and Labeyrie, L., 2001, New insights into the glacial latitudinal temperature gradients in the North Atlantic.

Results from UK^{37} sea surface temperatures and terrigenous inputs: v. 188, p. 509–519.

Clark, P.U., Archer, D., Pollard, D., Blum, J.D., Rial, J.A., Brovkin, V., Mix, A.C., Pisias, N.G., and Roy, M., 2006, The middle Pleistocene transition : characteristics, mechanisms, and implications for long-term changes in atmospheric pCO^2: Quaternary Science Reviews, v. 25, no. 23–24, p. 3150–3184, doi: 10.1016/j.quascirev.2006.07.008.

Combaz, A., 1964, Les palynofacies: Revue de Micropaléontologie, v. 7, p. 205–218.

Dale, B., 1976, Cyst formation, sedimentation, and preservation: factors affecting dinoflagellate assemblages in recent sediments from Trondheimsfjord, Norway: Review of Palaeobotany and Palynology, v. 22, p. 39-60

Dale, B., 1985, Dinoflagellate cyst analysis of upper Quaternary sediments in core GIK 15530-4 from the Skagerrak: Norsk Geologisk Tidsskrift, v. 65, p. 97–100.

Dale, B., 1996, Dinoflagellate cyst ecology: Modeling and geological applications, in Palynology: Principles and Applications, edited by J. Jansonius and D. C. McGregor, pp. 1249–1275, American Association of Stratigraphic Palynologists Foundation, Dallas, Texas.

De Schepper, S., Fischer, E.I., Groeneveld, J., Head, M.J., and Matthiessen, J., 2011, Deciphering the palaeoecology of Late Pliocene and Early Pleistocene dinoflagellate cysts: Palaeogeography, Palaeoclimatology, Palaeoecology, v. 309, no. 1–2, p. 17–32, doi: 10.1016/j.palaeo.2011.04.020.

De Schepper, S., and Head, M.J., 2008, New dinoflagellate cyst and acritarch taxa from the Pliocene and Pleistocene of the eastern North Atlantic (DSDP Site 610): Journal of Systematic Palaeontology, v. 6, no. 1, p. 101–117, doi: 10.1017/S1477201907002167.

De Schepper, S., and Head, M.J. In press. New late Cenozoic acritarchs: evolution, palaeoecology and correlation potential in high latitude oceans. *Journal of Systematic Palaeontology*.

De Schepper, S., Head, M.J., and Groeneveld, J., 2009a, North Atlantic Current variability through marine isotope stage M2 (circa 3.3 Ma) during the mid-Pliocene: Paleoceanography, v. 24, no. 1–17, doi: 10.1029/2008PA001725.

De Schepper, S., Head, M.J., and Louwye, S., 2009b, Pliocene dinoflagellate cyst stratigraphy, palaeoecology and sequence stratigraphy of the Tunnel-Canal Dock, Belgium: Geological Magazine, v. 146, p. 92–112, doi: 10.1017/S0016756808005438.

de Vernal, A., Eynaud, F., Henry, M., Hillaire-marcel, C., Londeix, L., Mangin, S., Matthiessen, J., Marret, F., Radi, T., Rochon, A., Solignac, S., and Turon, J.L., 2005, Reconstruction of sea-surface conditions at middle to high latitudes of the Northern Hemisphere during the Last Glacial Maximum (LGM) based on dinoflagellate cyst assemblages: Quaternary Science Reviews, v. 24, p. 897–924, doi: 10.1016/j.quascirev.2004.06.014.

de Vernal, A., Henry, M., Matthiessen, J., Mudie, P.J., Rochon, A., Boessenkool, K.P., Eynaud, F., Grosfeld, K., Guiot, J., Hamel, D., Harland, R., Head, M.J., Kunz-pirrung, M., Levac, E., et al., 2001, Dinoflagellate cyst assemblages as tracers of sea-surface conditions in the northern North Atlantic, Arctic and sub-Arctic seas: The new "n= 677" data base and its application for quantitative palaeoceanographic reconstruction: Journal of Quaternary Science, v. 16, no. 7, p. 681–698, doi: 10.1002/jqs.659.

de Vernal, A., and Mudie, P.J., 1989, Late Pliocene to Holocene palynostratigraphy at ODP Site 645, Baffin Bay: *in* Srivastava, S.P., Arthur, M., Clement B., et al., Proceedings of the Ocean Drilling Program, Scientific Results, v. 105, p. 387–399.

de Vernal, A., Turon, J.-L., and Guiot, J., 1993, Dinoflagellate cyst distribution in high-latitude marine environments and quantitative reconstruction of sea-surface salinity, temperature, and seasonality: Canadian Journal of Earth Sciences, v. 31, p. 48–62.

Devillers, R., and de Vernal, A., 2000, Distribution of dinoflagellate cysts in surface sediments of the northern North Atlantic in relation to nutrient content and productivity in surface waters: Marine Geology, v. 166, p. 103–124.

Donders, T.H., Weijers, J.W.H., Munsterman, D.K., Kloosterboer-van Hoeve, M.L., Buckles, L.K., Pancost, R.D., Schouten, S., Sinninghe Damste, J.S., and Brinkhuis, H., 2009, Strong climate coupling of terrestrial and marine environments in the Miocene of northwest Europe: Earth and Planetary Science Letters, v. 281, no. 3-4, p. 215–225, doi: 10.1016/j.epsl.2009.02.034.

Esper, O., and Zonneveld, K.A.F., 2007, The potential of organic-walled dinoflagellate cysts for the reconstruction of past sea-surface conditions in the Southern Ocean: Marine Micropaleontology, v. 65, p. 185–212, doi: 10.1016/j.marmicro.2007.07.002.

Evitt, W.R., 1963, A discussion and proposals concerning fossil dinoflagellates, hystrichospheres, and acritarchs. I. Proceedings of the National Academy of Sciences of the United States of America, v. 149, p. 158–164.

Evitt, W.R. 1984, Some techniques for preparing, manipulating and mounting dinoflagellates. Journal of Micropalaeontology, v. 3, p. 11–18.

Expedition 306 Scientists, 2006, Site U1313, in North Atlantic Climate 1, edited by J. E. T. Channell et al., Proc. Integrated Ocean Drill. Program, 303: doi:10.2204/iodp.proc.303306.112.2006, v. 303, p. 1–124, doi: 10.2204/iodp.proc.303306.112.2006.

Fagel, N., and Hillaire-Marcel, C., 2006, Glacial/interglacial instabilities if the western boundary under current during the last 365 kyr from Sm/Nd ratios of the sedimentary clay-size fractions at ODP Site 646 (Labrador Sea): Marine geology, v. 232, p. 87–99.

Fensome, R.A., Taylor, F.J.R., Norris, G., Sarjeant, W.A.S., Wharton, D.I., and Williams, G.L., 1993, A classification of living and fossil dinoflagellates: Micropaleontology special publication no. 7, 351 pp.

Fensome, R.A., and Williams, G.L., 2004, The Lentin and Williams Index of Fossil Dinoflagellates: AASP Contributions series, v. 42, 909 pp.

Ferretti, P., Crowhurst, S.J., Hall, M.A., and Cacho, I., 2010, North Atlantic millennial-scale variability 910 to 790 ka and the role of equatorial insolation forcing: Earth and Planetary Science Letters, v. 293, p. 28–41, doi: 10.1016/j.epsl.2010.02.016.

Gibbard, P.L., and Head, M.J., 2010. The newly-ratified definition of the Quaternary System/Period and redefinition of the Pleistocene Series/Epoch, and comparison of proposals advanced prior to formal ratification: Episodes, 33: 152–158.

Habib, D., 1976, Neocomian dinoflagellate zonation in the western North Atlantic. Micropaleontology, v. 21, p. 373–392. (Imprinted 1975)

Harland, R., and Pudsey, C.J., 2002, Protoperidiniacean dinoflagellate cyst taxa from the Upper Miocene of ODP Leg 178 , Antarctic Peninsula: Review of Palaeobotany and Palynology, v. 120, p. 263–284.

Hammer, Ø., Harper, D.A.T., and Ryan, P.D., 2001, Past: Paleontological statistics software package for education and data analysis: Paleontologia Electronica, v. 4 (1), p. 1–9.

Hammer, Ø., and Harper, D.A.T., 2006, Paleontological data analysis: Blackwell Publishing, 370 pp.

Harland, R., 1983, Distrobution maps of recent dinoflagellate cysts in bottom sediments from the North Atlantic Ocean and adjacent seas: Paleontology, v. 26, p. 321–387.

Harris, A.J., and Tocher, B. a., 2003, Palaeoenvironmental analysis of Late Cretaceous dinoflagellate cyst assemblages using high-resolution sample correlation from the Western Interior Basin, USA: Marine Micropaleontology, v. 48, no. 1–2, p. 127–148, doi: 10.1016/S0377-8398(03)00002-1.

Hays, J.D., Imbrie, J., and Shackleton, N.J., 1976, Variations in the Earth's orbit: pacemaker of the Ice Ages: Science, v. 194, no. 4270, p. 1121–1132.

Head, M.J., 1994, Morphology and paleoenvironmental significance of the Cenozoic dinoflagellate genera *Tectatodinium* and *Habibacysta*: Micropaleontology, v. 40, no. 4, p. 289–321.

Head, M.J., 2003, Neogene occurrences of the marine acritarch genus *Nannobarbophora* Habib and Knapp, 1982 emend., and the new species *N. gedlii*: Journal of Paleontology, v. 77, no. 2, p. 382–385.

Head, M.J., and Gibbard, P.L., 2005, Early–Middle Pleistocene transitions: an overview and recommendation for the defining boundary: Geological Society, London, Special Publications, v. 247, p. 1–18, doi: 10.1144/GSL.SP.2005.247.01.01.

Head, M.J., and Norris, G., 2003, New species of dinoflagellate cysts and other palynomorphs from the latest Miocene and Pliocene of DSDP Hole 603C, western North Atlantic: Journal of Paleontology, v. 77, no. 1, p. 1–15.

Head, M.J., Norris, G., and Mudie, P.J., 1989a, New species of dinocysts and a new species of acritarch from the upper Miocene and lowermost Pliocene, ODP Leg 105, Site 646, Labrador Sea. In Srivastava, S.P., Arthur, M., and Clement B., et al., Proceedings of the Ocean Drilling Program, Scientific results, v. 105, p. 1–14.

Head,M.J., Norris,G., and Mudie, P. J., 1989b. Palynology and dinocyst stratigraphy of the upper Miocene and lowermost Pleistocene, ODP Leg 105, Site 646, Labrador Sea. In Srivastava, S.P., Arthur, M., and Clement B., et al., Proceedings of the Ocean Drilling Program, Scientific Results, vol, 105. p. 467–514.

Head, M.J., Pillans, B., and Farquhar, S.A., 2008, The Early–Middle Pleistocene Transition: characterization and proposed guide for the defining boundary: Episodes, v. 31, no. 2, p. 255–259.

Head, M.J., Riding, J.B., Eidvin, T., and Chadwick, R.A., 2004, Palynological and foraminiferal biostratigraphy of (Upper Pliocene) Nordland Group mudstones at Sleipner, northern North Sea: Marine and Petroleum Geology, v. 21, p. 277–297, doi: 10.1016/j.marpetgeo.2003.12.002.

Heinrich, H., 1988, Origin and consequences of cyclic ice rafting in the northeast Atlantic Ocean during the past 130,000 years: Quaternary Research, v. 29, no. 2, p. 142–152.

Heiri, O., and Lotter, A.F., 2001, Effect of low count sums on quantitative environmental reconstructions: an example using subfossil chironomids: Journal of Paleolimnology, v. 26, p. 343–350.

Hemming, S.R., 2004, Heinrich events: Massive late Pleistocene detritus layers of the North Atlantic and their global climate imprint: Reviews of Geophysics, v. 42, p. 1–43, doi: 10.1029/2003RG000128.1.

Hemming, S.R., Gwiazda, R.H., Andrews, J.T., Broecker, W.S., Jennings, A.E., and Onstott, T.C., 2000, and Pb–Pb study of individual hornblende and feldspar grains from southeastern Baffin Island glacial sediments: Implications for the provenance of the Heinrich layers: Canadian Journal of Earth Sciences, v. 37, p. 879–890.

Hodell, D.A., Channell, J.E.T., Curtis, J.H., Romero, O.E., and Röhl, U., 2008, Onset of "Hudson Strait" Heinrich events in the eastern North Atlantic at the end of the middle Pleistocene transition (~640 ka)?: Paleoceanography, v. 23, no. 4, p. 1–16, doi: 10.1029/2008PA001591.

Hodell, D.A., Evans, H.F., Channell, J.E.T. and Curtis, J.H., 2010, Phase relationships of North Atlantic ice-rafted debris and surface-deep climate proxies during the last glacial period: Quaternary Science Reviews, v. 29, p. 3875–3886.

Hopkins, J.A., and McCarthy, F.M.G., 2002, Post-depositional palynomorph degradation in Quaternary shelf sediments: A laboratory experiment studying the effects of progressive oxidation: Palynology, v. 26, p. 167–184.

Huybers, P., 2007, Glacial variability over the last two million years: an extended depth-derived age model, continuous obliquity pacing, and the Pleistocene progression: Quaternary Science Reviews, v. 26, no. 1–2, p. 37–55.

Imbrie, J., Berger, A., Boyle, E.A., Clemens, S.C., Duffy, A., Howard, W.R., Kukla, G., Kutzbach, J., Martinson, D.G., Mcintyre, A., Mix, A.C., Molfino, B., Morley, J.J., Peterson, L.C., et al., 1993, On the structure and origin of major claciation cycles. 2. The 100,000-year cycle: Paleoceanography, v. 8, no. 6, p. 699–735.

Imbrie, J., Boyle, E.A., Clemens, S.C., Duffy, A., Howard, W.R., Kukla, G., Kutzbach, J., Martinson, D.G., Mclntyre, A., Mix, A.C., Molfino, B., Morley, J.J., Peterson, L.C., Pisias, N.G., et al., 1992, On the structure and origin of major glaciation cycles 1. Linear responses to Milankovitch forcing: Paleoceanography, v. 7, no. 6, p. 701–738.

Indelicato, S.R., and Loeblich, A.R., III, 1986, A revision of the marine peridinioid genera (Pyrrhophyta) utilizing hypothecal-cingular plate relationships as a taxonomic guideline: The Japanese Journal of Phycology, v. 34, p. 153–162.

Kokinos, J.P., Eglinton, T.I., Goñi, M.A., Boon, J.J., Martoglio, P.A., and Anderson, D.M., 1998, Characterization of a highly resistant biomacromolecular material in the cell wall of a marine dinoflagellate resting cyst: Organic Geochemistry, v. 28, no. 5, p. 265–288.

Kunz-Pirrung, M., 2001, Dinoflagellate cyst assemblages in surface sediments of the Laptev Sea region (Arctic Ocean) and their relationship to hydrographic conditions: Journal of Quaternary Science, v. 16, p. 637–649, doi: 10.1002/jqs.647.

Lang, N. and Wolff, E.W., 2011, Interglacial and glacial variability from the last 800 ka in marine, ice and terrestrial archives: Climate of the Past, v. 7, p. 361–380.

Lawrence, K.T., Herbert, T.D., Brown, C.M., Raymo, M.E., and Haywood, A.M., 2009, High-amplitude variations in North Atlantic sea surface temperature during the early Pliocene warm period: Paleoceanography, v. 24, p. 1–15, doi: 10.1029/2008PA001669.

Lisiecki, L.E., and Raymo, M.E., 2005, A Pliocene–Pleistocene stack of 57 globally distributed benthic δ18O records: Paleoceanography, v. 20, p. 1–17, doi: 10.1029/2004PA001071.

Louwye,S., Head,M.J., and De Schepper, S., 2004, Dinoflagellate cyst stratigraphy and palaeoecology of the Pliocene in northern Belgium, southern North Sea Basin. Geological Magazine, v. 141, p. 353–78.

Marret, F., and Zonneveld, K.A.F., 2003, Atlas of modern organic-walled dinoflagellate cyst distribution: Review of Palaeobotany and Palynology, v. 125, p. 1–200, doi: 10.1016/S0034-6667(02)00229-4.

Maslin, M.A., and Ridgwell, A.J., 2005, Mid-Pleistocene revolution and the "eccentricity myth": In: Head, M.J., and Gibbard, P.L., Early–Middle Pleistocene Transitions: the Land–Ocean Evidence; Geological Society, London, Special Publications, v. 247, p. 19–34, doi: 10.1144/GSL.SP.2005.247.01.02.

Matthiessen, J., 1995, Distribution patterns of dinoflagellate cysts and other organic-walled microfossils in recent Norwegian–Greenland Sea sediments: Marine Micropaleontology, v. 24, p. 307–334.

Mayer, L., Pisias, N., Janecek, T., et al., 1992, Proceedings of the Ocean Drilling Program, Initial Reptorts, 138: College Station, TX (Ocean Drilling Program).

McCarthy, F.M.G., Findlay, D.J., and Little, M.L., 2004, The micropaleontological character of anomalous calcareous sediments of late Pliocene through early Pleistocene age below the CCD in the northwestern North Pacific Ocean: Palaeogeography, Palaeoclimatology, Palaeoecology, v. 215, p. 1–15.

Miller, K.G., Kominz, M.A., Browning, J. V, Wright, J.D., Mountain, G.S., Katz, M.E., Sugarman, P.J., Cramer, B.S., Christie-Blick, N., and Pekar, S.F., 2005, The Phanerozoic Record of Global Sea-Level Change: Science, v. 310, p. 1293–1298, doi: 10.1126/science.1116412.

Moldowan, M.J., Dahl, J., Jacobson, S.R., Huizinga, B.J., Fago, F.J., Shetty, R., Watt, D.S., and Peters, K.E., 1996, Chemostratigraphic reconstruction of biofacies: Molecular evidence linking cyst-forming dinoflagellates with pre-Triasic ancestors: Geology, v. 24, no. 2, p. 159–162,

Moldowan, M.J., and Talyzina, N.M., 1998, Biogeochemical evidence for dinoflagellate ancestors in the Early Cambrian: Science, v. 281, p. 1168–1170, doi: 10.1126/science.281.5380.1168

Montresor, M., Zingone, A., and Marino, D., 1993, The calcareous resting cyst of *Pentapharsodinium tyrrhenicum* comb. nov. (Dinophyceae): *Journal of Phycology, v.* 29, p. 223–230.

Müller, P.J., G. Kirst, G. Ruhland, I. von Storch, and Rosell-Melé, A., 1998, Calibration of the alkenone paleotemperature index Uk′37 based on core-tops from the eastern South Atlantic and the global ocean (60°N–60°S): Geochimica et Cosmochimica Acta, v. no. 62 (10), p. 1757–1772, doi:10.1016/ S0016-7037(98)00097-0.

Naafs, B.D.A., Hefter, J., Ferretti, P., Stein, R., and Haug, G.H., 2011, Sea surface temperatures did not control the first occurrence of Hudson Strait Heinrich Events during MIS 16: Paleoceanography, v. 26, no. 4, p. 1–10, doi: 10.1029/2011PA002135.

Naafs, B.D.A., Stein, R., Hefter, J., Khélifi, N., De Schepper, S., and Haug, G.H., 2010, Late Pliocene changes in the North Atlantic Current: Earth and Planetary Science Letters, v. 298, no. 3–4, p. 434–442, doi: 10.1016/j.epsl.2010.08.023.

Van Nieuwenhove, N., and Bauch, H.A., 2008a, Last interglacial (MIS 5e) surface water conditions at the Vøring Plateau (Norwegian Sea), based on dinoflagellate cysts: Polar Research, v. 27, p. 175–186, doi: 10.1111/j.1751-8369.2008.00062.x.

Van Nieuwenhove, N., Bauch, H.A., and Matthiessen, J., 2008b, Last interglacial surface water conditions in the eastern Nordic Seas inferred from dinocyst and foraminiferal assemblages: Marine Micropaleontology, v. 66, p. 247–263, doi: 10.1016/j.marmicro.2007.10.004.

Oboh-Ikuenobe, F.E., Yepes, O., and Gregg, J.M., 1998, Palynostratigraphy, palynofacies, and thermal maduration of Cretaceous-Paleogene sediments from the Côte D'ivoire-Ghana transform margin, in Mascle, J., Lohmann, G.P., and Moullade, M. (Eds.), Proceedings of the Ocean Drilling Program, Scientific Results, v. 159, p. 277–318, doi:10.2973/odp.proc.sr.159.016.1998.

Oboh-Ikuenobe, F.E., Obi, C.G., and Jaramillo, C.A., 2005, Lithofacies, palynofacies, and sequence stratigraphy of Palaeogene strata in southeastern Nigeria: Journal of African Earth Sciences, v. 41, p. 79–101.

Parnell, J., Bowden, S., Andrews, J.T., and Taylor, C., 2007, Biomarker determination as a provenance tool for detrital carbonate events (Heinrich events?): Fingerprinting Quaternary glacial sources into Baffin Bay: Earth and Planetary Science Letters, v. 257, no. 1–2, p. 71–82, doi: 10.1016/j.epsl.2007.02.021.

Pospelova, V., de Vernal, A., and Pedersen, T.F., 2008, Distribution of dinoflagellate cysts in surface sediments from the notheastern Pacific Ocean (43–25ºN) in relation to sea-surface temperature, productivity and coastal upwelling: Marine Micropaleontology, v. 68 (1–2), p. 21–48.

Pospelova, V., Esenkulova, S., Johannessen, S.C., O'Brien, M.C., and Macdonald, R.W., 2010, Organic-walled dinoflagellate cyst production, composition and flux from 1996 to 1998 in the central Strait of Georgia (BC, Canada): a sediment trap study: Marine Micropaleontology, v. 75, p. 17–37.

Pospelova, V., Pedersen, T.F., and de Vernal, A., 2006, Dinoflagellate cysts as indicators of climatic and oceanographic changes during the past 40 kyr in the Santa Barbara basin, southern California: Paleoceanography, v. 21 (2), doi:10.1029/2005PA001251.

Powell, A.J., Dodge, J.D., and Lewis, J., 1990, Late Neogene to Pleistocene palynological facies of the Peruvian continental margin upwelling, in Suess, E., von Huene, R., et al., Proceedings of the Ocean Drilling Program, Scientific Results, v. 112, p. 297–321.

Price, A.M., and Pospelova, V., 2011, High-resolution sediment trap study of organic-walled dinoflagellate cyst production and biogenic silica flux in Saanich Inlet (BC, Canada): Marine Micropaleontology, v. 80, p. 18–43.

R Core Team, 2012, R: A language and environment for statistical computing. R Foundation for Statistical Computing, Vienna, Austria. ISBN 3-900051-07-0, http://www.R-project.org

Radi, T., Pospelova, V., de Vernal, A., and Barrie, J.V., 2007, Dinoflagellate cysts as indicators of water quality and productivity in British Columbia estuarine environments: Marine Micropaleontology, v. 62, p. 269–297.

Radi, T., and de Vernal, A., 2008a, Last Glacial Maximum (LGM) primary productivity in the northern North Atlantic Ocean: Canadian Journal of Earth Sciences, v. 45, p. 1299-1316, doi: 10.1139/E08-059.

Radi, T., and de Vernal, A., 2008b, Dinocysts as proxy of primary productivity in mid–high latitudes of the Northern Hemisphere: Marine Micropaleontology, v. 68, p. 84–114, doi: 10.1016/j.marmicro.2008.01.012.

Reichart, G.-J., and Brinkhuis, H., 2003, Late Quaternary *Protoperidinium* cysts as indicators of paleoproductivity in the northern Arabian Sea: Marine Micropaleontology, v. 937, p. 1–13.

Robinson, S.G., Maslin, M.A., and McCave, I.N., 1995, Magnetic susceptibility variations in upper Pleistocene deep-sea sediments of the NE Atlantic: implications for ice rafting and paleocirculation at the last glacial maximum: Paleoceanography, v. 10, p. 221–250.

Rochon, A., de Vernal, A., Turon, J., Matthiessen, J., and Head, M.J., 1999, Distribution of recent dinoflagellate cysts in surface sediments from the North Atlantic Ocean and adjacent seas in relation to sea-surface parameters: AASP Contributions Series, no. 35, p. 1–152.

Rosell-Melé, A., Maslin, M.A., Maxwell, J.R., and Schaefferi, P., 1997, Biomarker evidence for "Heinrich" events: Geochimica et Cosmochimica Acta, v. 61, no. 8, p. 1671–1678.

Ruddiman, W.F., 1977, Late Quaternary deposition of ice-rafted sand in the subpolar North Atlantic (lat. 40º to 65º N): Geological Society of America Bulletin, 88, p. 1813–1827, doi: 10.1130/0016-7606(1977)88<1813.

Ruddiman, W.F., Raymo, M.E., Martinson, D.G., Clement, B.M., and Backman, J., 1989, Pleistocene evolution: Northern Hemisphere ice sheets and North Atlantic Ocean: Paleoceanography, v. 4, no. 4, p. 353–412.

Schiebel, R., Bijma, J., and Hemleben, C., 1997, Population dynamics of the planktic foraminifer *Globigerina bulloides* from the eastern North Atlantic: Deep Sea Research Part I, v. 44, no. 9–10, p. 1701–1713.

Scott, R.W., Oboh-Ikuenobe, F.E., Benson, D.G., and Holbrook, J.M., 2009, Numerical age calibration of the Albian/Cenomanian boundary: Stratigraphy, v. 6, no. 1, p. 17–32.

Simaeys, S. Van, Munsterman, D., and Brinkhuis, H., 2005, Oligocene dinoflagellate cyst biostratigraphy of the southern North Sea Basin: Review of Palaeobotany and Palynology, v. 134, p. 105–128, doi: 10.1016/j.revpalbo.2004.12.003.

Sluijs, A., and Brinkhuis, H., 2009, A dynamic climate and ecosystem state during the Paleocene–Eocene Thermal Maximum: inferences from dinoflagellate cyst assemblages on the New Jersey Shelf: Biogeosciences, v. 6, no. 8, p. 1755–1781, doi: 10.5194/bg-6-1755-2009.

Sluijs, A., Schouten, S., Pagani, M., Brinkhuis, H., Sinninghe Damste, J.S., Dickens, G.R., Huber, M., Reichart, G., Stein, R., Matthiessen, J., Lourens, L.J., Pedentchouk, N., Backman, J., Moran, K., et al., 2006, Subtropical Arctic Ocean

temperatures during the Palaeocene/Eocene thermal maximum: Nature, v. 441, no. June, p. 610–613, doi: 10.1038/nature04668.

Snoeckx, H., Grousset, F., Revel, M., and Boelaert, A., 1999, European contribution of ice-rafted sand to Heinrich layers H3 and H4: Marine Geology, v. 158, p. 197–208, doi: 10.1016/S0025-3227(98)00168-6.

Stein, R., Hefter, J., Gru, J., Voelker, A., and Naafs, B.D.A., 2009, Variability of surface water characteristics and Heinrich-like events in the Pleistocene midlatitude North Atlantic Ocean : Biomarker and XRD records from IODP Site U1313 (MIS 16–9): Paleoceanography, v. 24, p. 1–13, doi: 10.1029/2008PA001639.

Susek, E., Zonneveld, K.A.F., Fischer, G., Versteegh, G.J.M., and Willems, H., 2005, Organic-walled dinoflagellate cyst production in relation to upwelling intensity and lithogenic influx in the Cape Blanc region (off North-West Africa): Phycological Research, v. 53, p. 97–112.

Telford, R.J., 2006, Limitations of dinoflagellate cyst transfer functions: Quaternary Science Reviews, v. 25, p. 1375–1382, doi: 10.1016/j.quascirev.2006.02.012.

Traverse, A., 2007, Paleopalynology: Springer, Dordrecht, The Netherlands. 816 pp.

Tyson, R.V., 1995, Sedimentary organic matter, organic facies and palynofacies: Chapman & Hall, London, UK. 615 pp.

Verleye, T.J., and Louwye, S., 2010, Recent geographical distribution of organic-walled dinoflagellate cysts in the southeast Pacific (25–53°S) and their relation to the prevailing hydrographical conditions: Palaeogeography, Palaeoclimatology, Palaeoecology, v. 298, no. 3–4, p. 319–340, doi: 10.1016/j.palaeo.2010.10.006.

Verleye, T.J., Mertens, K.N., Louwye, S., and Helge, W.A., 2009, Holocene salinity changes in the southwestern Black Sea: a reconstruction based on dinoflagellate cysts: Palynology, v. 33, p. 77–100.

Versteegh, G.J.M., and Zonneveld, K.A.F., 1994, Determination of (palaeo-) ecological preferences of dinoflagellates by applying Detrended and Canonical Correspondence analysis to Late Pliocene dinoflagellate cyst assemblages of the south Italian Singa section: Review of Palaeobotany and Palynology, v. 84, p. 181–199.

Versteegh, G.J.M., and Zonneveld, K.A.F., 2002, Use of selective degradation to separate preservation from productivity: Geology, v. 30, p. 615–618

Voelker, A.H.L., Rodrigues, T., Billups, K., Oppo, D., McManus, J., Stein, R., Hefter, J., and Grimalt, J.O., 2010, Variations in mid-latitude North Atlantic surface water properties during the mid-Brunhes (MIS 9–14) and their implications for the

thermohaline circulation: Climate of the Past, v. 6, no. 4, p. 531–552, doi: 10.5194/cp-6-531-2010.

Wall, D., and Dale, B., 1966, "Living fossils" in western Atlantic plankton: Nature, v. 211, p. 1025–1026.

Wall, D., Dale, B., Lohmann, G.P., and Smith, W.K., 1977, The environmental and climatic distribution of dinoflagellate cysts in modern marine sediments from regions in the North and South Atlantic oceans and adjacent seas: Marine Micropaleontology, v. 2, p. 121–200.

Wilkin, R.T., Arthur, M.A., and Dean, W.E., 1997, History of water column anoxia in the Black Sea indicated by pyrite framboid size distributions: Earth and Planetary Science Letters, v. 148, n. 3–4, p. 517–525.

Williams, G.L., Brinkhuis, H., Pearce, M.A., Fensome, R.A., and Weegink, J.W., 2004, Southern Ocean and global dinoflagellate cyst events compared: index events for the Late Cretaceous–Neogene: Proceedings of the Ocean Drilling Program, Scientific results, v. 189. 98 pp.

Wrenn, J.H., Hannah, M.J., and Raine, J.I., 1998, Diversity and palaeoenvironmental significance of late Cenozoic marine palynomorphs from the CRP-1 Core, Ross Sea, Antarctica: Terra Antartica, v. 5, no. 3, p. 553–570.

Wright, A.K., and Flower, B.P., 2002, Surface and deep ocean circulation in the subpolar North Atlantic during the mid-Pleistocene revolution: Paleoceanography, v. 17, no. 4, p. 1–16, doi: 10.1029/2002PA000782.

Zonneveld, K.A.F., Versteegh, G.J.M., and de Lange G.J., 2001, Palaeoproductivity and post-depositional aerobic organic matter decay reflected by dinoflagellate cyst assemblages of the Eastern Mediterranean S1 sapropel: Marine Geology, v. 172, p. 181–185.

Zonneveld, K.A.F., Bockelmann, F., and Holzwarth, U., 2007, Selective preservation of organic-walled dinoflagellate cysts as a tool to quantify past net primary production and bottom water oxygen concentrations: Marine Geology, v. 237, p. 109–126.

Zonneveld, K.A.F., Susek, E., and Fischer, G., 2010, Seasonal variability of the organic-walled dinoflagellate cyst production in the coastal upwelling region off Cape Blanc (Mauritania): a five-year survey: Journal of Phycology, v. 46, p. 202–215.

Zonneveld, K.A.F., Marret, F., Versteegh, G.J.M., Bogus, K., Bonnet, S., Bouimetarhan, I., Crouch, E., de Vernal, A., Elshanawany, R., Edwards, L., Esper, O., Forke, S., Grøsfjeld, K., Henry, M., Holzwarth, U., Kielt, J.-F., So-Young, K., Ladouceur, S., Ledu, D., Chen, L., Limoges, A., Londeix, L., Lu, S.-H., Mahmoud, M.S., Marino, G., Matsouka[sic], K., Matthiessen, J., Mildenhal[sic], D.C., Mudie, P., Neil, H.L.,

Pospelova, V., Qi, Y., Radi, T., Richerol, T., Rochon, A., Sangiorgi, F., Solignac, S., Turon, J.-L., Verleye, T., Wang, Y., Wang, Z., and Young, M., 2013, Atlas of modern dinoflagellate cyst distribution based on 2405 datapoints: Review of Paleobotany and Palynology, v. 191, p. 1–197.

APPENDIX 1

Remarks on selected taxa

Group Acritarcha Evitt, 1963

Genus *Lavradosphaera* De Schepper and Head, 2008

Lavradrosphaera sp. cf. *L. crista* De Schepper and Head, 2008

(Plate 4, figs. 1–3)

Description: Acritarch of spherical to spheroidal shape. Continuous to discontinuous spongy crests that divide the central body surface into unequal polygons. Crest structure can sometimes be fenestrate to foveolate. Thin crests (~0.5 µm) that generally become wider when intersecting to each other (~2 µm). Crest margins vary from regular to irregular. Central body surface smooth to microgranulate. Maximum diameter, including crests, 19 to 23 µm. Crest height varies between 2 and 3 µm. No pylome was discernible. Twelve specimens measured.

Genus *Pentapharsodinium* Indelicato and Loeblich III, 1986, emend. Montresor et al., 1993

Cysts of *Pentapharsodinium dalei* Indelicato and Loeblich III, 1986

(Plate 4, figs. 13–15)

Proximochorate to chorate cysts with spherical central body. Fibroreticulate processes, nontabular, solid, and with a rather heterogeneous morphology. Usually some processes bifurcate midway along their length. Archeopyle not discernible. Dimensions: central

body diameter varies between 16 and 18 µm. Process length: 4 to 5 µm. Eight specimens measured

Remarks: Certain specimens of *P. dalei* did not have any processes displaying characteristic bifurcation but were assigned to this category based on their size and the fibroreticulate morphology of the processes.

Genus ***Pyxidinopsis*** **Habib, 1976**

"Pyxidinopsis striatoconulus"

(Plate 5, figs. 4–6)

Gonyaulacacean cysts that are proximochorate with spherical to spheroidal body. Acavate. Processes are nontabular, with conical shape, rounded tips and parallel striations. Cyst wall about 1.0 µm thick and has a microgranulate surface. Archeopyle precingular. Dimensions: central body diameter varies between 34 and 36 µm. Process length: 1–2 µm. Ten specimens measured. The name "*Pyxidinopsis striatoconulus"* is not intended for formal publication in the present study.

APPENDIX 2

Plates

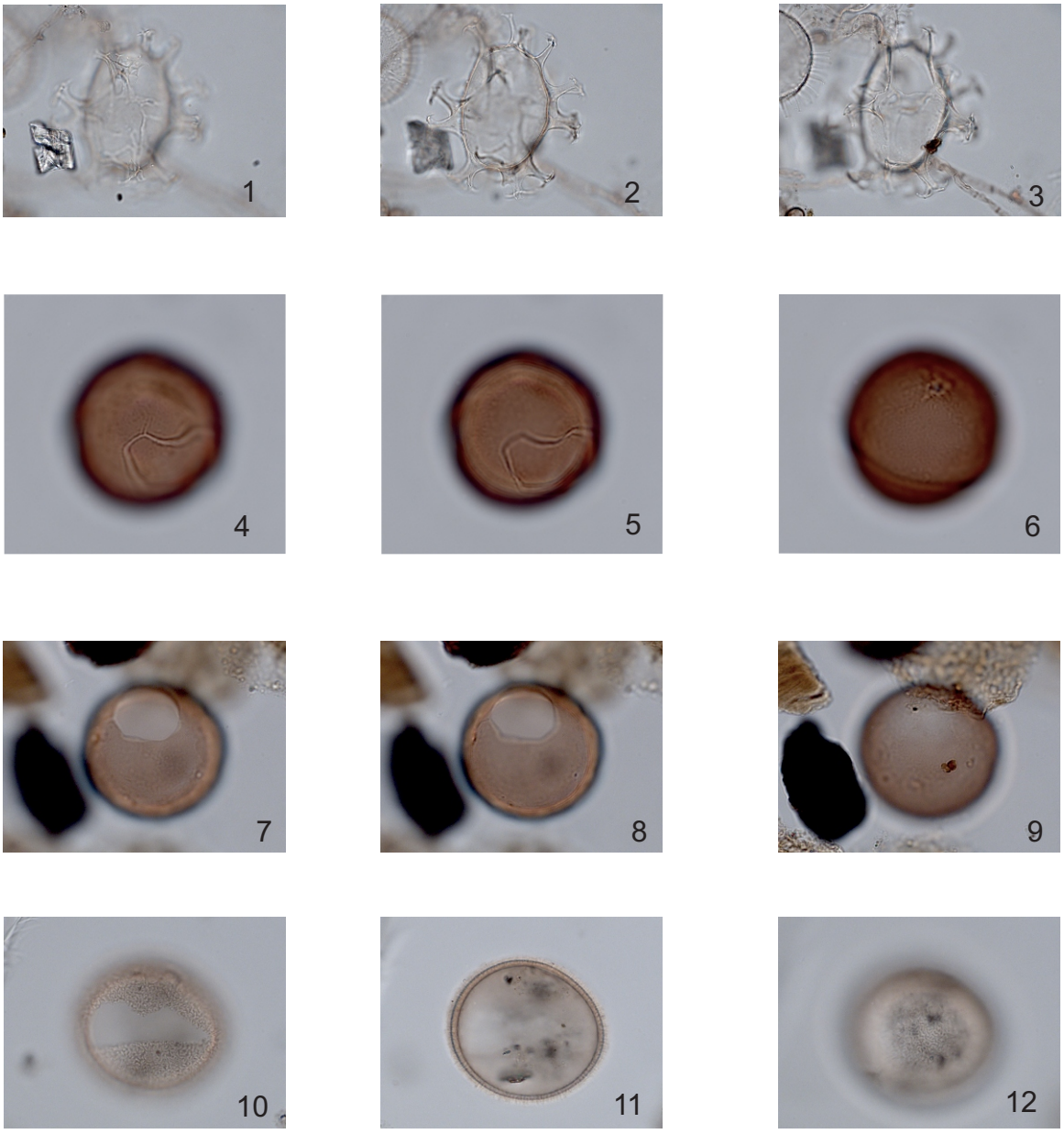

Plate 1

Figs. 1–3: *Achomosphaera andalousiensis* var. *andalousiensis*. Central body: 29x49 µm. Process length: 13–15 µm. Sample ID: 9; England Finder reference: V67/3.
Figs. 4–6: *Brigantedinium cariacoense*. Diameter: 33 µm. Sample ID: 62; England Finder reference: G54/2.
Figs. 7–9: *Brigantedinium simplex*. Diameter: 34 µm. Sample ID: 57; England Finder reference: E52/0.
Figs. 10–12: *Bitectatodinium tepikiense*. Dimensions: 40x46 µm. Sample ID: 12; England Finder reference: S61/2.

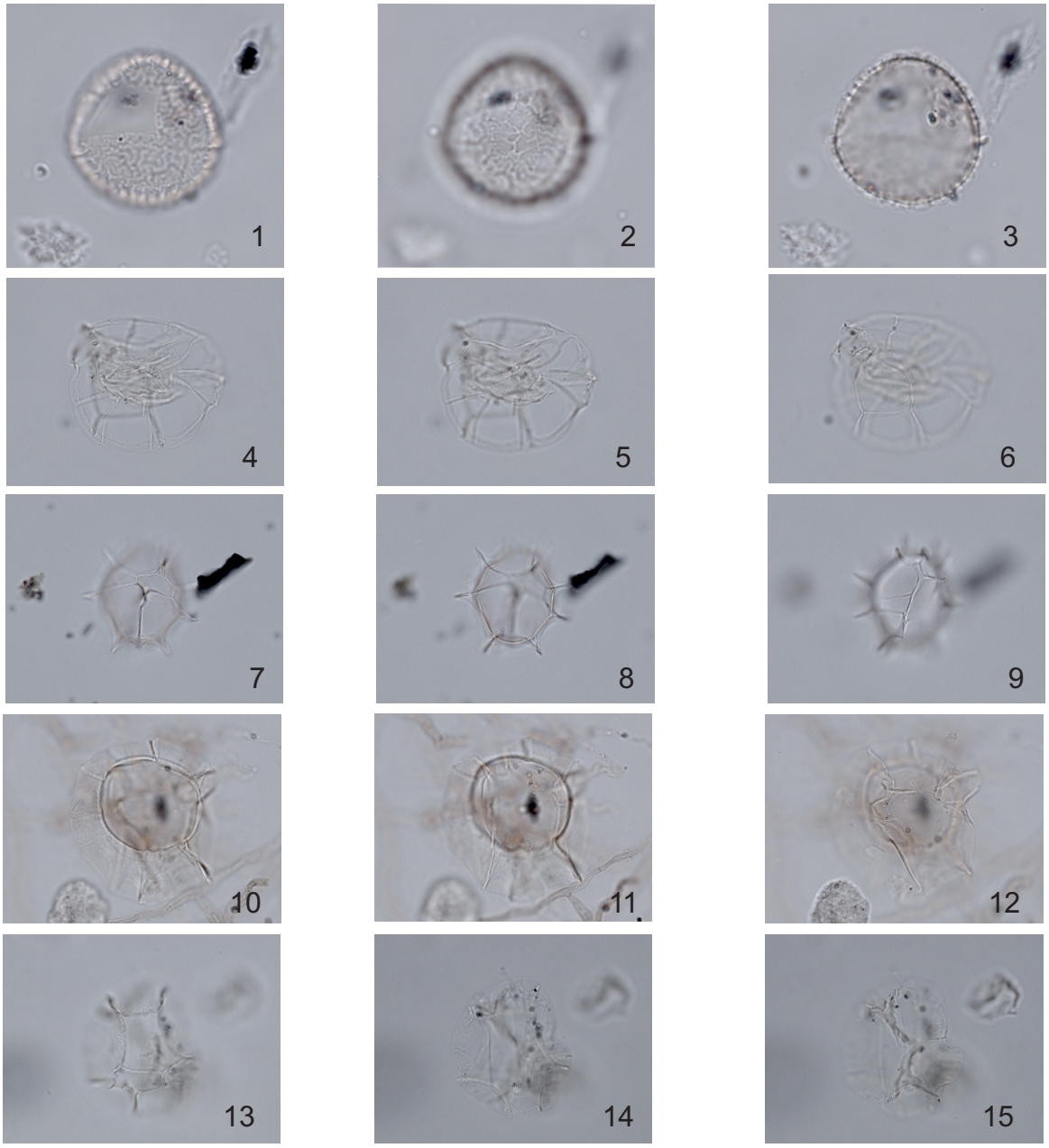

Plate 2

Figs. 1–3: *Corrudinium*? *labradori*. Diameter: 20 µm. Sample ID: 5; England Finder reference: L49/1.
Figs. 4–6: *Dalella chathamensis*. Dimensions of central body: 35x17 µm. Process length: 6–13 µm. Trabecula thickness: 2–3 µm. Sample ID: 65; England Finder reference: O47/2.
Figs. 7–9: *Impagidinium aculeatum*. Dimensions of central body: 48x36 µm. Crest acuminations: 5 µm. Sample ID: 68; England Finder reference: P52/2.
Figs. 10–12: *Impagidinium cantabrigiense*. Diameter of central body: 30 µm. Crest and tegillum varies from 5 µm at the apex to 12 µm at the antapex. Sample ID: 7; England Finder reference: U62/4.
Figs. 13–15: *Impagidinium palidum*. Dimensions: 45x50 µm including crests. Crest length varies between 7 and 10 µm. Sample ID: 56; England Finder reference: M57/2.

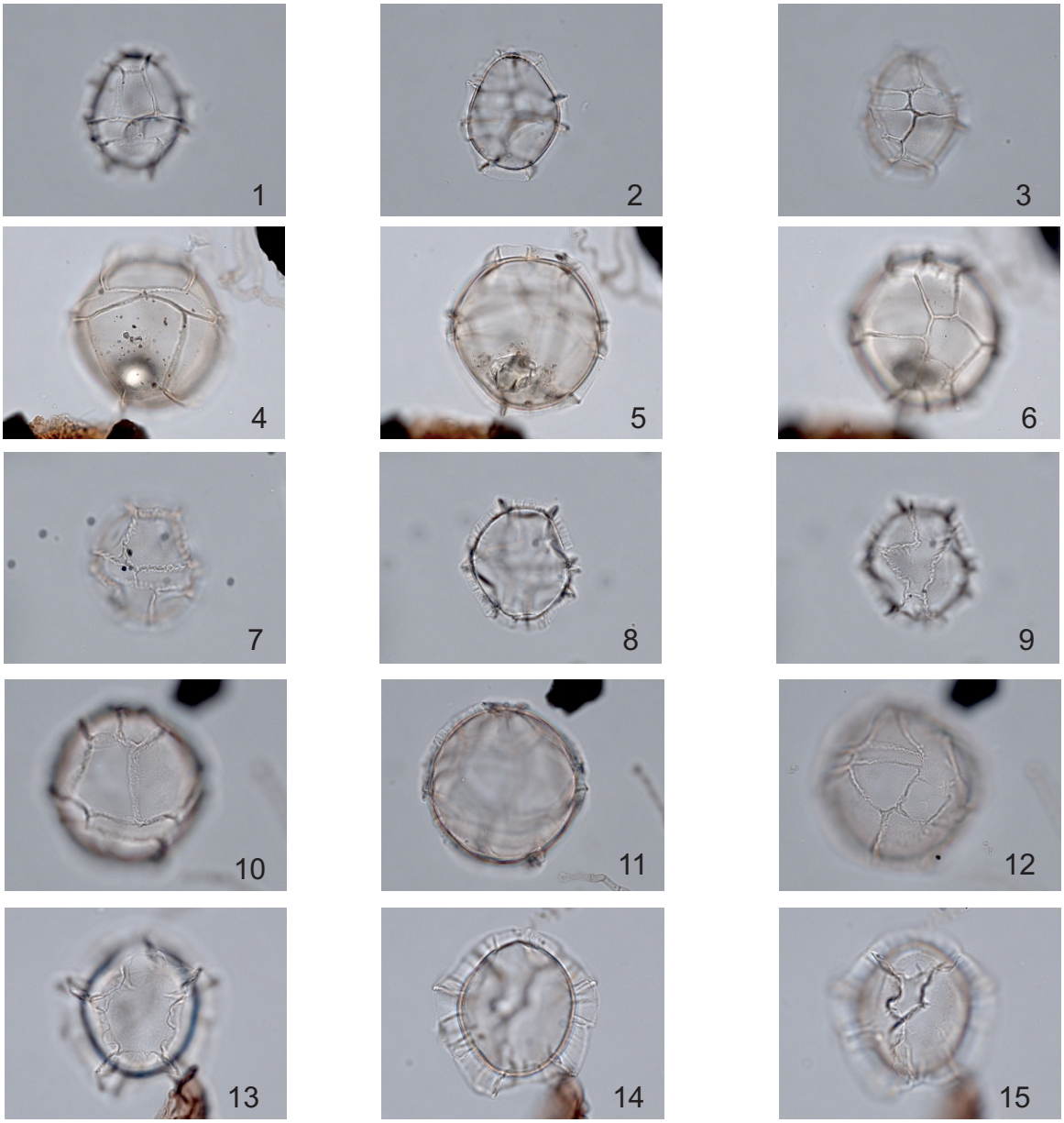

Plate 3

Figs. 1–3: *Impagidinium paradoxum*. Central body: 32x26 µm. Crest length: 2.5 µm. Sample ID: 61; England Finder reference: T55/1.
Figs. 4–6: *Impagidinium patulum*. Diameter of central body: 63 µm. Crest length: 5 µm. Sample ID: 20; England Finder reference: N60/3.
Figs. 7–9: *Impagidinium plicatum*. Diameter of central body: 32 µm. Crest length: 3 µm. Sample ID: 21; England Finder reference: K57/4.
Figs. 10–12: *Impagidinium sphaericum*. Diameter of central body: 56 µm. Crest length: 2 µm. Sample ID: 49; England Finder reference: T55/0.
Figs. 13–15: *Impagidinium strialatum*. Diameter of central body: 29 µm. Crest length: 6 µm. Sample ID: 57; England Finder reference: R53/0.

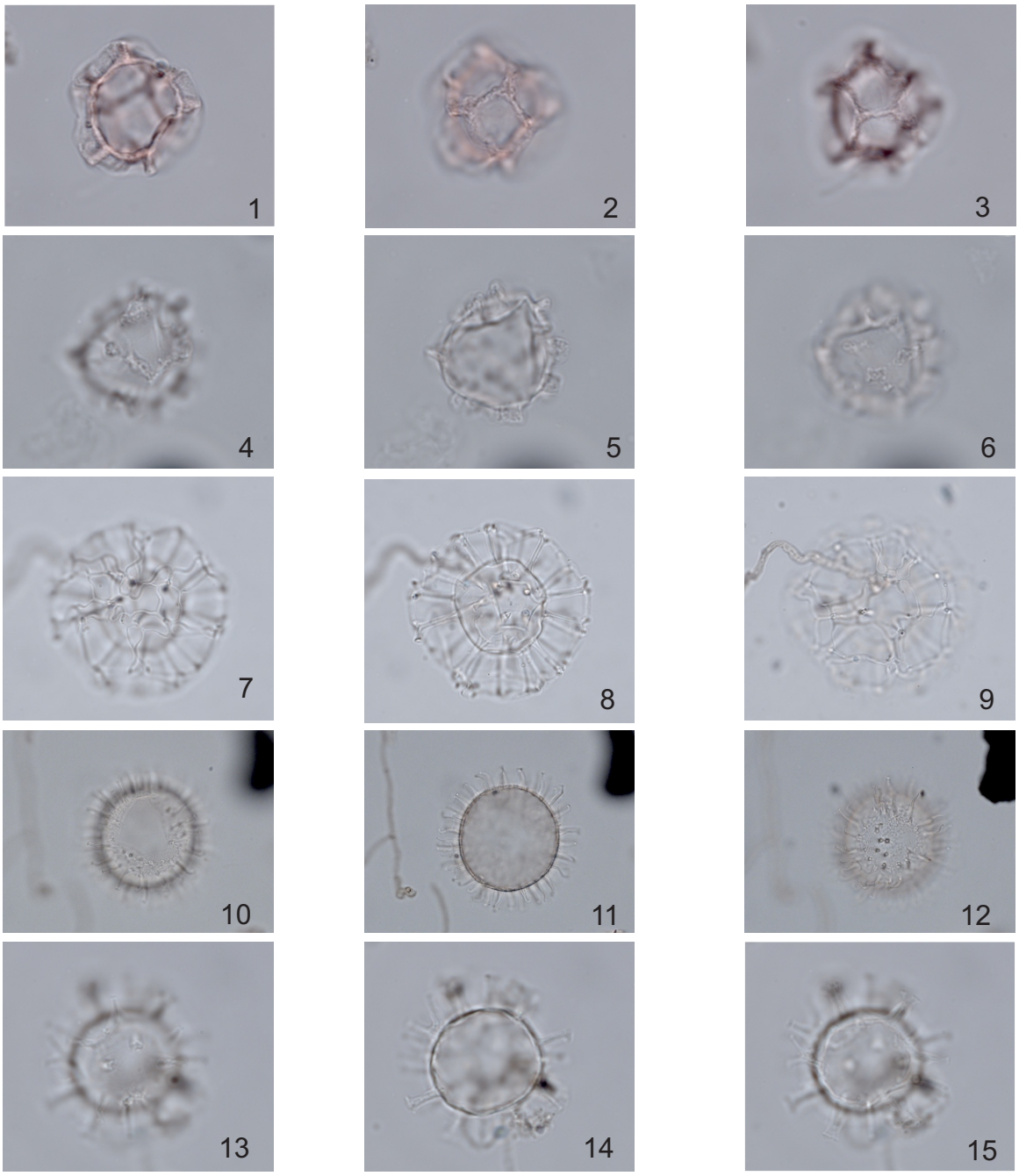

Plate 4

Figs. 1–3: *Lavradosphaera* cf. *crista*. Diameter of central body: 16 µm. Crest length: 3 µm. Sample ID: 39; England Finder reference: R58/0.
Figs. 4–6: *Lavradosphaera* cf. *crista*?. Diameter of central body: 16 µm. Crest length: 1–3 µm. Sample ID: 14; England Finder reference: P55/4.
Figs. 7–9: *Nematosphaeropsis labyrinthus*. Diameter of central body: 25 µm. Process length: 15 µm. Thickness of trabecula: 1 µm. Sample ID: 28; England Finder reference: J40/3.
Figs. 10–12: *Operculodinium centrocarpum* sensu Wall & Dale, 1966. Diameter of central body: 33 µm. Process length: 6 µm. Sample ID: 6; England Finder reference: K51/1.
Figs. 13–15: Cysts of *Pentapharsodinium dalei*. Diameter of central body: 17 µm. Process length: 3–4 µm. Sample ID: 52; England Finder reference: H57/4.

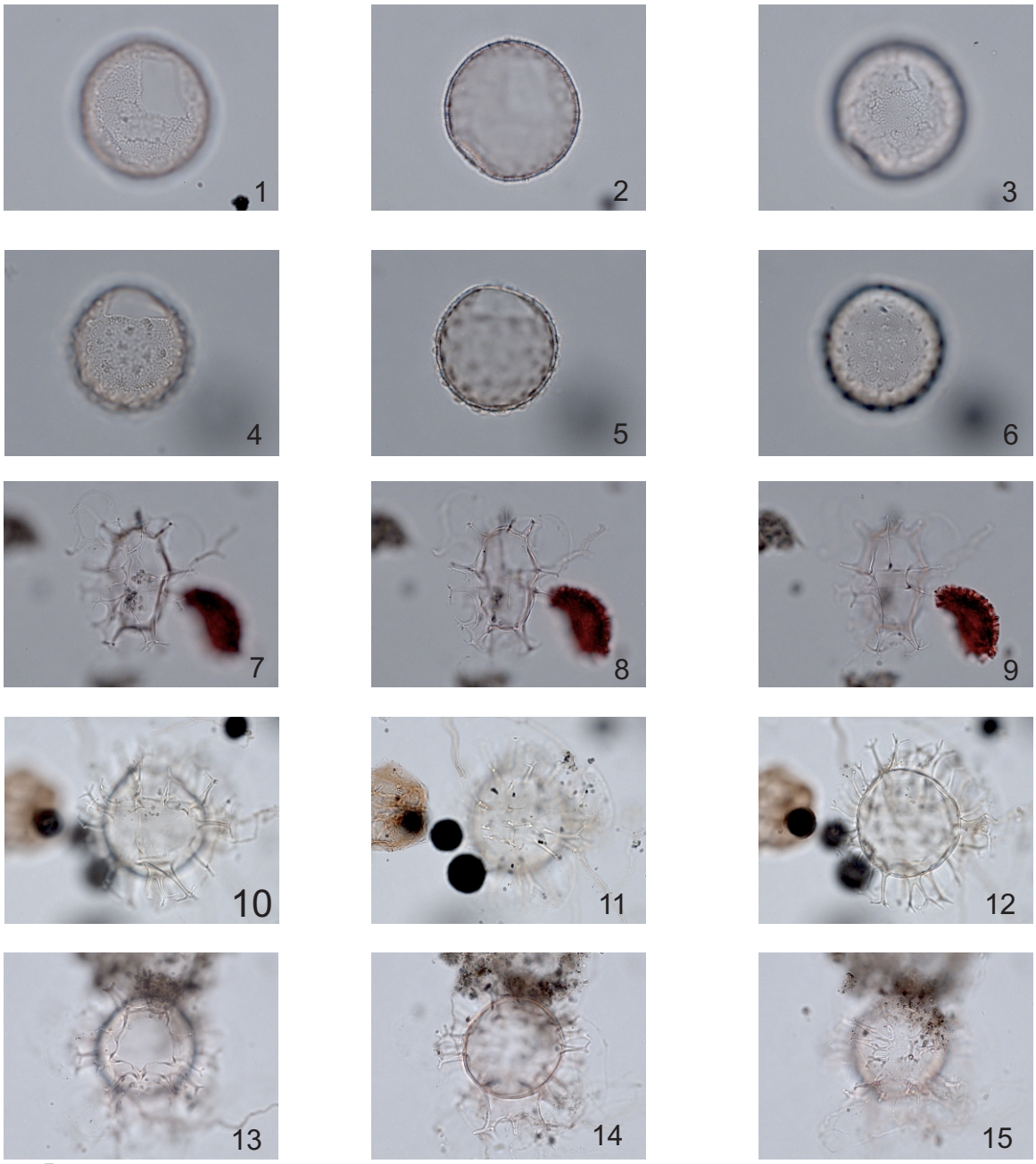

Plate 5

Figs. 1–3: *Pyxidinopsis reticulata*. Diameter of central body: 35 µm. Sample ID: 25; England Finder reference: F61/3.
Figs. 4–6: "*Pyxidinopsis striatoconulus*". Diameter of central body: 35 µm. Process length: 1 µm. Sample ID: 49; England Finder reference: D48/3.
Figs. 7–9: *Spiniferites elongatus*. Dimensions of central body: 25x36 µm. Process length: 6–8 µm. Sample ID: 38; England Finder reference: H40/4.
Figs. 10–12: *Spiniferites hyperacanthus*. Diameter of central body: 55 µm. Process length: 20 µm. Sample ID: 4; England Finder reference: P52/0.
Figs. 13–15: *Spiniferites mirabilis*. Diameter of central body: 53 µm. Process length: 20 µm. Sample ID: 39; England Finder reference: L33/4.

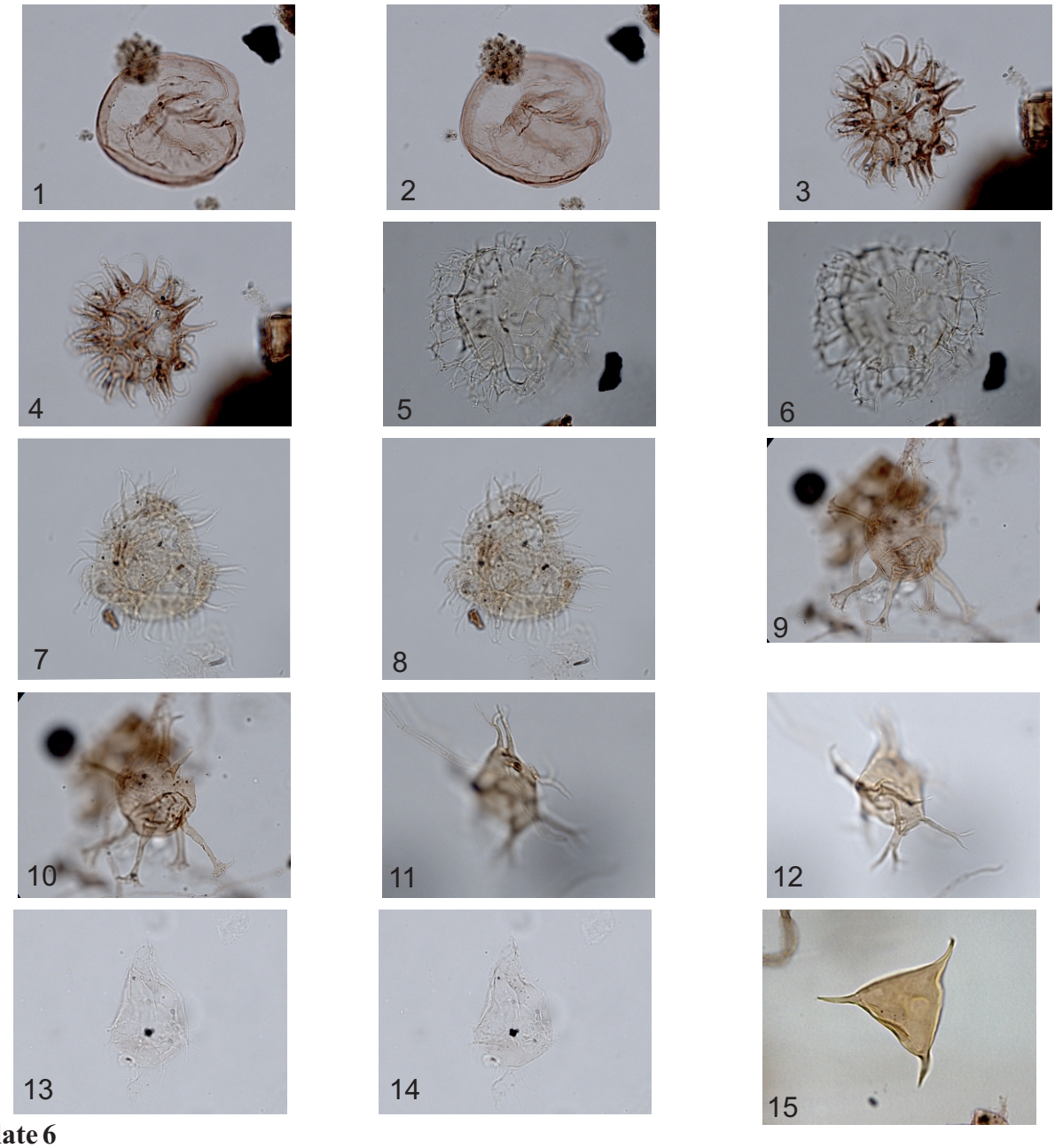

Plate 6

Figs. 1, 2: *Selenopemphix nephroides*. Diameter: 38 µm. Sample ID: 36; England Finder reference: O47/2. **Figs. 3, 4**: *Selenopemphix quanta*. Diameter of central body: 25 µm. Process length: 10 µm. Sample ID: 26; England Finder reference: V56/3. **Figs. 5, 6**: *Glaphyrocysta* sp. (RW). Dimensions of central body: 55x60 µm. Process length: 15–20 µm. Sample ID: 66; England Finder reference: H53/3. **Figs. 7, 8**: *Hystrichodinium* cf. *pulchrum*. Diameter of central body: 38 µm. Process length: 20 µm. Sample ID: 59; England Finder reference: N53/0. **Figs. 9, 10**: *Oligosphaeridium complex*. Diameter of central body: 47 µm. Process length: 40 µm. Sample ID: 5; England Finder reference: C43/4. **Figs. 11, 12**: *Multiplicisphaeridium*? sp. (RW). (Grouped as unidentified acritarch). Diameter of central body: 25 µm. Process length: 16–18 µm. Sample ID: 4; England Finder reference: Q58/4. **Figs. 13, 14**: *Palaeohystrichophora infusorioides* (RW). Dimensions: 68x30 µm. Sample ID: 5; England Finder reference: D61/3. **Fig. 15**: *Veryhachium* spp. (RW). Dimensions: 30 µm from the process to the opposite edge. Sample ID: 13; England Finder reference: F62/2.

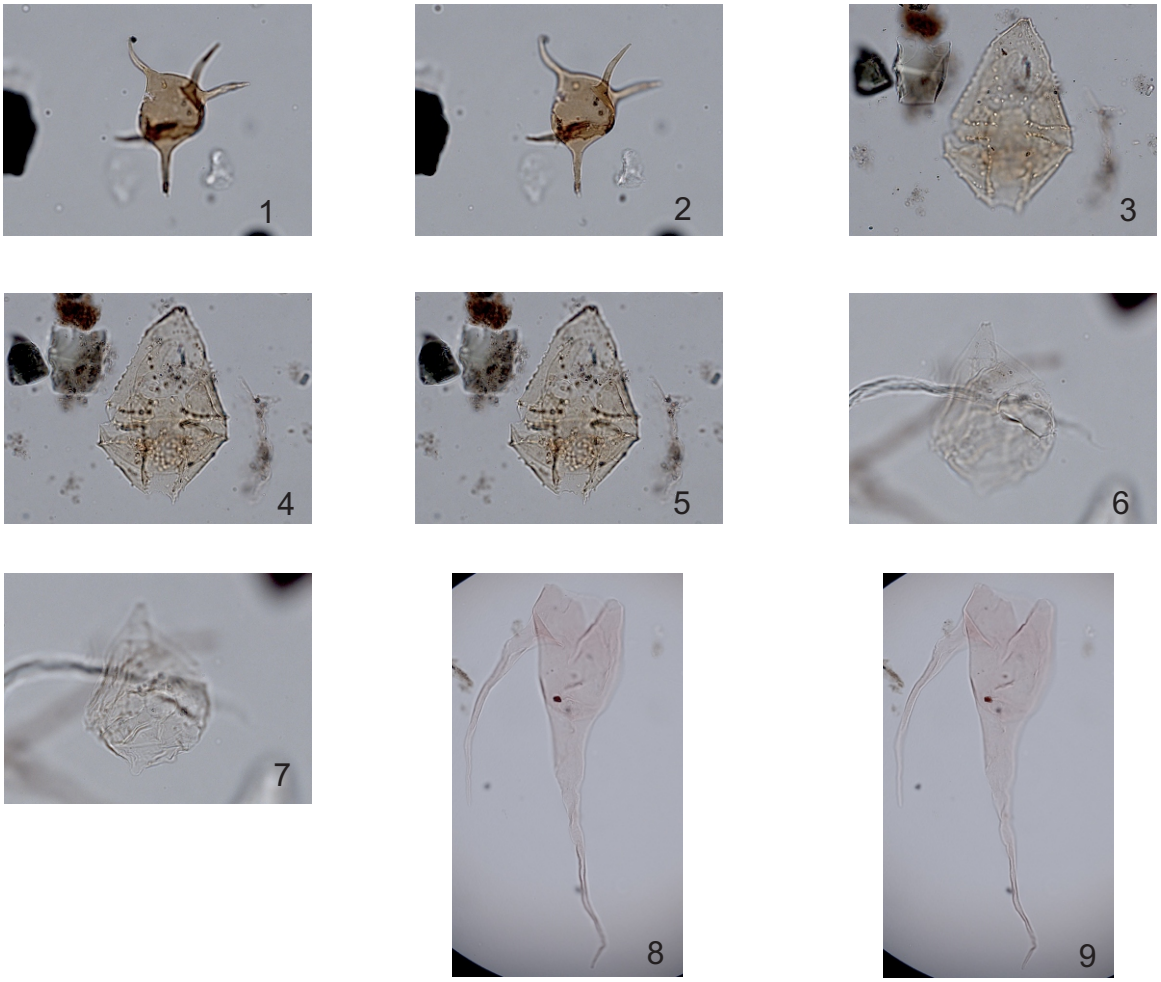

Plate 7

Figs. 1, 2: *Micrhystridium*? sp. (RW) (grouped as unidentified acritarch). Dimensions: 35 µm from the tip of the process to the opposite edge. Process length: 15 µm. Sample ID: 5; England Finder reference: H46/3.
Figs. 3–5: *Spinidinium* sp. (RW). Dimensions: 69x45 µm. Sample ID: 33; England Finder reference: L65/2.
Figs. 6, 7: *Subtilisphaera* sp. (RW). Dimensions: 48x35 µm. Sample ID: 5; England Finder reference: O60/4.
Figs. 8, 9: *Odontochitina operculata* (RW). Dimensions: 145x40 µm. Sample ID: 1; England Finder reference: Q73/1.

APPENDIX 3

Protocol for processing palynological samples

The following protocol for sample processing is adapted from methods already used at Brock University, with the specific aims of minimizing the loss of organic residue while maintaining the highest standards to prevent contamination. Minimizing processing losses is crucially important when the original sample size is small. The protocol described below was developed for deep-sea sediment samples that had been disaggregated in distilled water, and wet sieved at 63 µm to remove foraminifera for later geochemical analysis. The filtrate had been retained in a 1L glass beaker, allowed to settle, decanted, and dried. This dried sediment was scraped from the base of each glass beaker, and stored in plastic bags for future palynological analysis. The above preparation was conducted at the University of Cambridge under the direction of Dr Patrizia Ferretti who then supplied the dried sediment for the present study.

1. Wash 400 ml beakers in preparation for sample processing. First, soak in warm soapy water, then clean vigorously with a soft, non-abrasive cloth using non-abrasive soap. Clean with hot tap water and rinse thoroughly with distilled water to remove any tap water (which in the St. Catharines area comes from the Decew Falls Water Treatment Plant on a reservoir complex that includes lakes Moody and Gibson, adjacent to Brock University). The St Catharines tap water is likely to be contaminated with aquatic palynomorphs. A piece of parafilm is placed over the beaker to prevent airborne contamination prior to and during processing.

2. When the beakers are dry, remove any existing external markings with solvent. Using an indelible marker, number each beaker with a designated lab number (keeping the numbering simple, e.g. 1 to 24) in two places: high on one side and low on the opposite side (as a precaution). Write this number also on the sample bag to correlate the sample number with the lab number. Note also in lab note book. If more than one person is using the lab, write initials on the beaker.

3. Crush the dried pieces of dried sediment gently between fingers in the plastic bag, breaking larger pieces into fragments of about 5 mm in diameter.

4. Place a paper baking cup onto the cleaned weighing plate of an electronic balance. Zero the balance. Transfer contents of the sample bag into the baking cup, and weigh the sediment. Note sample weight in grams to one decimal place.

5. Transfer contents of baking cup into a clean 400 ml beaker, ensuring that the sample is tipped gently onto the bottom of the beaker and thereby prevent a cloud of dust from forming. Dispose of empty baking cup. Re-seal beaker with Parafilm. Note that using a baking cup rather than pouring the sample directly from the sample bag into the beaker: 1) potentially reduces errors in weighing because of the minimal weight of the baking cup relative to the sample weight, 2) avoids the risk of transferring any contaminant from the outside of the bag into the beaker, and 3) allows the sample to be lowered gently to the base of the beaker.

6. When all samples have been weighed and placed in beakers, the beakers are transferred to the fume hood and small amounts of 20% conc. cold HCl are added in turn to each sample, using a squirt bottle. It is important to add the acid in minute increments

to avoid any possibility of bubbling over. Gradually add 150 ml of acid to each beaker, swirling the sediment into suspension several times, and allow to stand overnight to dissolve all carbonates. Make sure that the Parafilm is securely attached to the top of the beaker.

7. After standing overnight, swirl the sediment into suspension and add distilled water vigorously up to about 500 ml. Allow to stand for about 9 hours. Then vibrate the beaker by dragging briefly and by abrupt short twisting movements to flocculate any fine material adhering to the sides of the beaker as the result of electrostatic forces. Allow 3 more hours for this flocculant to settle.

8. Rinse a glass pipette with distilled water and connect it to the hose attached to the side of the siphon. Then open the faucet and allow water to run to produce suction (Venturi effect) through the pipette.

9. Carefully place the beaker next to the tap avoiding any abrupt movement or twisting that could bring sediment back into suspension; open the Parafilm cover and insert the pipette to suck the supernatant. While removing this supernatant, prevent the pipette from contacting the sides of the beaker to minimize the risk of contamination. Slowly begin tilting the beaker when the liquid reaches around 150 mL. This helps to prevent the tip of the pipette from getting too close to the sediment in the bottom. Remove the pipette when reaching the lowest safe level of supernatant to avoid any chance of losing sediment. Re-seal beaker with Parafilm.

10. Rinse the tip of the pipette with tap water and allow re-circulation (tap water being sucked through the pipette), then repeat using distilled water. Keep the tap water running

at all times to maintain the suction and prevent tap water back-flowing into the hose connected to the pipette.

11. Transfer the beaker to the fume hood and swirl the sediment back into suspension. Add distilled water vigorously up to 500 mL and allow to stand for 9 hours. Subsequently, repeat the procedure for flocculation mentioned in step 7.

12. Repeat steps 8 to 11 until reaching a pH of about 6 (pH of distilled water). When measuring the acidity, use one end of the pH paper to test the sample and add a small amount of distilled water on the other end for comparison. Then, remove the supernatant as before.

13. Swirl the sediment into suspension and add 38% conc. cold HF up to 150 mL. Due to the hazardous nature of this acid, is essential to wear all the safety elements (lab coat, gloves, mask etc.) when manipulating it. Look for any drips at all times. If there is a suspicion of drips, rinse the affected area(s) with a sodium carbonate solution using a cloth. Also, dip gloves in this solution always before removing them from the fumehood.

14. Swirl the sediment into suspension 3 times a day for 5 days.

15. Twist and drag the beakers to produce flocculation of particles in the sides of the beaker. Allow to stand for three hours.

16. Peel back the Parafilm cover from the beaker. Make sure to avoid the drops condensed on its inner side since they could contain HF. Begin decanting the HF from the samples to a 1 L beaker by slow tilting to avoid any abrupt movement of the sediment that could bring it into suspension. Reverse the tilt if the sediment at the bottom of the

beaker begins to cascade. Stop decanting if there is any chance of losing organic residue. Label a plastic bottle with “Waste HF” and then transfer the content of the 1 L beaker to this bottle. It is important not to accumulate too much HF in the 1 L beaker. Hence, it is recommended that the decanted acid be transferred to the waste HF bottle after every other sample.

17. Swirl beakers to bring the residue into suspension and add distilled water up to around 500 mL and allow to stand overnight.

18. Repeat steps 15 and 16 until the supernatant is neutral.

19. Label 50 mL screw-top disposable conical test tubes with the same designated lab number used in the beakers. Label in two different places: high on one side and low on the opposite side. Also label the screw top.

20. Decant the supernatant and transfer the residue from the beaker to a 50 mL test tube. Make sure the number in the test tube matches the number on the beaker.

21. Add about 40 mL of HCl to the test tubes and allow stand for 3 hours. This helps to remove any precipitates formed during HF treatment. Then fill the tubes with distilled water.

22. In a centrifuge, set the RPM at 3500 and spin the test tubes for 3 minutes, then remove the supernatant. Repeat until reaching a pH of 6, this being the pH of distilled water.

23. Add the desired number of *Lycopodium clavatum* tablets (usually around 1 to 3 per 10 grams of dry sediment) to each sample and dissolve them adding some HCl. Is important to aim approximately for an ideal ratio of dinoflagellate cysts to spores of *L. clavatum*, but this requires estimating the dinocyst concentration in advance which is best achieved by consulting previous studies of dinocysts under similar settings. Fill the test tube with distilled water after the tablet(s) is (are) completely dissolved.

24. Spin down the samples using the same parameters mentioned in step 22. Then, remove approximately 3/4 of the supernatant and mix the residue using the vortex mixer being careful always to bring all the residue into suspension.

25. Sieve the sediment using a 10 µm nylon mesh. After sieving, make a wet preparation to see if ultrasound treatment is needed due to high amounts of AOM. Also it is possible to add more *Lycopodium* tablets at this point if necessary. Then transfer the sieved material to a 15 mL test and add two drops of stain if desired. Mix the material with the stain using the vortex mixer then sieve again to remove superfluous stain. Transfer the residue back to the 15 mL test tube.

26. Place a cover slip on a slide warmer and using a pipette add 2 or 3 drops of glycerin jelly and 6 drops of distilled water. Mix using a toothpick or cocktail stick. Make sure to cover all the cover slip's surface with the mix. Use a pipette to mix the sieved residue thoroughly, and promptly transfer about 10 drops of residue evenly over the cover slip, then cover the slide warmer and let the cover slip dry for at least an hour.

27. Ensure that all superfluous water has evaporated from the cover slip. This can be done by placing a cold microscope slide over the cover slip to check for condensation.

Put approximately 12 drops of glycerine jelly on a microscope slide and carefully invert the cover slip onto the glucerine jelly, avoiding any air bubbles from becoming trapped. Then remove the microscope slide quickly from the slide warmer and let it rest horizontally for a few hours. Slide-making follows the methodology of Evitt (1984).